UNIVERSITAT POLITÈCNICA DE VALÈNCIA

Escuela Técnica Superior de Ingeniería del Diseño

UNIVERSITAT POLITÈCNICA DE VALÈNCIA

Escuela Técnica Superior de Ingeniería del Diseño

OPTIMIZATION STRATEGY FOR THE COMBINATION OF HIGH-PRESSURE AND LOW-PRESSURE EGR TO REDUCE FUEL CONSUMPTION AND NOX EMISSIONS IN A LIGHT DUTY COMMERCIAL VEHICLE

TRABAJO FINAL DEL

Grado en Ingeniería Mecánica

REALIZADO POR

Carlos Javier Blanco Chuecos

TUTORIZADO POR

Benjamín Pla Moreno

FECHA: **Valencia, septiembre, 2019**

Universitat Politècnica de València
Escuela Técnica Superior de Ingeniería del Diseño
Departamento de Máquinas y Motores Térmicos

UNIVERSITAT POLITÈCNICA DE VALÈNCIA

Optimization strategy for the combination of High Pressure and Low Pressure EGR to reduce fuel consumption and NOx emissions in a Light Duty Commercial Vehicle

Trabajo Fin de Grado (TFG)
Mechanical Engineering
Presented by:
Carlos J. Blanco
Advised by:
Dr. Benjamin Pla

Valencia, September 2019

Resumen. El presente trabajo aborda una alternativa basada en modelado para la optimización del consumo de combustible y de las emisiones de NO_x en un motor Diesel; creando una calibración óptima basada en mapas para la partición de EGR de alta y baja presión, relacionada con las condiciones de funcionamiento del motor. El método se lleva a cabo mediante un estudio previo de las condiciones estacionarias en diferentes puntos de operación, identificando la proporción óptima de EGR de Baja-Alta presión en cada punto. Esta información es transformada en un mapa de calibración que se implementa en la unidad de control del modelo para ser evaluado en condiciones transitorias de conducción real, donde se pueden obtener mejoras tanto en emisiones de NO_x como en consumo de combustible.

Abstract. This work presents a model-based approach for optimizing both fuel consumption and NO_x emissions, for a given Diesel engine, creating a map-based optimal calibration for LP-HP EGR split, regarding the engine operating conditions. The method involves a prior steady-state study for several operating points, identifying optimal LP-HP EGR ratios for each of the points. This data is converted into a calibration map that is later implemented to the model control unit for a transient state test with real driving conditions, where improvements in NO_x emissions and fuel consumption can be achieved.

Agradecimientos

He dejado para el final este pequeño espacio, que nos sirve para dar la nota personal. Viene siendo la única parte del documento escrita en Castellano, en función a las personas a las que van dirigidas estas palabras.

Como suele ocurrir, son muchas las personas e instituciones que han hecho posible el desarrollo de este Trabajo Final de Carrera, ya que uno considera que, en este documento, no entra únicamente el esfuerzo y el tiempo de unos cuantos meses en los que se realiza el proyecto, sino de todos aquellos momentos importantes, durante el transcurso de la carrera de Ingeniería Mecánica, que nos desafiaron y nos sirvieron de enseñanza, personal y profesional. Es aquí donde la guía, las palabras de ánimo, los buenos momentos y el apoyo incondicional brindan las fuerzas necesarias para continuar por un camino que no todos pueden culminar.

Me llena de alegría poder mirar atrás y ver la cantidad de personas que jugaron un papel importante en esto, empezando por mis padres, que supieron equilibrar perfectamente el balance entre ser la rama protectora del nido y la plataforma de despegue para el polluelo. Gracias por enseñarme a valerme por mí mismo y a confiar en mis capacidades. No quedan atrás mis hermanos, que estuvieron cerca en los momentos más difíciles. Entre risas, disputas y juegos hicieron más ameno el camino. A ellos, gracias.

Gracias también a todas esas personas ejemplares que me enseñaron el buen hacer en el camino profesional; profesores como Derwis Rivas, Rolando Rodríguez, Pablo Olmeda y Rafael Ruiz, y compañeros de trabajo como Varun Pandey (Thank you, Varun) y mi tutor Benjamín Pla.

Gracias, por supuesto a la UPV por recibirme en este país y permitirme el honor de culminar mi carrera en ella, pero también gracias a "mi universidad" ULA en Mérida-Venezuela, que me inició y me confirmó mi pasión por la profesión. En ella di mis primeros pasos en este rubro, junto a compañeros y amigos como Dariana López y Jesús Herrera. Gracias también a ellos.

Por último, y no menos importante, gracias a Mª Paula Mendoza (Lala), por estar tan cerca de mí, fortaleciéndome, enseñándome y alegrándome cada día de los últimos maravillosos meses.

Contents

I Report 1

1. Introduction 2

Background-Motivation ... 2

LP-HP EGR outlines for Diesel Engines ... 3

LP-HPEGR impact on gas exchange processes ... 4

LP-HPEGR impact on combustion process ... 7

LP-HPEGR impact in some ICE systems of interest ... 10

LP-HPEGR combination and potential ... 18

Objectives ... 24

Methodology ... 24

2. Model Description and Identification 26

Introduction ... 26

Intake Manifold ... 27

Exhaust Manifold ... 29

Turbocharger ... 29

Compressor ... 30

Turbine ... 31

Mechanical coupling ... 32

EGR System ... 32

Coolers (WCAC & EGR heat exchangers) ... 33

Cylinders ... 33

Control System....35
Model Identification....35
3. **EGR circuit evaluation: Analysis of simulated performance** **38**
Introduction....38
Validation for Base Engine Model (only HP-EGR circuit)....40
Steady State behavior (HPEGR)....43
Transient Model behavior (HPEGR)....50
Exploration of Low-Pressure Model (only LP-EGR circuit)....51
Steady State behavior (LPEGR)....52
Transient behavior (LPEGR)....60
Testing for Hybrid Model ($NO_{x_{Opt}}$, M_{Opt})....63
Steady State engine behavior with optimal calibration maps....69
Transient engine behavior with optimal calibration maps....76
4. **Conclusion** **85**
References and Bibliography **86**
II Project Budget....89
Introduction....90
I. Prices Breakdown Appendix....90
1. 0-D Engine Modeling and Calibration....90
2. Model Exploration and Optimization Activities....91
3. Development of Data-Management and Analysis Programs....93
II. Measurements & Partial Budget....94
1. 0-D Engine Modeling and Calibration....94
2. Model Exploration and Optimization Activities....94
3. Development of Data-Management and Analysis Programs....94
III. Budget Summary....94

Nomenclature

HPEGR	High-Pressure Exhaust Gas Recirculation
LPEGR	Low-Pressure Exhaust Gas Recirculation
VGT	Variable-Geometry Turbine
WCAC	Water-Charge Air Cooler
ICE	Internal Combustion Engine
HC emissions	Unburned Hydrocarbons (unburned fuel)
BSFC	Break-Specific Fuel Consumption
WLTP	Worldwide Light-duty vehicle Test Procedure
NEDC	New European Driving Cycle
MAF	Air mass flow
MAP	Intake Pressure (also referred as P2=P2'=P2'')

I Document

Report

Chapter 1

Introduction

Contents:

Background-Motivation 2
LP-HP EGR outlines for Diesel Engines 3
LP-HPEGR impact on gas exchange processes 4
LP-HPEGR impact on combustion process 7
LP-HPEGR impact in some ICE systems of interest 10
LP-HPEGR combination and potential 18
Objectives 24
Methodology 24

Background-Motivation

These days, research concerning Light Duty Commercial Vehicles in the EU is mainly focused on developing techniques concerning the control of emissions, which are derived from the combustion process, without compromising engine performance. Internal Combustion Engines (ICE), both diesel- and petrol-powered, are affected by this, so the motivation for projects of this kind is the production of efficient vehicles which fulfill the ever-changing European Emission Standards. The present academic work is no exception of this, being the result of a project developed by a team of the Control Department at *CMT - Motores*

Térmicos, driven to a contract between said institution and *Groupe PSA.* The task assigned was the exploration of the potential upgrade of an existing EURO6 engine, from this manufacturer. The idea is introducing new air-management techniques, which allows the engine to fall in the frame of EURO7 regulations.

The implemented method has been obtained from previous works and experiences carried out at the *CMT*, where insights and highlights of Exhaust Gas Recirculation (EGR) tactics have been verified and translated into the base knowledge of this project. The selected approach deals with application of this knowledge through engine modelling, simulation and calibration; serving as a firm guideline for future phases of the contract with *PSA*, where experimental execution will take place. The given solution consists in the introduction of a LPEGR circuit that works parallelly to the already functional HPEGR of the PSA engine DW12RU. In this sense, advantages showcased in both EGR architectures can be maximized by developing an engine control calibration, for the entire engine operating map, based in the optimal combined use of both EGR systems. The optimization is mainly guided towards the reduction of fuel consumption and NO_x emissions.

The first chapter of this work serves as an introduction and a guide for the current state of the matter in relation with EGR technologies. It is also intended to reflect the necessary reasons that justify the viability of the project, as well as the specific objectives pursued and the methodology used. In followings chapters, specifications of the modelling process are discussed, giving first a full description of the model, identifying and validating its execution, and ultimately analyzing its performance under real driving conditions simulated as a homologation procedure cycle. Finally, conclusions are drawn from the obtained results.

It is important to underline that the results obtained are useful to observe general trends for the LPEGR system to be designed, but final performance will strongly depend on the design of the engine, the EGR system and on the final application.

LP-HP EGR outlines for Diesel Engines

Nowadays, knowledge about the characteristics and implementation of both LP and HP EGR architectures is widespread, being well documented in several publications and tested in various engines (check references). However, the aim of this section is to make use of current knowledge and show a

comparative between the two systems, to identify and analyze how engine operative parameters change between architectures and how this affects the engine performance.

In this sense, the comparative is stated in the first blocks of the section. Each block deals with different aspects of the engine and describes how it is influenced by each EGR architecture. This description is carried out by explaining the nature of the changes in performance and highlighting the benefits that can be obtained from both EGR circuits. Finally, an overview of the potential from combining both systems is given.

LP-HPEGR impact on gas exchange processes

The properties of the gas that intervenes in the combustion process have a major impact on engine performance. Given that those properties are directly dependent on the way gas is treated on its way to the cylinder, it is imperative to acknowledge the influence of the systems involved in this gas exchange process. Since the EGR circuit is among these, changes in EGR architecture lead to important effects on said process.

Intake charge temperature, pressure and density. Engine performance is usually improved by increasing the amount of air mass flow introduced in the combustion process. To achieve this, without modifying engine size, air density is intended to be augmented by increasing the pressure and reducing temperature in the intake manifold. Accordingly, turbocharging is implemented aft to pursue higher pressures, while heat exchangers are used in the intake to keep temperatures as low as possible.

For HPEGR systems, the exhaust gas extraction for recirculation is taken from the exhaust manifold, which is at high temperatures. This leads to a challenge when trying to increase the amount of EGR introduced in the intake manifold without reaching temperatures that would boost the production of thermal NO_x. Even though current Diesel engines incorporate EGR coolers to avoid this issue, the small size of the heat exchanger, due to packing restrictions mostly, prevents EGR temperatures from getting as low as desired, so only certain rates of EGR can be used, since otherwise the temperature in the intake will increase. This behavior is shown in figure 1.1.

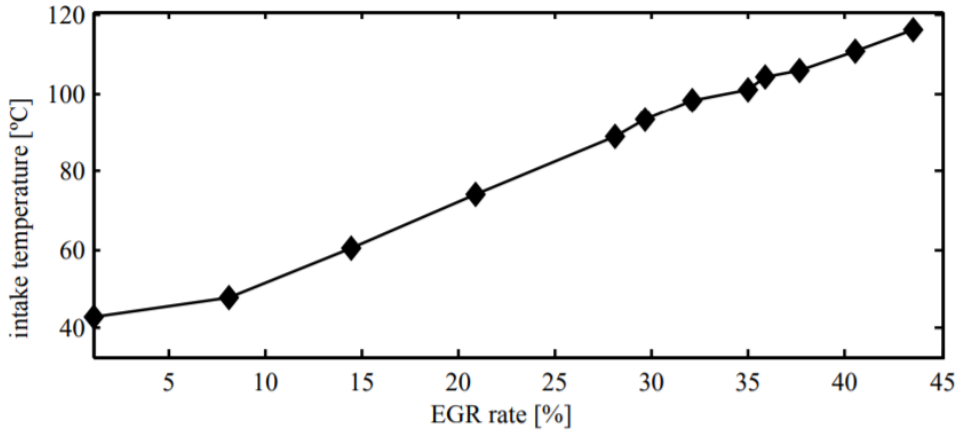

Figure 1.1: HPEGR rate effect on the intake temperature for a 2 liters HSDI engine at 1582 rpm - 42 Nm

Another direct consequence of the increase in intake temperature is what's called "Thermal throttling". As stated before, temperatures in the intake manifold should remain as low as possible so the density increases as well as air flow, therefore the increase in temperature acts as a throttle, preventing the flow of fresh air to remain constant, leading to a decrease instead. If the pressure in the intake manifold remains constant, intake mass flow also decreases as a consequence of the dilution effect created by EGR flow taking its place. Figure 1.2 illustrates phenomena.

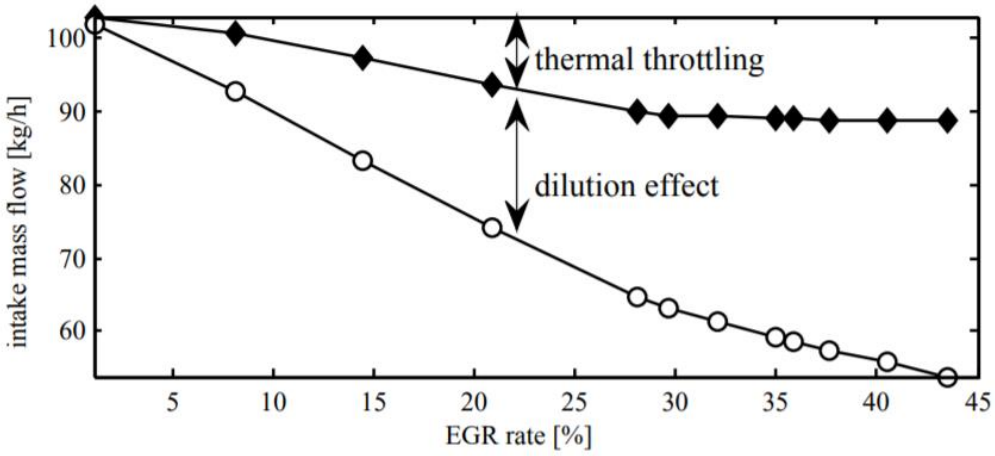

Figure 1.2: Reduction in the fresh air admitted by the engine as a function of the HPEGR rate for a 2 liters HSDI engine at 1582 rpm - 42 Nm.
♦: intake mass flow. ○: air mass flow.

To decrease NO_x emissions by introducing inert exhaust gases that absorb heat from the combustion, it would appear interesting to make temperatures in the intake independent of EGR rate. Importance of EGR rate associated with thermal throttling in the intake manifold diminishes when working with LPEGR, as the effect of WCAC is predominant on the temperature of the combined fresh air and recirculated gases, mixed before the compressor. Furthermore, the interest in a cooling system intended to reduce temperature of recirculated gas alone, when using LPEGR, takes importance only to avoid excessive temperatures at the compressor outlet that may damage it.

To sum up, given the relative independence available in LPEGR circuits concerning intake temperature in relation with EGR rates, this type of EGR architecture offers an elegant solution for thermal throttling. However, a high amount of recirculated gases in the intake manifold, maintaining the same pressure, will continue to lead to dilution effect, i.e. reduction in air mass flow that leads to lower air-to-fuel ratios. Fortunately, intake pressure obtained with a LPEGR architecture tends to be higher than its equivalent in HPEGR circuits, considering that the former's mass flow in the exhaust manifold is not fractionated for recirculation as the latter's, therefore the energy available in the VGT is inherent to the entire mass flow and does not substantially change with the EGR rate. The VGT is then delivering more power to the compressor through the coupling, thus the intake pressure is proportionally higher. This is how LPEGR systems make possible to work in a way that both burned gas concentration and air-to-fuel ratio are higher than those achieved in HPEGR, allowing the reduction of NO_x emissions with lower smoke-opacity penalization in comparison.

Intake charge composition (EGR maximum rates). At certain loads, it is possible to find an issue that makes more difficult the recirculation of exhaust gases. It comes to the lack of the necessary difference of pressures between the gas extraction and delivery point to stablish the desired amount of recirculated gas. As showed in upper plot of figure 1.3, it is clear how, for HPEGR architectures, operating points located at high loads (and usually low engine speeds) will fall into this problem. The same difficulty is found in LPEGR when operating at low loads.

This problematic is often mended, for all version of EGR, with the use of throttling devices to increase the pressure difference at the expense of pumping loses. For HPEGR systems, an intake throttle expands the air flow after the WCAC, which diminish the pressure, so it can be mixed with the right amount

of EGR before entering the intake manifold. LPEGR systems may use a similar mechanism, but the throttle should be installed in the inlet, before the compressor and the EGR delivery; although, the use of a back pressure valves may be chosen instead, located in the exhaust line, after the EGR extraction, so the pressure rises in this point and the desired pressure difference, in relation with the EGR delivery, is achieved.

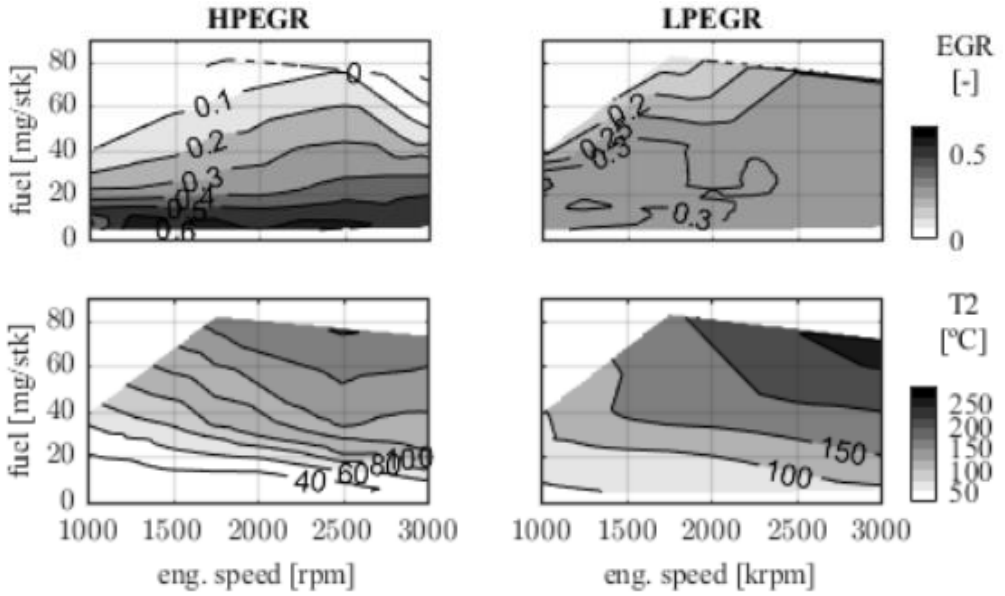

Figure 1.3: EGR rate and compressor outlet temperature (T2) maps for a 2 liters Diesel engine without throttling devices (modelling results)

When it comes to facing the regulations, assuring EGR rates for high loads is decisive to guarantee reduction in NO_x emissions, due to significant full load operation of especially Commercial and Heavy Duty Vehicles at real driving conditions. It is at this demanding operative state where the NO_x emissions peak, so LPEGR shows a clear advantage in this matter, for it is not in need of a throttling device to meet EGR requirements. However, the bottom plot of figure 1.3 shows a limitation of using this type of EGR architecture. Temperatures after the compressor may reach values too high to be withstood for the materials of the compressor wheel, which would impose a restriction in the achievable EGR rate with LPEGR.

LP-HPEGR impact on combustion process

Once understood how gas treatment in the intake manifold changes between EGR systems and how this influences its properties, the next step is to

consider how those variations influence the combustion process. Previous sections state that the main properties affected by the change between architectures are gas composition and its physical conditions inside the intake manifold and later in the cylinder. Both the reduction in the intake temperature and increase in EGR rate with LPEGR generally lead to a slower combustion process, therefore shifting the combustion towards the expansion stroke. Works in this area, such as referenced [5; 6; 20], conveys that, if intake pressure and air mass flow are intended to remain as in its HPEGR counterpart, LPEGR systems are expected to obtain some reduction in NO_x emissions at expense of some increase in fuel consumption, unburned hydrocarbons (HC) and CO emissions.

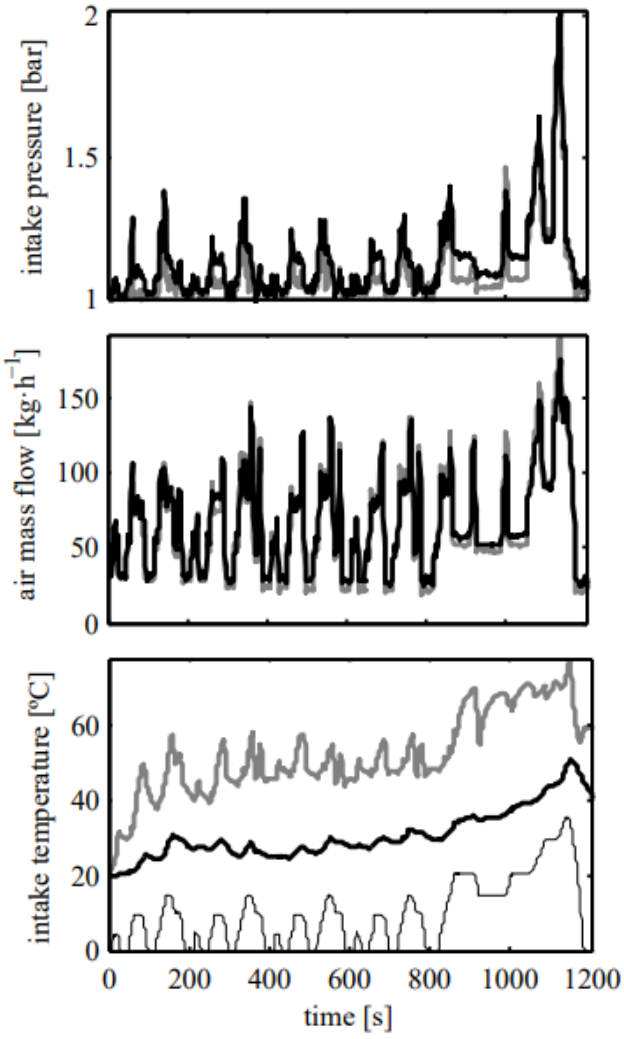

Figure 1.4: Evolution of the air mass flow, intake pressure and intake temperature during the NEDC with LPEGR (black line) and HPEGR (grey line).

Insight into the effects of HP and LPEGR in a driving cycle. The evolution of some parameter of interest during engine operation in NEDC are shown in figure 1.4. Engine control parameters were kept the same for both tests, with different EGR architecture for each.

In the first plot, evolution of intake pressure is shown, falling in line with the concepts already discussed: even though VGT follows the same evolution in both cases, the greater exhaust gas flow that goes through the turbine, in case of LPEGR, increases turbine power, leading to higher compressor mass flow and higher intake pressure. Moreover, this relation can be confirmed in the second plot, where air mass flow is roughly the same, due to unchanged control parameters, but tends to be somewhat higher for LPEGR in those moments when intake pressure also increases. This is a consequence of the EGR valve being completely open, but not being able to dilute the air because of higher intake density.

Intake temperature is another parameter that plays a major role in the combustion process. The third plot in figure 1.4 shows an important reduction in the temperature of the intake gasses when the LPEGR architecture is used. The increase in mass flow, discussed in the previous paragraph, is achievable also thanks to the lower intake temperature, which leads to a noticeable increase in intake density. This also involves a higher amount of recirculated gas in the case of using the LPEGR circuit. Combustion is a physical-chemical process, and therefore closely related to the composition, pressure and temperature conditions of the elements involved in the reaction. In this sense, changes in intake gas properties lead to noticeable variations in the engine NO_x emissions and fuel consumption depending on the EGR architecture.

Figure 1.5 shows the instantaneous and accumulated values for fuel consumption, NO_x emissions and unburned hydrocarbons emissions (HC). The slight increase in fuel consumption is due to two main causes:

- Higher mass flow through intake and exhaust systems leads to higher pumping losses. It is also important to consider that, while applying LPEGR, the recirculated gas flows through more components, such as WCAC and after-treatment systems; this not being the case for HPEGR.
- As stated before, both the lower intake temperature and the higher amount of burnt gases recirculated contribute to a later combustion, with lower temperatures but also with lower efficiency.

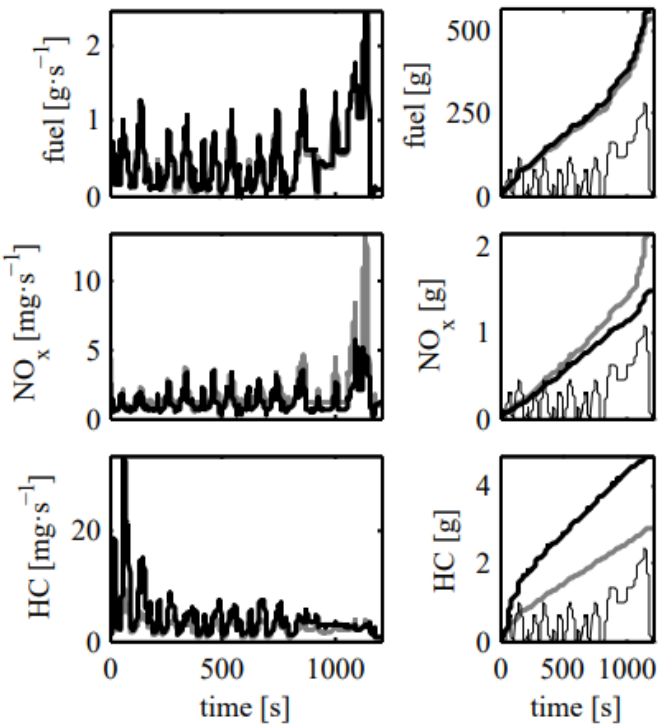

Figure 1.5: Evolution of the accumulated fuel consumption and NO_x emissions during the NEDC with LPEGR (black line) and HPEGR (grey line).

Regarding the last point, the lower combustion temperature, reached with the LPEGR circuit, greatly influences the physical mechanisms involving the increase in fuel consumption, that are also the same which lead to a reduction in NO_x emissions and an increase in HC, at the same time. Figure 1.5 shows lower NO_x emissions with the LPEGR during the whole test, independently of the operating conditions. Consequently, at the end of the cycle a noticeable reduction in the NO_x emissions can be observed. On the contrary, the LPEGR produces a greater increase in the HC emissions respect to HPEGR.

LP-HPEGR impact in some ICE systems of interest

Turbocharging. As EGR and turbocharger are systems that affects directly the gas conditions in the intake manifold, both share a close relation. The different influences of EGR architectures on the turbocharger appear clear by following the path traversed by the exhaust recirculated gases in each case. When applying LPEGR architecture, the entire engine mass flow passes through both Turbine and Compressor, while only the flow that corresponds to air goes through turbocharging elements when HPEGR is used.

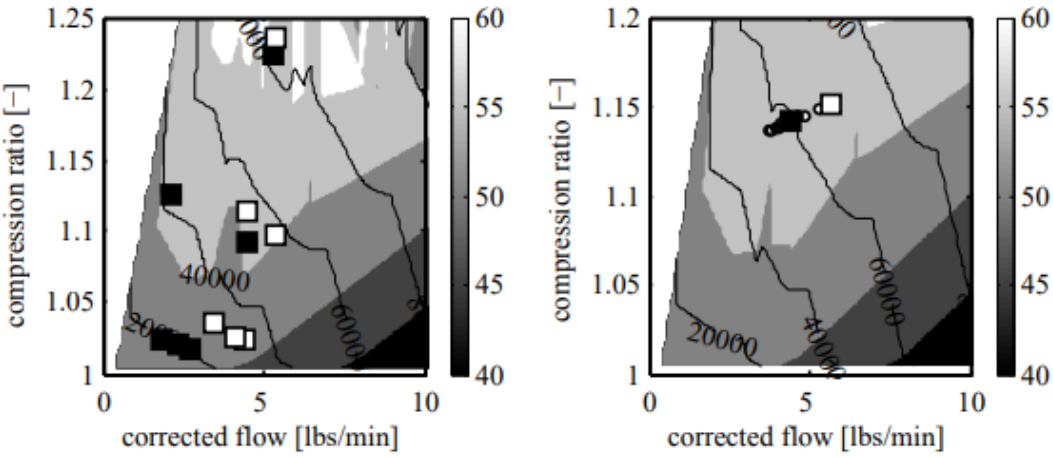

Figure 1.6: EGR architecture effect on the operating point in the compressor map. ■: HPEGR system. □: LPEGR system. ○: evolution with increasing the HPEGR rate from 0 (right) to maximum value (left)

Because of higher flows in the turbocharger when LPEGR is active, the operating point in the compressor and turbine maps is displaced towards higher corrected mass flows, moving away from the surge line, as illustrated in figure 1.6. Also, the right plot of the same figure shows how increasing HPEGR rate decreases mass flow through the turbocharger because exhaust gasses are fractionated before entering the VGT, leading to a power decrease in the compressor, reducing both corrected mass flow and compression ratio. This does not take place when the LPEGR architecture is implemented, for the power available upstream VGT is always the same, being independent of EGR rate. However, in LPEGR systems, if EGR rate changes, there may be a small displacement of the operating point of the compressor due to the effect of gas temperature on the corrected flow, but it can be considered roughly the same.

In light duty vehicles, since the conditions in which the EGR is carried out are usually located at low engine speeds and loads, operating point displacement towards higher corrected mass flows usually means an increase in efficiency for the turbocharger, so performance of the compressor with LPEGR tends to be, in general, enhanced in relation with that obtained with the HPEGR system.

Higher angular velocities in the coupling for LPEGR allows faster response to transients, in fact, as turbocharger speed is practically independent of LPEGR rate, closing the EGR valve allows the instantaneous substitution of recirculated gas for fresh air in the same amount, reducing delay of the turbo group.

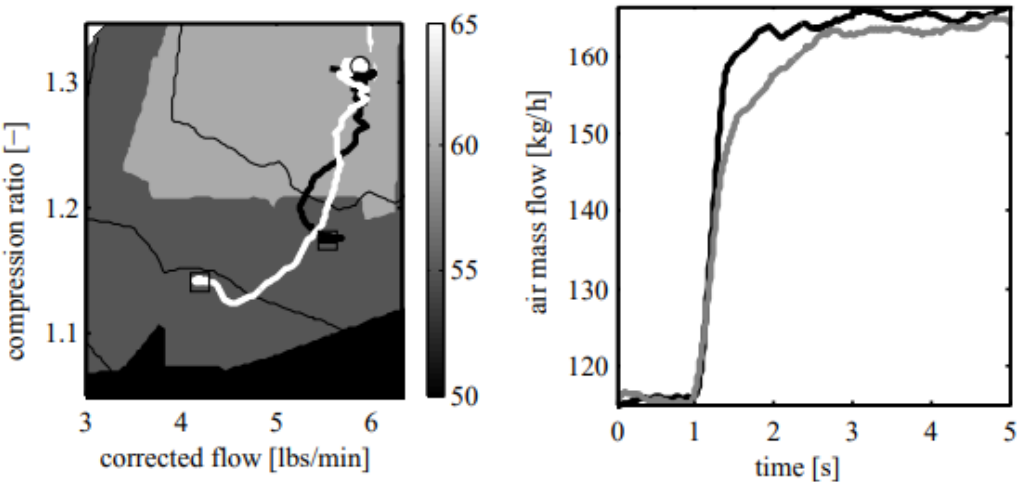

Figure 1.7: Evolution of the turbocharger operating conditions (left) and air mass flow (right) during a tip-in. ——: LPEGR. ——: HPEGR. □: initial conditions. ○: final conditions.

One way to see the advantage of the higher mass flow provided for LPEGR architecture is when the tip in (load transient) test is carried out. This procedure evaluates the response of the air loop system in a turbocharged engine. It consists in increasing the injected fuel, increasing the energy provided to the VGT. In HPEGR systems, a very high amount of that energy is lost by overcoming first the inertia of the turbocharger, so the energy invested in effective work of the compressor comes at a later moment. The left plot of figure 1.7 shows that, due to higher corrected flows in LPEGR, the compressor speed is already closer to the demanded point, so it doesn't lose much energy due to the acceleration of the turbocharger, leading to a faster compressor ratio build up which covers the air flow demand in a shorter amount of time, as shown in the right plot of figure 1.7.

Diesel vehicles have a smoke limiter that restricts the injection of fuel beyond a certain value calculated from some engine operating parameters. This value falls into a criterion of air-to-fuel ratio, given that a significant decrease of this ratio would increase specific fuel consumption, smoke emissions and even NO_x emissions via prompt mechanism. In this sense, the time needed to accelerate the turbocharger is a major cause of the delay in torque response in a turbocharged diesel engine, since the air response limits the fuel injection. An example of this can be seen in figure 1.8, where according to the lower time response of the LPEGR system, the smoke limiter allows, in this case, a higher injection rate, providing more energy to the engine. For this reason, the torque presents a faster

response when this architecture is used, reaching 90% of the final torque in 0.95 seconds, as opposed to the 1.8 seconds required by the engine with the HPEGR system.

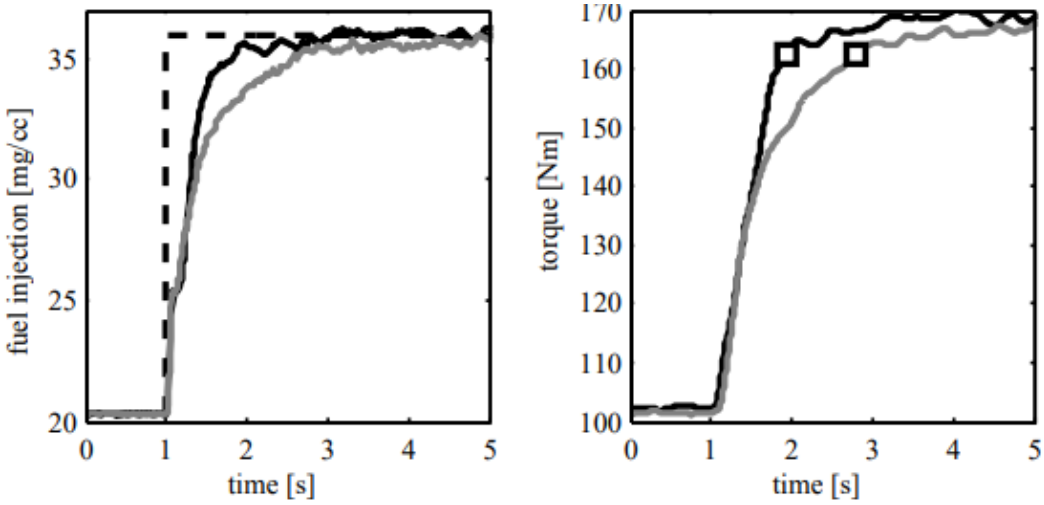

Figure 1.8: Evolution of the fuel injected (left) and engine torque (right) during a tip-in. ——: LPEGR. ——: HPEGR. □: 90% of the final torque.

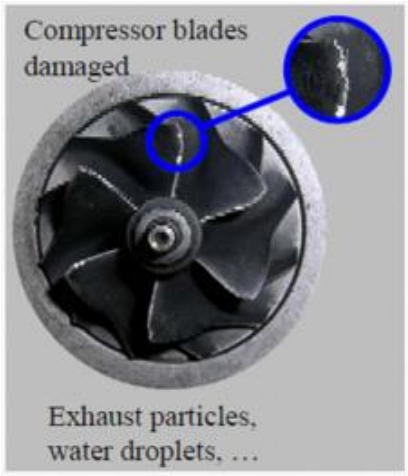

Figure 1.9: Compressor wheel damaged at CMT facilities after intensive LPEGR testing.

A particular downside of applying LPEGR architecture is the damage dealt to intake elements caused by soot and moisture passing through the compressor and WCAC. These agents aid to the formation of fouling, acidic condensation that degrade components, specially the compressor wheel, where water droplets and particles from aged after-treatment components may damage the blades, as

shown in figure 1.9. Despite this, technology is evolving to create stronger after-treatment elements to reduce the importance of this problem, and it has permitted LPEGR to become almost a standard device in current diesel vehicles, but considerations about the issue should still be made when designing an intake line.

Control. One of the most difficult tasks concerning EGR is coordinating it with turbocharging, due to their strong coupling. In general, LPEGR coupling with the VGT tends to be simpler, with a reduce effort in calibration in comparison to HPEGR. This is connected to the fact that HPEGR splits the power available in the exhaust manifold between the EGR and the VGT, while for LPEGR the amount of energy remains always the same at the entrance of the VGT, despite of EGR rate. Three main cases can be explored concerning VGT-EGR coupling controls:

- Effect on the air mass flow:

When the HPEGR valve remains closed, the air mass flow decreases as the turbine opens, however, when the HPEGR valve is fully open exactly the opposite behavior can be observed. In this way, the gain of the relation between the VGT position and the air mass flow changes from positive to negative depending on the HPEGR opening. This leads to important difficulties for a controller, in fact, it is the reason why the air mass flow is usually not used as a direct feedback for the VGT control, and only the intake pressure is used for this purpose. Regarding the behavior of the air mass flow with the LPEGR system shown in figure 1.10, it is possible to check that independently on the LPEGR valve position, opening the VGT always entails a reduction in the air mass flow, simplifying the control.

- Effect on the intake pressure:

It is clearly illustrated in figure 1.11 how the LPEGR valve has virtually no effect on the control of intake pressure, achieving a successful decoupling of the VGT position, so only this one is influencing the parameter. When HPEGR is employed, there are more interactions between EGR and VGT that involve a stronger coupling.

- Effect on the EGR concentrated at the intake:

In this case, figure 1.12 shows the independency of the VGT position related to intake burnt gas fraction (as representation of EGR) when applying the LPEGR architecture, while HPEGR has a slightly greater dependency on EGR opening, specially at higher values.

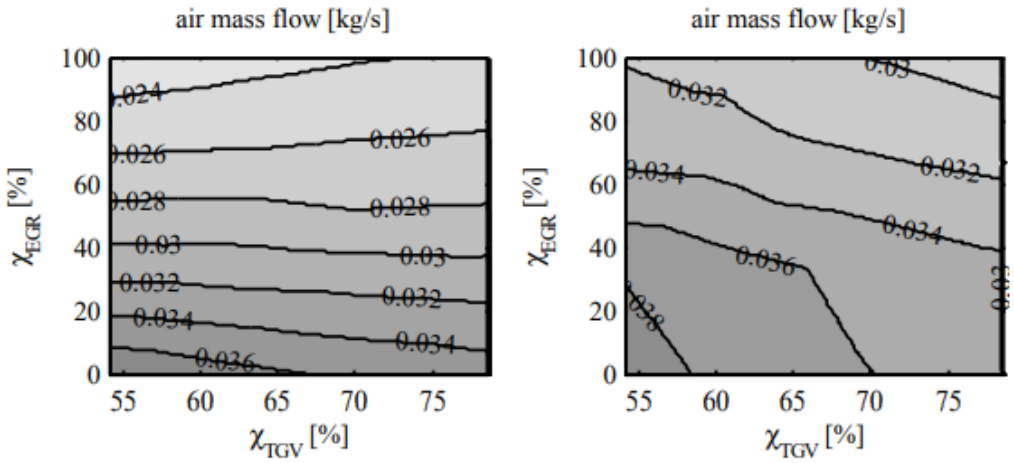

Figure 1.10: VGT and EGR coupling at steady state.
Effect of the VGT position and EGR valve opening for LP and HPEGR systems in the air mass flow of a 2 liters Diesel engine at 2250rpm - 102Nm.
Left: HPEGR system. Right: LPEGR system.
χ represents percentage of opening.

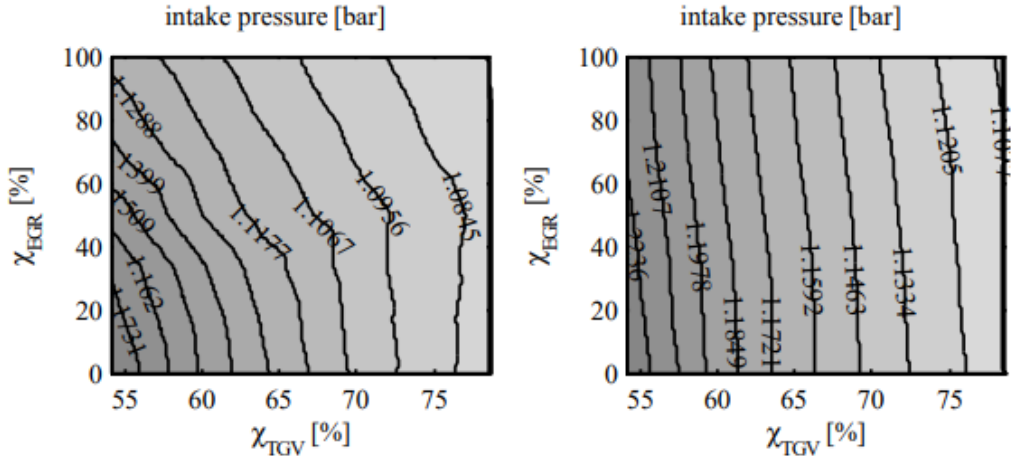

Figure 1.11: VGT and EGR coupling at steady state.
Effect of the VGT position and EGR valve opening for LP and HPEGR systems in the intake pressure of a 2 liters Diesel engine at 2250rpm - 102Nm.
Left: HPEGR system. Right: LPEGR system.
χ represents percentage of opening.

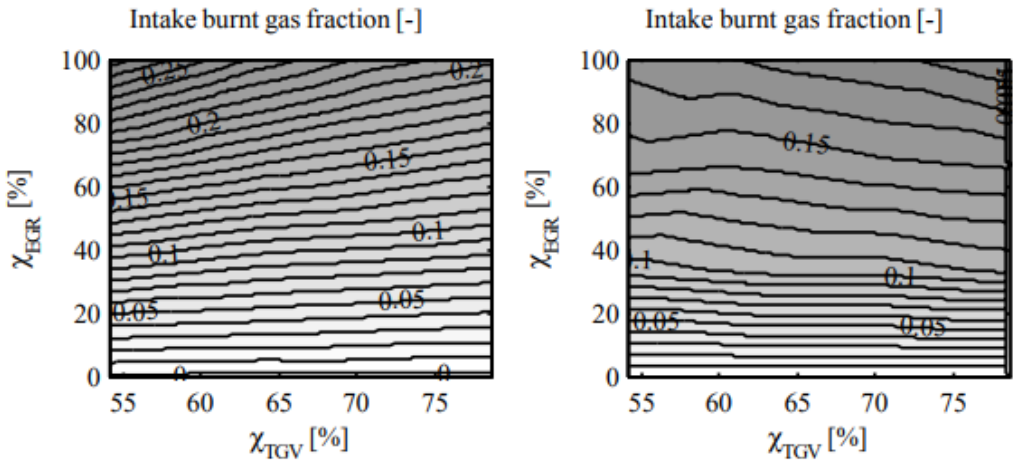

Figure 1.12: VGT and EGR coupling at steady state.
Effect of the VGT position and EGR valve opening for LP and HPEGR systems in the intake burnt gas fraction of a 2 liters Diesel engine at 2250rpm - 102Nm.
Left: HPEGR system. Right: LPEGR system.
χ represents percentage of opening.

The transient response to steps in the VGT or the EGR openings also shows a peculiar behavior, in HPEGR systems, known as non-minimum phase. This behavior consists in showing a trend in one direction at the beginning of the transient, known as “fast dynamics”; while as the process continues, the trend is reversed and is given the name “slow dynamics”.

This phenomena is depicted in figure 1.13, where the non-minimum behaviour concerning the pressure in the intake manifold is found when a HPEGR system faces a step in EGR opening. During the transient response, the flow through the HPEGR line rapidly increases because of the high difference in pressure between intake and exhaust, filling the intake with higher concentrations of EGR, as shown in the third plot of figure 1.13. Then, intake and exhaust pressures are progressively equalized as a consequence of connecting the two manifolds. In this way, the intake pressure increases at the beginning of the transient (fast dynamics), however, since there is a reduction in the energy availability in the turbine due to exhaust gas being deflected to the EGR valve, the turbocharger progressively slows down (slow dynamics) and finally the intake pressure decreases. The second effect is predominant, but slower as a result of the inertia of the turbocharger. When the LPEGR system is used, the EGR does not directly affect the conditions in the intake and exhaust manifolds, so there is hardly any variation in the inlet pressure with the EGR step.

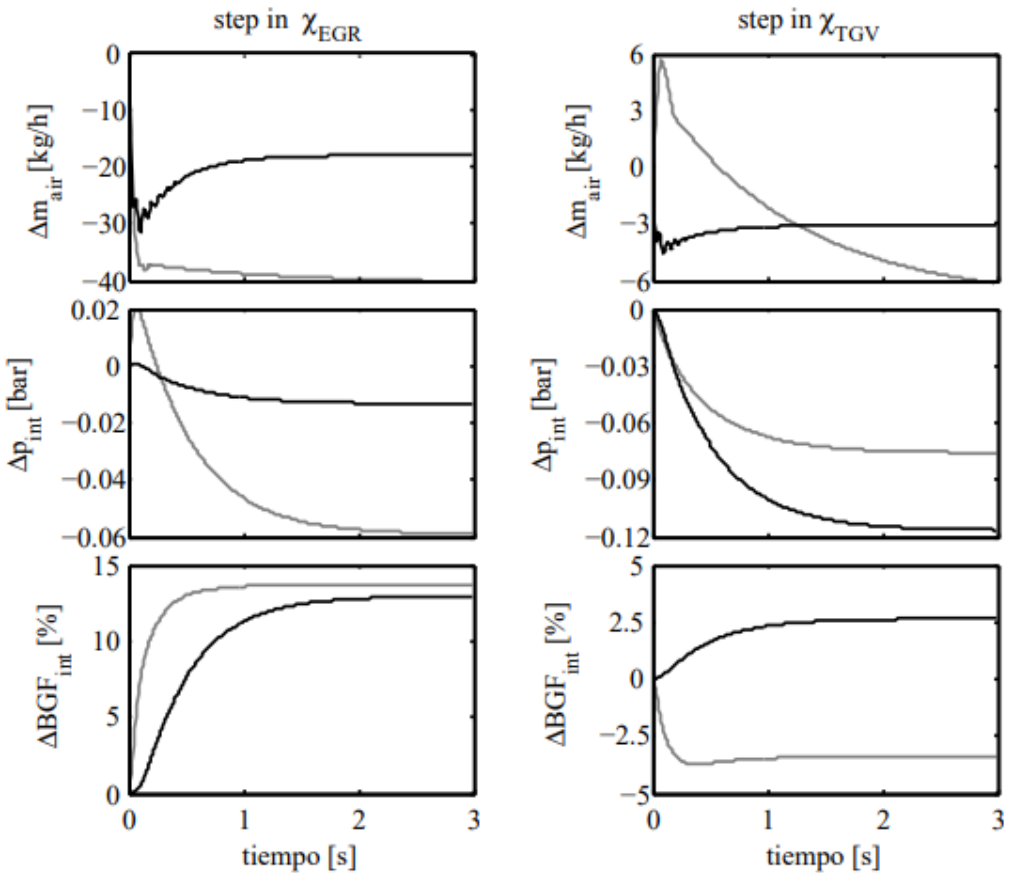

Figure 1.13: Dynamic response in the air mass flow, intake pressure and intake burnt gas fraction for steps in the EGR (left) and VGT (right) openings for a 2 liters Diesel engine at 2250rpm - 102Nm.
——— : LPEGR system. ——— : HPEGR system.

Another example of a non-minimum behavior can be observed in the case of HPEGR systems in front of a VGT step opening, regarding intake air mass flow. By opening the VGT, a pressure drop is experienced inside the exhaust manifold, so the HPEGR flow decreases and fails to fill the intake with exhaust gas, as depicted in the third plot. The absence of EGR is rapidly satisfied with a higher air mass flow (fast dynamics), but the drop in exhaust pressure diminish, once again, the power available at the entrance of the turbine and ends up decelerating the turbocharger (slow dynamics), so the air flow is progressively reduced.

Since all the above behaviors depend on operating factors such as the engine speed, fuel injected and VGT and EGR valve positions, the system control

entails an important calibration effort. In effect, it will be necessary to plan the gain of the controller based on several parameters, thus increasing the size of the cartographies and the time and tests necessary to fill them. It is clear, then, that LPEGR offers a simpler calibration process, but issues with the transport delay of the LPEGR gas, shown in the third plot of figure 1.13, are experienced due to the longer distance from the compressor inlet to the cylinders, in comparison to shorter HPEGR tracks. This must be considered when calibrating the VGT-EGR coupling.

LP-HPEGR combination and potential

All the information about benefits and disadvantages of each EGR architecture discussed in the previous blocks can be summarized in the following table:

HPEGR	LPEGR
High intake temperatures	Low intake temperature
Limited EGR at high load	Limited EGR at low load
Lower flows & pumping losses	Higher flow & pumping losses
Low energy available at the VGT	High energy available at the VGT
Compressor closer to surge line	Compressor far from the surge limit
VGT-EGR coupling	Reduced VGT-EGR coupling
Slower turbocharger response (air, torque)	Faster turbocharger response (air, torque)
Fast EGR response (short path)	Slower EGR rate response (long path)
No compressor reliability issues	Compressor reliability issues
Higher NOx emissions	Lower NOx emissions
Higher soot emissions	Lower soot emissions
Higher HC emissions	Lower HC emissions
Lower fuel consumption	Higher fuel consumption

Table 1: Characteristics of HP & LPEGR architectures

Implementing a system that makes use of a dual-loop EGR seems to be an interesting method to embrace the advantages of HP and LPEGR routes, given the complementarity reviewed in table 1. Considering two different EGR systems working simultaneously makes the air loop control more complex, and extra considerations must be made concerning EGR fraction estimation and control. However, there already are engines that use a combined control of EGR circuits to reach the necessary intake conditions which lead to desired fuel consumption and emissions.

A possible approach, which appears simplistic enough, is applying each circuit only when the engine operative conditions serves the benefits of a specific architecture and keep switching between the two systems to make the best of their characteristics, depending of the requirements. In consequence, HPEGR use would be aimed towards the reduction of HC which would impact positively the fuel consumption. In the same way, LPEGR would be dedicated to lowering NO_x emissions.

Another important contribution of this *Sequential* switching technique is fulfilling the EGR requirements in those areas of the engine map where small pressure differences don't allow a suitable quantity of exhaust gas flow to be recirculated nor air mass flow requirements to be fulfilled. As stated in past blocks, this problem is usually solved by implementing throttle devices, but it may not be necessary when combining both architectures, as one complements the other in this aspect. In this sense, it appears more convenient to use LPEGR at high loads while employing HPEGR at low loads, or at least use HPEGR to complement LPEGR in situations where the air mass flow demands cannot be reached. However, regarding this last declaration, a *Dual or Hybrid* EGR is required, so an exhaustive study of the combination of EGR rates, evaluating LP-HP ratios, must be carried out.

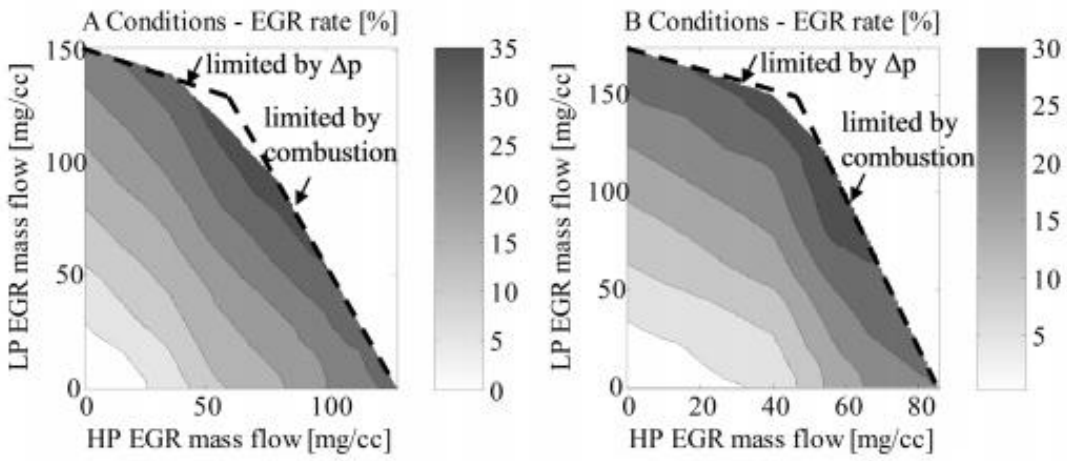

Figure 1.14: EGR rate as a function of the flow through HP & LPEGR Systems at two operating conditions in a 2 liters Diesel engine.
Left: 1970rpm low load. Right: 2250rpm and medium load.

In figure 1.14 the possible combinations of HP and LPEGR flows are shown, thus the EGR rate measured at the different tested conditions versus the mass flows through both EGR circuits is represented. For both operating

conditions the LPEGR rate is limited by the pressure difference between the DPF outlet and the compressor inlet. The LPEGR rates achieved in this study could be increased by using a backpressure valve in the exhaust line, after the EGR extraction, which increases the pressure difference in the LPEGR line. Nevertheless, this solution will increase the engine pumping losses and will have a negative impact in BSFC (Break-Specific Fuel Consumption). On the contrary, the HPEGR rate is limited by an excessive reduction in the intake O_2 concentration, which involves an important increase in opacity and BSFC.

The differences in the intake temperature and O_2 concentration lead to differences in the engine behavior. Results concerning engine performance are shown in figure 1.15. Here the trade-off NO_x-opacity is represented for the previous operating points represented in figure 1.14. The gray scale represents the BSFC, from dark (high BSFC) to light (low BSFC). The results obtained indicate that, for a given EGR rate, the higher the LPEGR contribution, the lower emissions (points are moved towards the origin of coordinates). Also, for both operating conditions, the absolute minimum BSFC is obtained for HPEGR, but provided a NO_x emission limit, the LPEGR system can improve both the BSFC and opacity of the HPEGR layout.

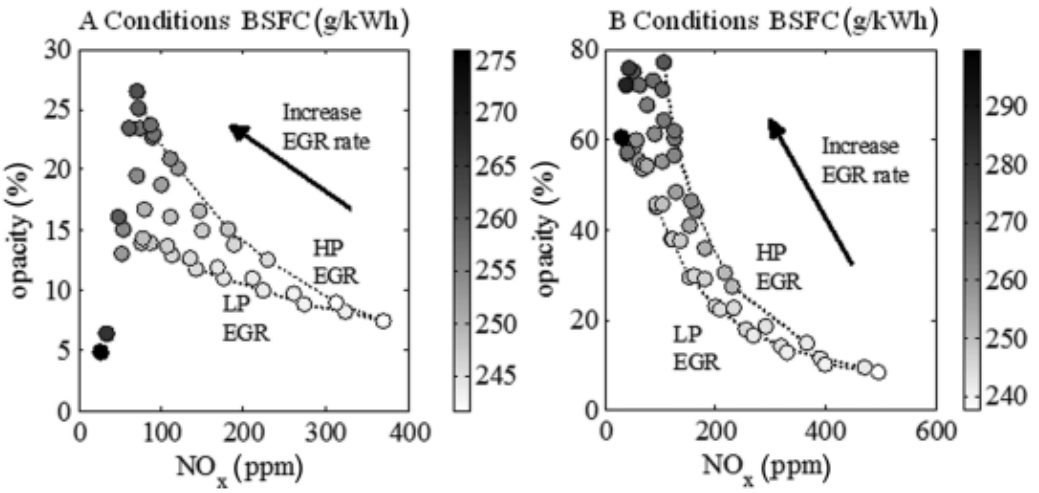

Figure 1.15: Trade-off NO_x-opacity
at 1970rpm low load (left) and 2250rpm medium load (right).
The gray scale represents the BSFC from low (white) to high (black)

An example of *Sequential* EGR and *Dual or Hybrid* EGR can be observe in a previous project carried out at the *CMT – Motores Térmicos*, where a model of another Diesel engine (a 2 liters GT-power model) was created and simulated considering hybrid EGR. The references used to make the Dual EGR simulation

were set equal to the one where only HPEGR was used, which is the original architecture incorporated in the engine, so both simulations share the speed and torque profile, air mass flow and intake pressure setpoints and other calibration maps (smoke limiter, PID values, throttle to fuel mapping, etc.). In the case of the Hybrid EGR simulation, the MAF controller output has been split in two actuations, one for the HPEGR valve and other for the LPEGR valve. Figure 1.16 shows the calibration implemented for such a split. For low loads (throttle) only HPEGR was used and the ratio between LP and HPEGR actuators progressively increased up to 98% LPEGR at loads higher than 30%.

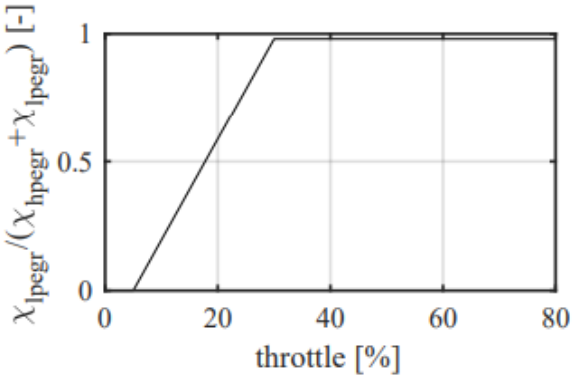

Figure 1.16: Hybrid EGR calibration

The results obtained with such a system are represented in figure 1.17 and 1.18. In particular, figure 1.17 shows a zoom of the last phase of the implemented cycle, where it can be observed that at idling conditions and low load, high EGR rates can be achieved with the Hybrid EGR due to the HPEGR valve opening (black dotted line in the last plot) while at high conditions the required EGR rates are obtained with the LPEGR circuit. Regarding fuel consumption, figure 1.18 shows that, at the end of the cycle, the Hybrid EGR allows a fuel saving of 0.31%.

On the one hand, it can be observed that there is still room for improvement in the first part of the cycle: the calibration shown in figure 1.16 can be improved, some sequential EGR can be implemented. On the other hand, again it should be remembered that those results came from a model with little experimental validation, but trends remain sensible.

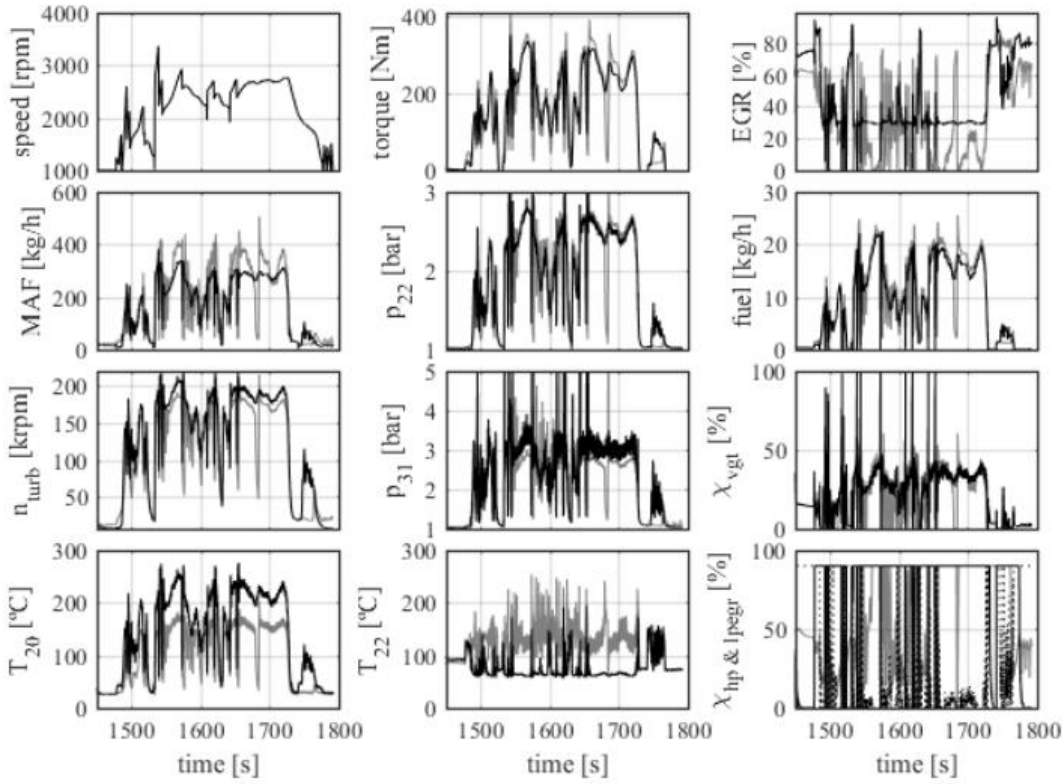

Figure 1.17: Zoom of the last part of the implemented cycle evaluated with Hybrid EGR (black) and HPEGR (grey) in a 2.0 liters Diesel engine by modelling (1D code)

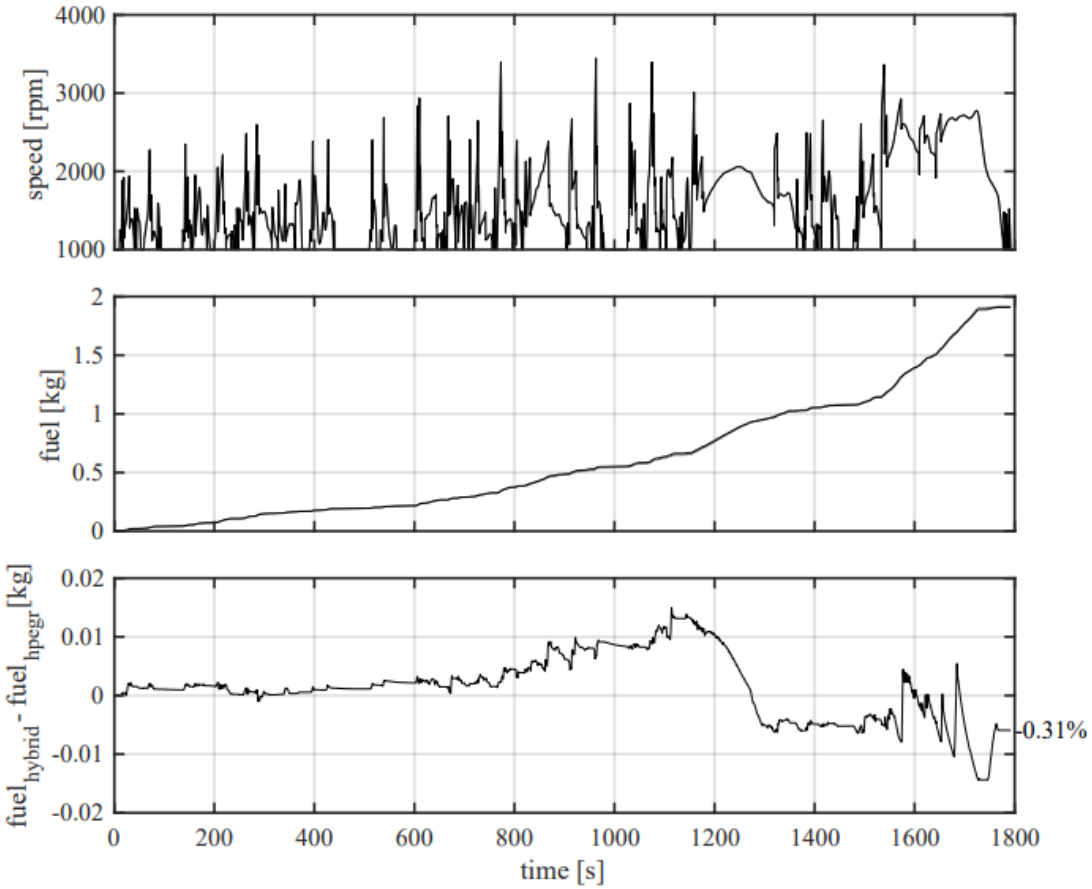

Figure 1.18: Fuel consumption in the implemented cycle evaluated with Hybrid-EGR (black) and HPEGR (grey) in a 2.0 liters Diesel engine by modelling (1D code)

Objectives

Having stated the current situation regarding EGR systems, and given the problem derived from the project at hand, the objectives of this academic work are the following:

General

Identify the potential reduction of both fuel consumption and NO_x emissions in the *PSA* engine DW12RU, when LPEGR & WCAC are incorporated along with Hybrid EGR calibration, pursuing the fulfillment of EURO7 regulations for Light Duty Commercial Vehicles.

Specifics

- Create, calibrate and validate a 0-D data-based engine model for DW12RU, from information received from *Groupe PSA,* which would serve as the estimation tool.

- Design a calibration strategy that would serve as a method of reference for future experimental tests of real in-engine calibration.

- Develop two types of calibrations: a first mainly oriented to fuel consumption reduction, without rising current NO_x emissions; and a second mainly oriented to reduction in NO_x emissions, maintaining fuel consumption.

Methodology

A 0-D data-based model has been developed for DW12RU engine in MathWorks Simulink. The model combines physical and empirical models for the different subsystems and control volumes. An effort has been made to produce a continuous and smooth engine model for control purposes, avoiding any sharpness. Model corresponds to a Euro 6 Diesel turbocharged internal combustion engine (ICE) with VGT and High-Pressure Exhaust Gas Recirculation systems (HPEGR). Model parameters are fitted to a set of experimental data consisting mainly of a set of steady state experiments (“BL7.xls”), provided by *Groupe PSA,* that explore different combinations of

operating conditions and controls. This information can be fairly checked in Chapter 2 (figure 2.3).

Special attention has been paid in incorporate the data set for the turbogroup. Manufacturer maps for the turbocharger have been extrapolated, preventing any malfunction that could be derived for the operating point displacement caused by the change of the applied EGR architecture.

Following its design, the model has been validated on another set of steady state operating points (“BL8.xls”) of the same nature. This experimental data is shown in Chapter 3 (figures 3.3 to 3.12). In order to provide a fair benchmarking, transient validation has been carried out through emulation of the data presented by the contracting party in another file, which contains the registered performance of DW12RU engine in a WLTP cycle class 3, featuring different dynamics. This information is shown in Chapter 3 (figure 3.13)

The developed base model has been modified to include Low-pressure EGR circuit, maintaining the same calibration maps and control dynamics, such as air flow and pressure setpoints. This model has been utilized to make an optimization study based on combined use of LP and HP EGR to reduce fuel consumption and NO_x emissions.

Chapter 2

Model Description and Identification

Contents:

Introduction 26
Intake Manifold 27
Exhaust Manifold 29
Turbocharger 29
Compressor 30
Turbine 31
Mechanical coupling 32
EGR System 32
Coolers (WCAC & EGR heat exchangers) 33
Cylinders 33
Control System 35
Model Identification 35

Introduction

In this section, the 0-D model has been described in detail, including all subcomponents, namely, the turbocharger, intake and exhaust manifold, EGR circuits, Coolers, Cylinder and engine control unit. The model was built in MathWorks Simulink, starting from information given by *Groupe* PSA, as

commented in the Methodology section in Chapter 1. A schematic of the developed engine is presented in figure 2.1, which is followed by the details of each subsystem.

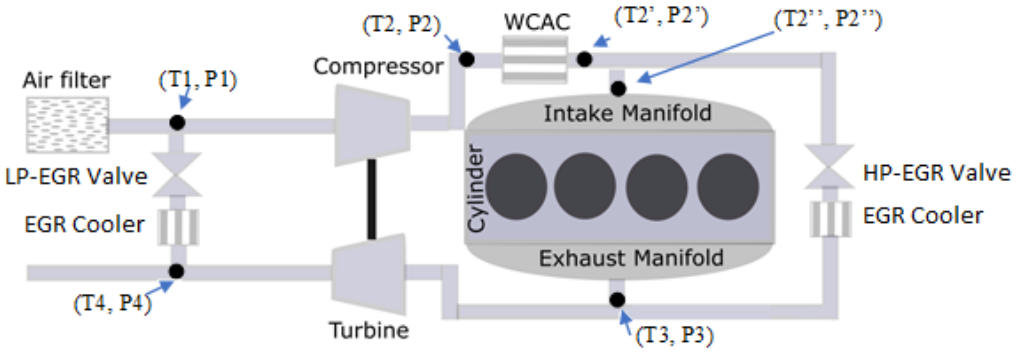

Figure 2.1: Engine Schematic

Note that, pressure drop across WCAC has been neglected and therefore, P2=P2'=P2''

Intake Manifold

Intake manifold has been modelled as an open system, specifically a control volume or *reservoir*, where gases coming from the compressor, through the WCAC, and recirculation gases from the HPEGR loop are mixed together. Cylinders breathe gases from this reservoir. The equilibrium between the incoming and outgoing gases produces a variation on the reservoir pressure, energy and composition. These quantities are solved using the mass and energy conservation principles:

$$\dot{m}(t) = \dot{m_{us}}(t) - \dot{m_{ds}}(t) \qquad eq.1$$

$$\dot{U}(t) = \dot{H_{us}}(t) - \dot{H_{ds}}(t) + \dot{Q}(t) \qquad eq.2$$

With $\dot{m}(t)$ the mass of gas in the reservoir at any given time t, $\dot{U}(t)$ the internal energy of that gas, $\dot{H}(t)$ the enthalpy of incoming and outgoing flows, and $\dot{Q}(t)$ the heat flow exchanged with the environment. Note that the energy conservation principle can be deducted from the definition of the internal energy stored in a control volume:

$$\dot{E_{us}} = \dot{m_{us}}(u_{us} + pv_{us} + 0.5c_{us}^2 + \rho_{us} z_{us})$$

$$\dot{E_{ds}} = \dot{m_{ds}}(u_{ds} + pv_{ds} + 0.5c_{ds}^2 + \rho_{ds} z_{ds})$$

$$\dot{U} = \dot{Q} - \dot{W} + \dot{E_{us}} + \dot{E_{ds}} \qquad eq.3$$

where subscripts ds and us represent downstream and upstream conditions respectively. The work $\dot{W}$ of the manifold along with the kinetic ($0.5c^2$) and potential (ρz) energy of the fluid are neglected. Additionally, heat flow exchange $\dot{Q}$ through the walls of the manifold has not been considered, due to its rapid dynamics and relatively low temperatures compared to other parts of the engine, so intake manifold has been considered an adiabatic system. The gas inside the reservoir can be modelled as an ideal gas:

$$pV = mR\theta \qquad eq.4$$

with R the specific gas constant, obtained by dividing the universal gas constant by the molar mass of the gas, p the pressure, V the manifold volume, m the mass of the gas inside the volume and θ the temperature. Note that the explicit dependency on time has been neglected for simplicity of the nomenclature. The energy associated to the reservoir gas temperature is:

$$U = c_v m\theta \qquad eq.5$$

with c_v as the specific heat of the gas at constant volume. Introducing the ideal gas law in the above expression, the energy results:

$$U = \frac{1}{\gamma - 1} pV \qquad eq.6$$

Note that the relations $R = (c_p - c_v)$ and $\gamma = c_p/c_v$ have been used to reach the above expression. The enthalpy of upstream and downstream flows can be calculated as:

$$\dot{H_{us}} = c_p \dot{m_{us}} \theta_{us} \qquad eq.7$$

$$\dot{H_{ds}} = c_p \dot{m_{ds}} \theta_{ds} \qquad eq.8$$

Variation in temperature can modelled as eq.9 by substituting equations 7 and 8; and the derivative of eq.5 ($\dot{U} = c_v(m\dot{\theta} + \dot{m}\theta)$), in eq.2.

$$\dot{\theta} = \frac{R\theta}{pV}[\dot{m_{us}}(\gamma\theta_{us} - \theta) - \dot{m_{ds}}(\gamma\theta_{ds} - \theta)] \qquad eq.99$$

Introducing equations 7 and 8; and the derivative of eq.6 ($\dot{U} = \frac{1}{\gamma - 1}\dot{p}V$) in the energy conservation relation (eq.2), and neglecting $\dot{Q}(t)$, due to the adiabatic hypothesis previously introduced, the variation of the pressure in the reservoir can be modelled as in eq.10:

$$\dot{p} = \frac{\gamma R}{V}[\dot{m_{us}}\theta_{us} - \dot{m_{ds}}\theta_{ds}] \qquad eq.10$$

Note that the temperature of the downstream flow is the same than that in the intake manifold, as perfect mixing is assumed. Also, the intake manifold model can be simplified by considering it as an isothermal system, because it is rapidly filled of gas and depleted in an instant. In this case, the polytropic coefficient serves $\gamma = 1$, so eq.10 can turn into the equation for the ratio of instantaneous change in pressure, like this:

$$\dot{p} = \frac{R\theta}{V}[\dot{m_{us}} - \dot{m_{ds}}] \qquad eq.10$$

Converting the above equation for the considered ICE, the dynamics of the pressure in the intake manifold are modelled as:

$$\dot{p_{im}} = \frac{R\theta_{im}}{V_{im}}\left[\dot{m_c} + \dot{m_{hpegr}} - \dot{m_{ei}}\right] \qquad eq.11$$

where the subscript im refers to intake manifold, while subscripts c, $hpegr$ and ei refer to compressor (WCAC) outlet, HPEGR duct outlet and engine inlet (cylinders inlet). In addition, eq.9 for temperature dynamics is neglected since temperature dynamics are much slower than pressure dynamics.

Exhaust Manifold

Following the same ideas than intake manifold, the exhaust manifold is modelled as an adiabatic reservoir. The same mass and energy conservation equations used in intake manifold modelling have been applied in this subcomponent. Assigning the appropriate quantities to these equations according to the engine layout, they result in:

$$\dot{p_{em}} = \frac{R\theta_{em}}{V_{em}}\left[\dot{m_{eo}} - \dot{m_{hpegr}} - \dot{m_t}\right] \qquad eq.12$$

where the subscript em refers to exhaust manifold, while subscripts t, $hpegr$ and eo refer to turbine inlet, HPEGR duct inlet and engine out (cylinders outlet), respectively.

Turbocharger

This subcomponent has been modeled with special attention, for it is one with a heavier coupling to EGR. The turbocharger model consists of three

subsystems, that is, a compressor, turbine and a mechanical coupling. These subsystems are described in the following subsections.

Compressor

The purpose of the compressor is to increase the amount of gas flow that enters the engine, by increasing the pressure inside the intake manifold and forcing an amount of air, coming through air filter, to reduce its density, so a higher quantity of mass can flow through. The power employed to achieve this is transformed from the mechanical energy produced by the turbine.

For a given pressure ratio Π_c, between upstream and downstream, and a corrected rotational speed ω_{tc}, the compressor propels a known mass flow, which can be modelled as using the maps provided by the supplier ($\dot{m}_c = \dot{m}_c(\omega_{tc}, \Pi_c)$). Compressor efficiency is estimated using the same approach, obtaining it from the compressor map by checking the pressure ratio and corrected speed ($\eta_c = \eta_c(\omega_{tc}, \Pi_c)$). The maps used were provided by *PSA*.

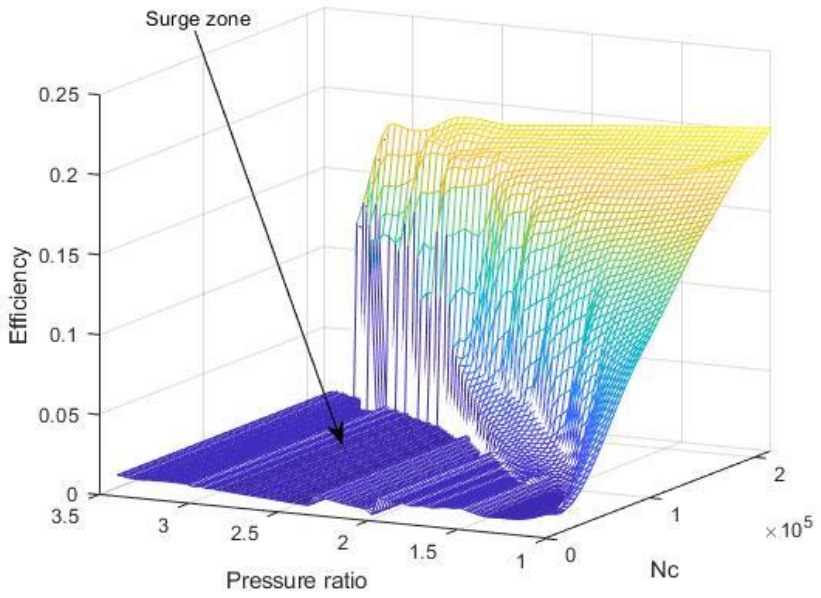

Figure 2.2: Clipping of the surge zone for the compressor efficiency map

Compressor surge is a phenomenon that happens when the fluid-dynamics are too unstable to sustain the regular flow inside the compressor. It is generally produced by an excessive pressure ratio, causing the blades to stall. This should be avoided at all cost. The surge limit on the compressor plays a critical role in the model, since it represents a discontinuity on the compressor behavior and has

been modelled by clipping the provided maps in the surge zone, as shown in figure 2.2.

The compression can be considered an adiabatic process with an isentropic efficiency η_c. Therefore, the power required to produce the compression process is:

$$P_c = \frac{1}{\eta_c}\frac{\gamma R}{\gamma-1}\dot{m}_c\theta_{bc}\left[\Pi_c^{\frac{\gamma-1}{\gamma}} - 1\right] \qquad \textit{eq.13}$$

where subscripts c and bc represent compressor and before compressor respectively. The temperature increase of the fluid has been modelled according to an adiabatic compression as:

$$\theta_{ac} = \left[\Pi_c^{\frac{\gamma-1}{\gamma}} - 1\right]\frac{\theta_{bc}}{\eta_c} + \theta_{bc} \qquad \textit{eq.14}$$

where subscript ac represents conditions after the compressor.

Turbine

This subsystem complements the compressor, taking profit of the thermal energy of the exhaust gases by expanding them, in order to obtain the necessary torque to carry out the compression process. It transmits the gathered mechanical energy through a coupling shaft that links both subsystems. Turbines in the present model have movable stator blades (VGT), in order to produce a variable pressure-drop and control the boost pressure.

As in the case of the compressor, manufacturer's maps have been used to model the flow through turbine and efficiency of turbine as a function of pressure ratio Π_t, turbo speed ω_{tc} and VGT position $\mathbf{xvgt}$.

$$\dot{m}_t = \dot{m}_t(\omega_{tc}, \Pi_t, xvgt)$$

$$\eta_t = \eta_t(\omega_{tc}, \Pi_t, xvgt)$$

The thermodynamic process in the turbine is considered an adiabatic expansion with an isentropic efficiency η_t . The power that this process develop in the shaft is:

$$P_t = \eta_t\,\frac{\gamma R}{\gamma-1}\dot{m}_t\theta_{bt}\left[1 - \Pi_t^{\frac{1-\gamma}{\gamma}}\right] \qquad \textit{eq.15}$$

Since the expansion is an adiabatic process, the temperature of the gas at the turbine outlet is:

$$\theta_{at} = \theta_{bt} - \eta_t \theta_{bt} \left[1 - \Pi_t^{\frac{1-\gamma}{\gamma}} \right] \qquad eq.16$$

Note that the turbine inlet temperature is assumed the same than the exhaust manifold temperature θ_{bt}. It might be an unrealistic hypothesis due to the heat losses at the exhaust manifold and pipelines connecting to the turbine, but this effect can be included in the exhaust temperature model (see Cylinders).

Mechanical coupling

The compressor and turbine are mechanically linked through a shaft. There is a balance between the power developed by the turbine P_t and the power that the compression process requires P_c. Depending on the sign of this balance and the moment of inertia I_{tc} of the rotating mass, the turbocharger will accelerate, decelerate or hold speed. The speed of this set follows the ODE:

$$\dot{\omega}_{tc} = \left[\frac{P_t - P_c}{I_{tc}\omega_{tc}} \right] \qquad eq.17$$

EGR System

Both the EGR systems (LP and HP) have been modelled as the nozzle model like maps with fixed efficiency exchangers. Flow across the EGR valves is modelled as a function of engine operating point (speed and fuel injected) and pressure ratio PI across the valves. In the case of HPEGR the pressure ratio is across intake/exhaust manifold and in case of LPEGR the pressure ratio is before compressor/after turbine. A generic model is in eq.19.

$$Qegr = c_d(n, mf) \times Qegr_0\left(PI, u_{egr}\right) \qquad eq.18$$

where, $Qegr$ is the flow across the EGR pipe, c_d is discharge coefficient that is mapped with the operating conditions and $Qegr_0$ is a reference EGR flow obtained from the nozzle equation as a function of the pressure ratio and the EGR valve opening calibrated from the measurements.

Coolers (WCAC & EGR heat exchangers)

Intake gas coming from the compressor goes through an intercooler (WCAC) to increase density before going to the intake port. EGR ducts also include a cooler for performance reasons. These elements are represented with a simple model of a heat exchanger. Coolers from EGR valves transfer thermal energy from the gas to another fluid–engine coolant. The gas flow inside the intake intercooler (WCAC) exchanges heat with water, for this is the custom intercooler setup in the testing facility. Note that the coolers have been designed as fixed efficiency η_{ic} exchangers for preliminary studies.

$$\theta_{ds} = [1 - \eta_{ic}]\theta_{us} + \eta_{ic}\,\theta_{cf} \qquad eq.19$$

where θ_{cf} is the temperature of the cooling fluid. Note this expression is also valid for air-to-air heat exchangers.

Cylinders

The events taking part at the cylinder are complex and highly nonlinear, involving chemical, thermodynamic and fluid-dynamic processes at every single engine cycle. Physically detailed models with crank angle resolution follow all these processes throughout the duration of a cycle and can make a good approximation to the cylinder dynamics. However, they need a substantial amount of information to be calibrated and have high computational cost. From a control point of view, and if no intra-cycle control is to be performed, the cylinder is a system whose dynamics extend to few milliseconds, then much faster than the typical dynamics during a driving cycle, so mean value models are generally an adequate estimation. In this line, the cylinder model developed for this project is a quasi-steady model to be used for the engine optimization, not requiring extra consideration for in-cylinder dynamics.

This model avoids complex equations that would limit its control capabilities, given that the in-cylinder processes are not the control target. To be specific, the cylinder is represented as map-based models, whose principal inputs are the engine speed and fueling rate. Other inputs, such as mass of air flow into the cylinder and temperature of the gases entering the cylinder are also values introduced to provide corrections. This approximation is simplistic but captures the important phenomenon related to flow and temperatures on the engine

outputs, like torque and emissions. Therefore, the relevant engine outputs have been modelled as in eq. 21.

$$y = y_0(n, mf) + \Delta y_{MAF}(n, mf, \Delta MAF) + \Delta y_{T_{im}}(n, mf, \Delta T) \quad eq.20$$

where y is the model output containing torque, NO_x and exhaust temperature ($y = [torque,\ NO_x,\ T_{em}]$), the map $y_0(n, mf)$ represents a baseline for the outputs depending on the operating conditions defined as engine speed (n) and fuelling rate (m_f). Those baselines are corrected with terms (Δy_{MAF} and $\Delta y_{T_{im}}$), depending on how actual air mass flow deviates from the reference air mass flow at a given operating condition (ΔMAF) and how actual intake temperature deviates from the reference intake temperature at a given operating condition (ΔT). Note that the terms Δy_{MAF} and $\Delta y_{T_{im}}$ are necessary to consider the following phenomena:

- The impact of modifying the air-loop calibration: Modifying the air mass flow set point should have an impact on combustion that may affect torque, NO_x and exhaust temperature. This term cannot be taken into account if only the term $\mathrm{y_0(n, mf)}$ is considered
- The impact of LPEGR: As pointed out in chapter 1, the main difference between HP and LPEGR is that the intake temperature is strongly reduced with LPEGR. That leads to direct effects on combustion but also important impact on the air loop due to the higher amount of gases that can be admitted by the engine for a given intake pressure. Considering the term $\mathrm{\Delta y_{T_{im}}}$ allows to take into account the impact of the lower intake temperature with LPEGR on combustion.
- The impact of engine (air loop) dynamics: During transient conditions, the air mass flow suffers excursions from the reference value, the term $\mathrm{\Delta y_{MAF}}$ allows to correct the engine outputs when the air mass flow is different from the reference one.

The map $\mathrm{\Delta y_{MAF}(n, mf, \Delta MAF)}$ has been obtained from experimental information from *Groupe PSA*, including EGR sweeps at different operating conditions. As the given file only contains information for 10 operating conditions, 10 nodes have been created and the model takes the impact from the nearest node to the actual operating conditions of the engine.

A similar approach has been used for the correcting map $\Delta y_{T_{im}}(n, mf, \Delta T)$, which takes into account the effect of the intake temperature that, at the end, is the main impact of replacing HPEGR by LPEGR. In this case, since no information was available for the DW12 engine, previous experimental

information from *CMT - Motores Térmicos* regarding LPEGR in a DW10 was used.

Despite this model entails an important simplification, it is a reasonable hypothesis since the characteristic time of the air path is several orders of magnitude higher than in-cylinder phenomena. In addition, the previous simplification hypothesis allow the model to operate around 20 times faster than real-time in a standard PC (Intel® Core™ i7-8550U CPU @1.80GHz, 8.00GB RAM), i.e. takes 67 seconds simulate a complete WLTC of 1800 seconds, which allows to run a wide set of simulations for exploring the impact of different parameters.

Control System

State of the art control architecture has been used to control VGT rack and EGR valve positions with a set of PID controller that track set points for MAP and MAF obtained from a calibration. These set points are mapped by engine speed and fueling rate; and interpolated during operation. Initial guess for VGT and EGR position has also been used as feedforward to speed up the engine response during transients. The dynamics of controller can be seen in figure 2.4.

The steady state model has also been upgraded to run transient cycles, provided by *Groupe PSA,* on demanded speed and torque profiles for WLTP cycle. In this case fueling rate is controlled in a close loop based on the error between demanded and actual torque using a PID. An initial guess for fueling rate is provided by a map derived from measurements as a feedforward.

Model Identification

The model has been identified using the steady state measurement data provided by *Groupe PSA* `(BL7.xlsx)`. In figure 2.3, the error in the engine states (MAF and MAP) and engine outputs (Torque and NO_x emissions) are presented. In particular, the y_{error} is defined as:

$$y_{error} = \frac{y_{meas} - y_{model}}{y_{meas}}$$

Priority has been given to MAF estimation since the Torque, NOx emissions are MAF dependent, as explained in Cylinders section (see equation 21).

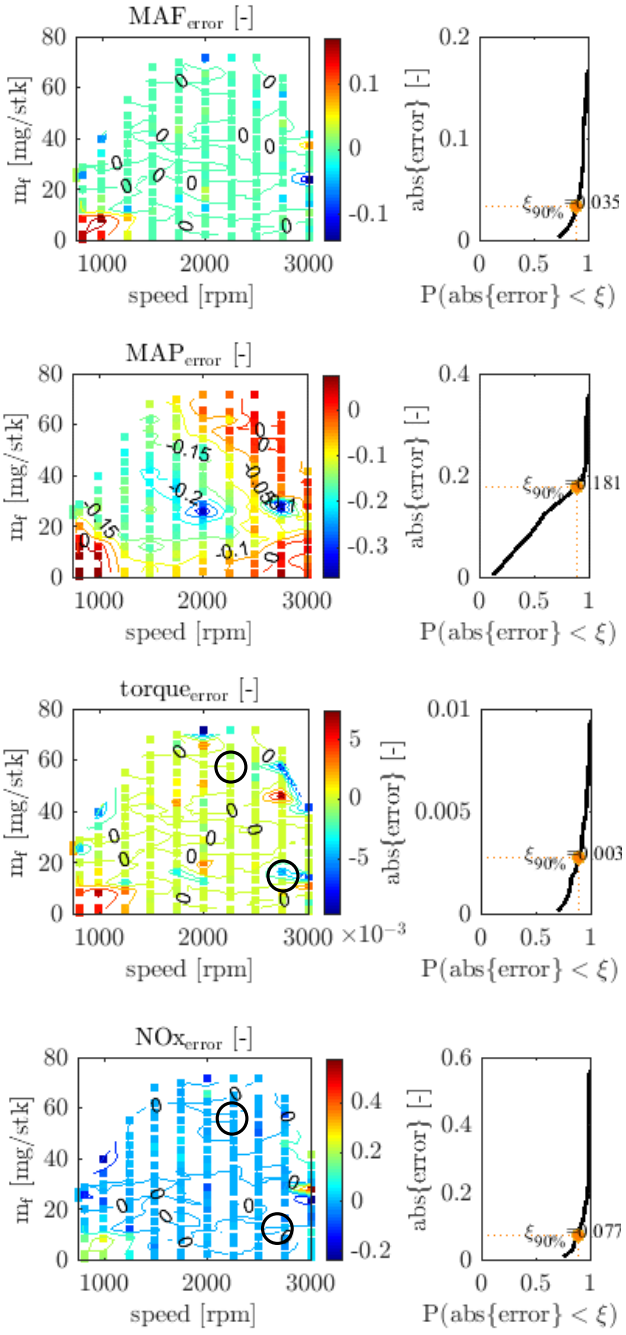

Figure 2.3: Error (y_{error}) between model and experimental results for air mass flow (MAF_{error}), intake pressure (MAP_{error}), torque ($torque_{error}$) and NOx (NOx_{error})

$\xi_{90\%}$ represents a level such that the 90% of all the simulated points have an error (y_{error}) below this level. It can be noticed in figure 2.3, that the error in MAF and MAP for 90% of the operating points is less than 3.5% and 18%,

respectively. The subsequent error in torque and NO_x is below 1% and 7%, respectively, for the 90% of simulated points.

Two typical simulations for engine operating points (2250rpm, 60mg/stk) and (2750rpm, 15mg/stk) are shown in figure 2.4Figure . The dynamics in MAF and MAP are controlled by *uvgt* and *uhpegr* valve positions that evolve to reach the desired set points. It can be noticed that, for the first case (2250rpm-60mg/stk), the controller is not able to reach desired value of MAP even though the VGT is fully closed. In this sense, this is a limitation of the model while the controller is performing suitably. Note that since the model outputs are not dependent on the intake pressure, the measured values of torque and NO_x are captured by the model. In the operating conditions shown at the right (2750rpm-15mg/stk) the model can reach the air mass flow and intake pressure set points, then leading to a satisfying matching with the experimental results in the output variables (NOx and torque).

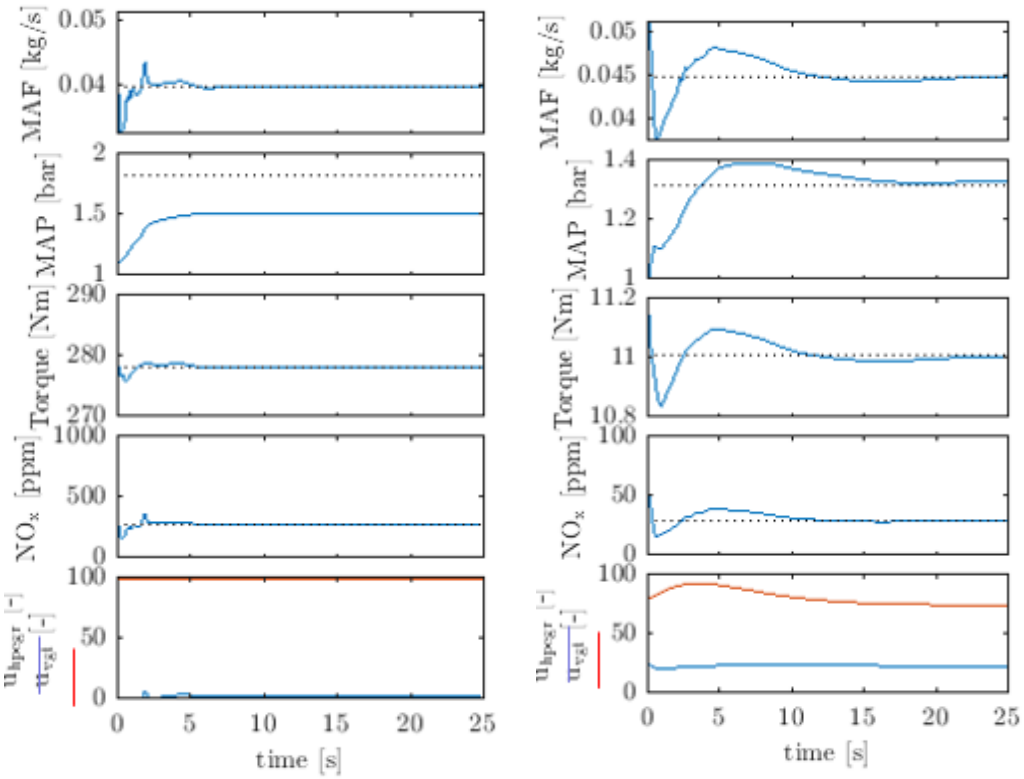

Figure 2.4: Evolution of the model variables during a simulation for two operating conditions: 2250rpm, 60mg/stk (left) and 2750rpm, 15mg/stk (right)

Chapter 3

EGR circuit evaluation: Analysis of simulated performance

Contents:

Validation for Base Engine Model (only HP-EGR circuit) 40

Steady State behavior (HPEGR) 43

Transient Model behavior (HPEGR) 50

Exploration of Low-Pressure Model (only LP-EGR circuit) 51

Steady State behavior (LPEGR) 52

Transient behavior (LPEGR) 60

Testing for Hybrid Model ($\boldsymbol{NO_{x_{Opt}}}$, $\boldsymbol{M_{Opt}}$) 63

Steady State engine behavior with optimal calibration maps 69

Transient engine behavior with optimal calibration maps 76

Introduction

In this chapter, simulations run during the study are discussed, along with the results. The identified model described in the previous Chapter has been prepared to run steady state (imposed engine speed and fueling rate) and transient simulations (imposed engine speed and desired torque), and presented as follows:

- Validation: In this section, the model validation results have been presented for two types of simulations.

- Steady State simulation: this engine model has been run for a set of engine operating points provided by *Groupe PSA* in "BL8.xls" file. In these simulations, the MAF and intake pressure set points from the *BL8* map have been used instead of those of the *BL7,* used for model identification, and differences in the obtained torque and NO_x emissions are evaluated. This analysis is useful to check the accuracy of the combustion model.
- Transient simulations: The transient engine model has been used to run WLTP cycle (following speed and torque demands) provided by *Groupe PSA*. The results from simulations for fuel consumption, NO_x emissions and temperature downstream the turbine have been compared with the measured data from the provided file (figure 3.13).

- Pure LPEGR potential: After engine model validation, the LPEGR circuit was added to the base model and following simulations were made. The results of these simulations are discussed in the second section of this chapter.

  - Steady State simulations: these were carried out by inactivating the HPEGR circuit and implementing and activating LPEGR. A control variable called $LP-HPEGR_{ratio}$ allows the model to switch between both EGR architectures. This switch could be set to one in order to activate LPEGR and zero to activate HPEGR; and any rational values between zero and one could be set to achieve a desired combination of LP and HP EGR.

$$LP-HPEGR_{ratio}=\frac{m_{lpegr}}{m_{lpegr}+m_{hpegr}}$$

    In this phase, the variable $LP-HPEGR_{ratio}$ has been set to 1 (LPEGR) and the results obtained have been compared with those with the HPEGR circuit (keeping the same engine calibration).
  - Transient simulations: The transient model was used to run WLTP cycle with $LP-HPEGR_{ratio}$ equal to 1 and results have been compared with the transient simulations with HPEGR keeping the same engine calibration.

- Hybrid EGR potential: After the addition of LPEGR circuit, parametric study was conducted to explore all the possible range of $LP-HPEGR_{ratio}$, between 0 and 1. This study was done to generate steady state optimal calibration maps for $(LP-HPEGR_{ratio})^{steadyOpt}$ and MAF set point

($MAF_{sp}^{steadyOpt}$). Two different calibrations were generated from this study: one focused on efficiency (but keeping the NO_x emissions from the HPEGR simulations) and one focused on minimizing NO_x (but keeping the efficiency of the HPEGR simulations). The potential of the hybrid system with the obtained calibrations was compared with the results of the HPEGR system in:

- Steady State: engine simulations for the same engine operating points used during validation.
- Transient simulations: initially the optimal calibration maps ($(LP-HPEGR_{ratio})^{steadyOpt}$; $(MAF_{sp}^{steadyOpt})$) obtained in steady state conditions were used to run WLTP cycle as a transient study. Even though some improvements in engine performance was observed, they were not as optimal as those suggested at steady state. Therefore, another iteration of optimization was performed by also including cycle dynamics during the optimisation process. In this case, the calibration obtained in steady state ($MAF_{sp}^{steadyOpt}$) has been used as a starting point and has been linearly corrected with engine speed and fuelling rate. The next equation shows the structure of the final air mass flow set point:

$$MAF_{sp}^{Opt} = MAF_{sp}^{steadyOpt} \cdot (b_0 + b_1 \cdot n + b_2 \cdot m_f)$$

  The optimal map MAF_{sp}^{Opt} has been obtained by exploring around the $MAF_{sp}^{steadyOpt}$, with b_0, b_1 and b_2 coefficients to be calibrated in the following range:

```
b0= [0.95 1.05]; b1= [-0.025 +0.025]; b2= [-0.025 +0.025];
```

  To optimize the calibration, the WLTP is run with different combinations of coefficients b_0, b_1 and b_2. Then, the obtained results are analysed in order to choose the coefficient combinations that minimizes fuel consumption or NO_x emissions.

Validation for Base Engine Model (only HP-EGR circuit)

The most important parameters, which were used to identify the model, have been presented in this section for engine validation. Note that while the model was calibrated with "BL7.xls", the model is evaluated in this section with "BL8.xls", in order to check its expected accuracy. It can be noticed in figure 3.1 that the error in MAF and MAP for 90% of the operating points is

below 4.5% and 20%, respectively. The subsequent error in torque and NO_x is lower than 1% and 9%, respectively.

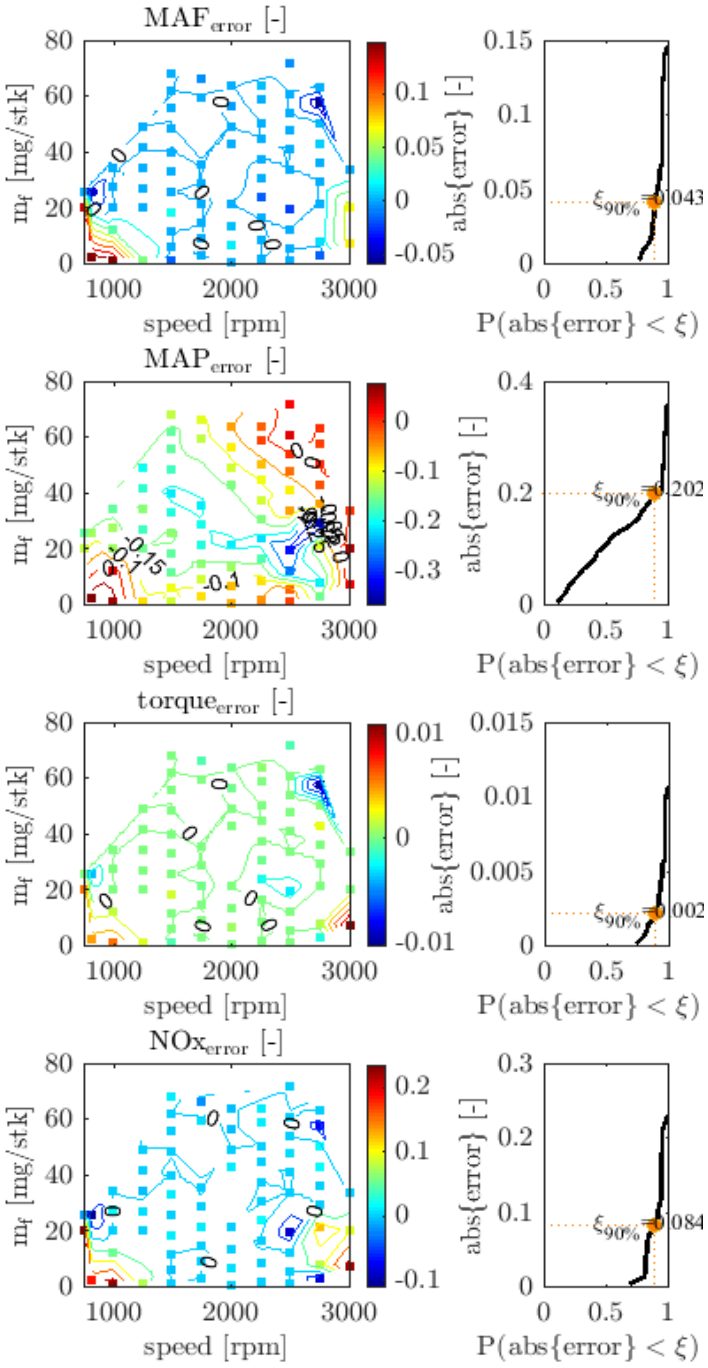

Figure 3.1: Error (y_{error}) between model and experimental results for air mass flow (MAF_{error}), intake pressure (MAP_{error}), torque ($torque_{error}$) and NOx (NOx_{error}) for `"BL8.xls"` conditions.

Figure 3.5 shows the errors obtained in a validation process with a 1-D high fidelity engine model (GT power) in a turbocharged diesel engine with similar displacement with LP and HPEGR.

One can observe that error levels are in the same order of magnitude than those obtained with the current simplified model.

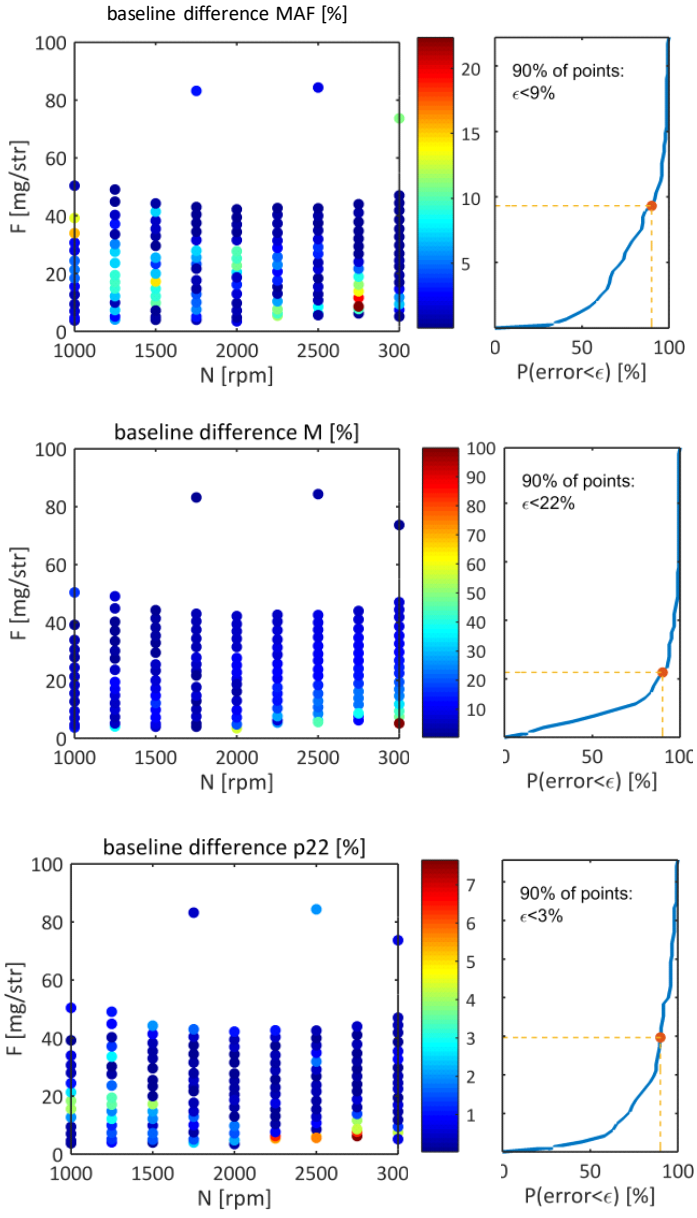

Figure 3.2: Error (y_{error}) between model and experimental results for air mass flow (MAF_{error}), intake pressure (MAP_{error}) and torque ($torque_{error}$), with a detailed 1D code in a turbocharged Diesel engine with LP and HPEGR circuits and 2 liters displacement.

In the following subsection, one on one comparison of important engine parameters (MAF, T2, T2', T2'', P2'', T3, T4, NO_x and Qegr) from experimental and simulated results for 45 engine operating conditions are presented. For the sake of clarity, all the figures share the same structure: the top plot to the left presents the measured results, right top plot shows the results from simulations, the bottom left plot shows the y_{error} between the measured and simulations and bottom right plot presents error limit for 90% of the operating points.

Steady State behavior (HPEGR)

Figure 3.3 shows the comparison between measured and modelled air mass flow (MAF).

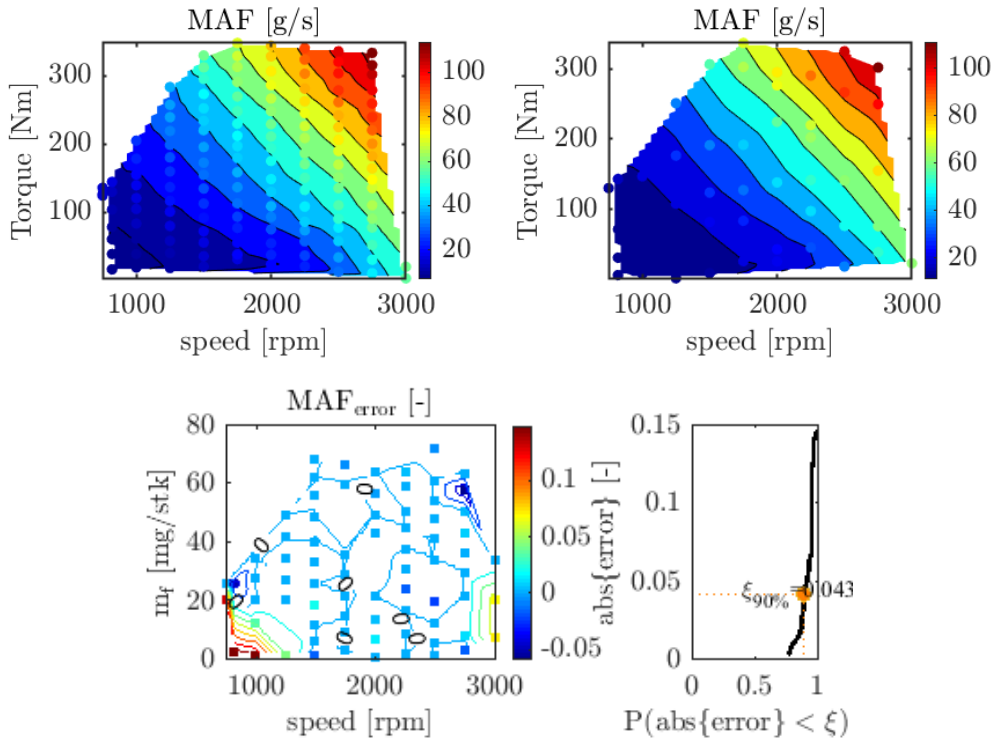

Figure 3.3: Measured air mass flow, modelled air mass flow, error in the MAF and error distribution (same reading order).

Error in MAF estimation is less than 5% for 90% of the considered operating points.

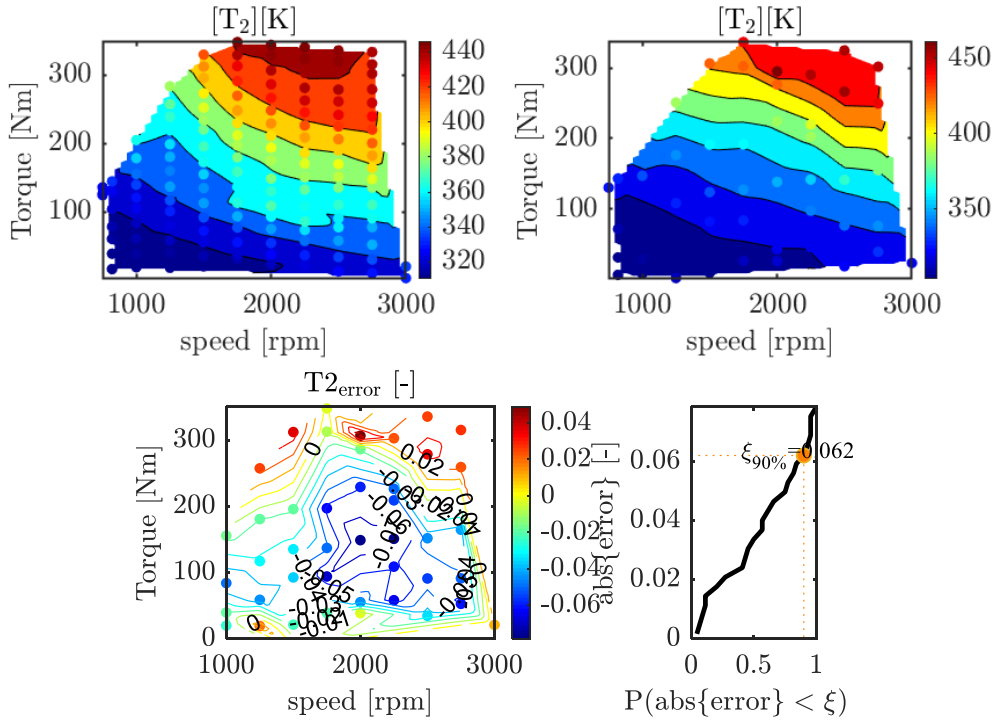

Figure 3.4: Measured compressor outlet temperature,
modelled compressor outlet temperature,
error map and error distribution (same reading order).

Results in figure 3.4 show that the error in temperature after the compressor (T2) is about 6% for 90% of the operating points. This temperature is critical for the model because addition of LPEGR circuit to the system would directly affect T2, which is critical in compressor blade design. Note that even with the HPEGR system at full load, temperatures above 440K (167ºC) are achieved.

Considering a fixed WCAC efficiency of 85%. Figure 3.5 shows a linear reduction from T2 to T2' (temperature after WCAC). This reduction in temperature leads to a reduction in y_{error} that for T2' is less than 2%.

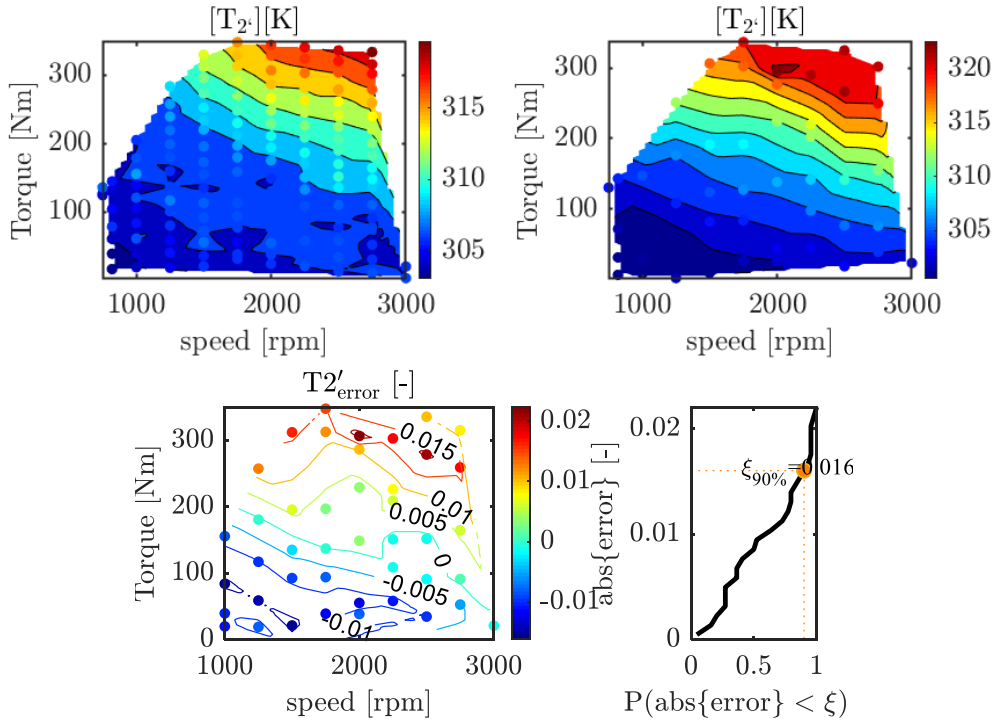

Figure 3.5: Measured WCAC outlet temperature, modelled WCAC outlet temperature, error map and error distribution (same reading order).

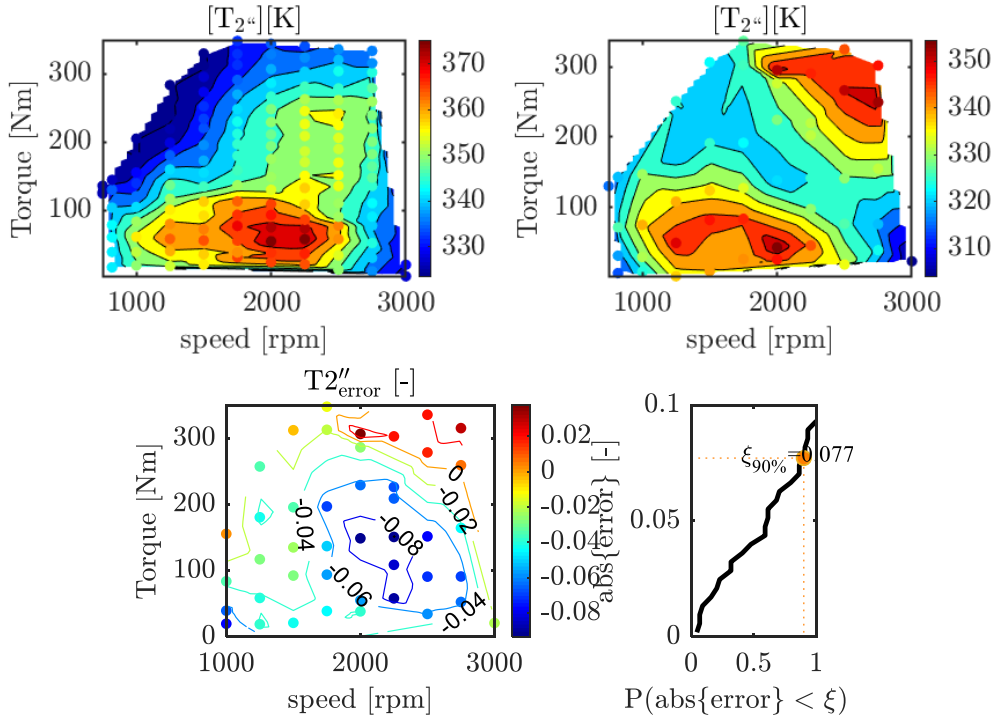

Figure 3.6: Measured intake temperature, modelled intake temperature, error map and error distribution (same reading order).

Figure 3.6 shows how the measured temperature in the manifold is maximum in the area of expected maximum EGR rates. The model behaves accordingly as can be checked looking at Qegr in figure 3.12. The error in temperature in the manifold is high at 2250rpm and medium load. This could be because of the higher error in intake pressure in the same region of the engine map, shown in figure 3.7. Hence, differences in the modelled intake pressure with regards to the measured values may lead to differences in the EGR rate, that finally involve differences in the intake temperature. In any case the error is bounded below 8%.

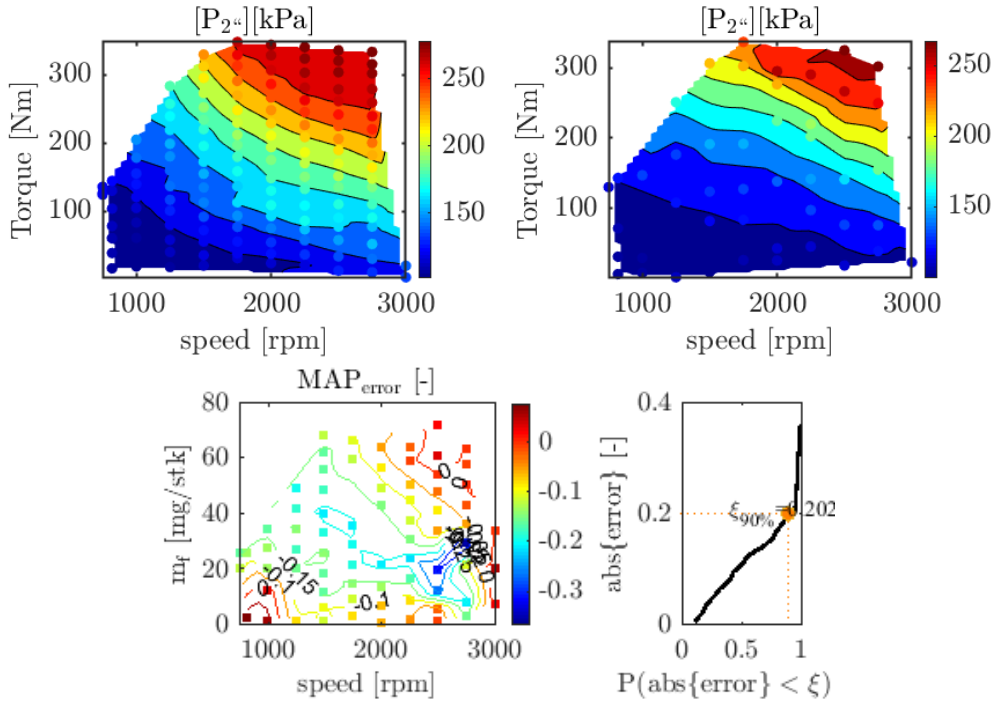

Figure 3.7: Measured intake pressure, modelled intake pressure, error map and error distribution (same reading order).

The error in the intake manifold pressure (P2'') is 20% for 90% of the operating points as shown in Figure, which is in similar order of the results from model identification. Similar uncertainty can be observed in exhaust pressure as depicted in figure 3.8.

Regarding the exhaust temperature conditions, figure 3.9 and figure 3.10 show the temperatures at the turbine inlet (T3) and outlet (T4), respectively.

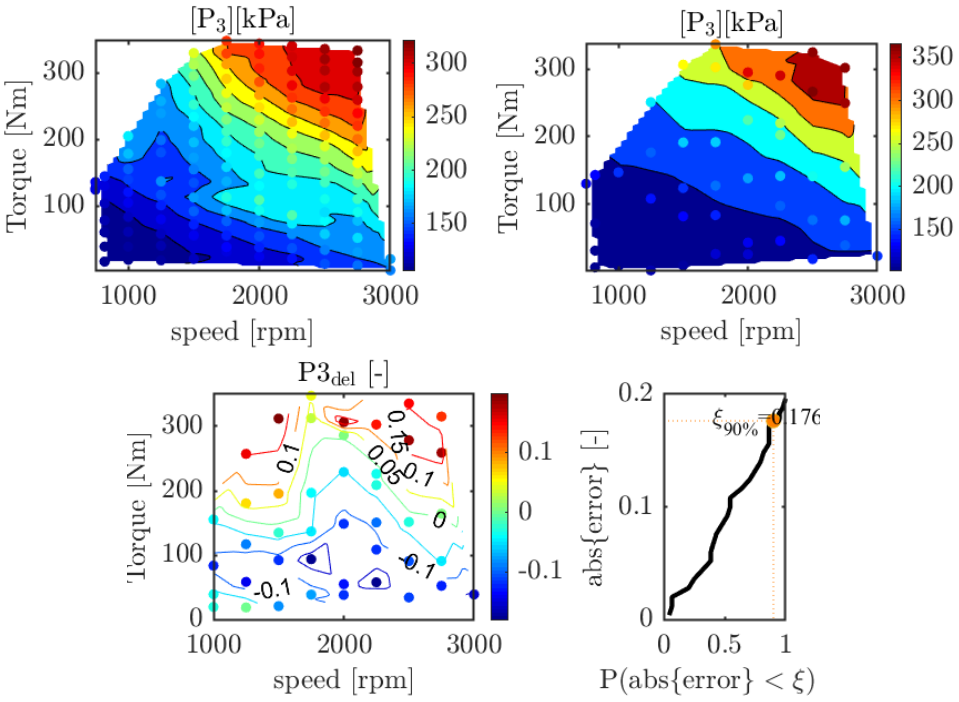

Figure 3.8: Measured exhaust pressure, modelled exhaust pressure, error map and error distribution (same reading order).

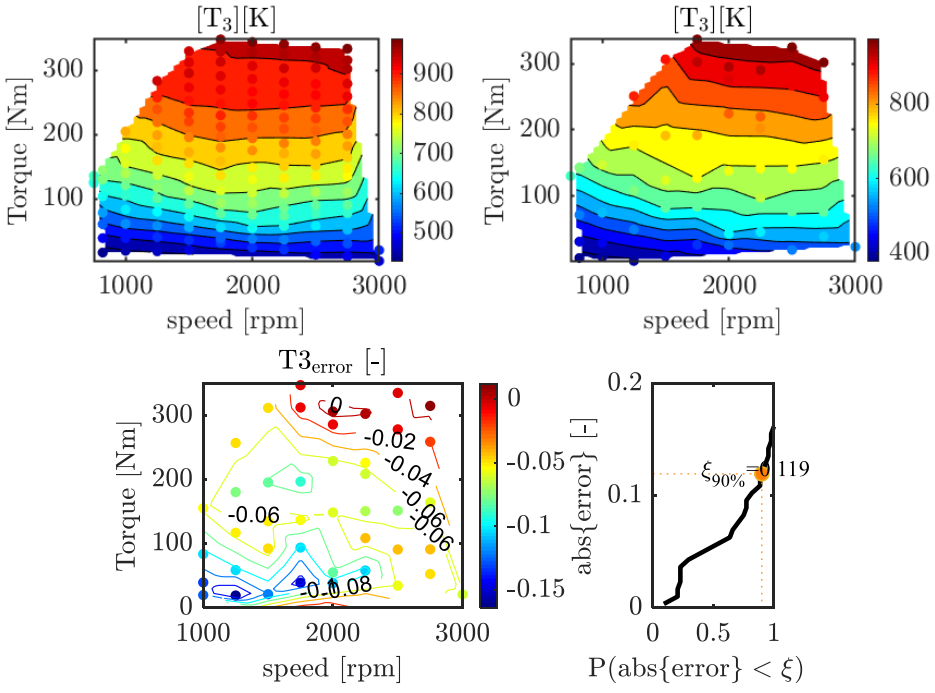

Figure 3.9: Measured exhaust manifold temperature, modelled exhaust manifold temperature, error map and error distribution (same reading order).

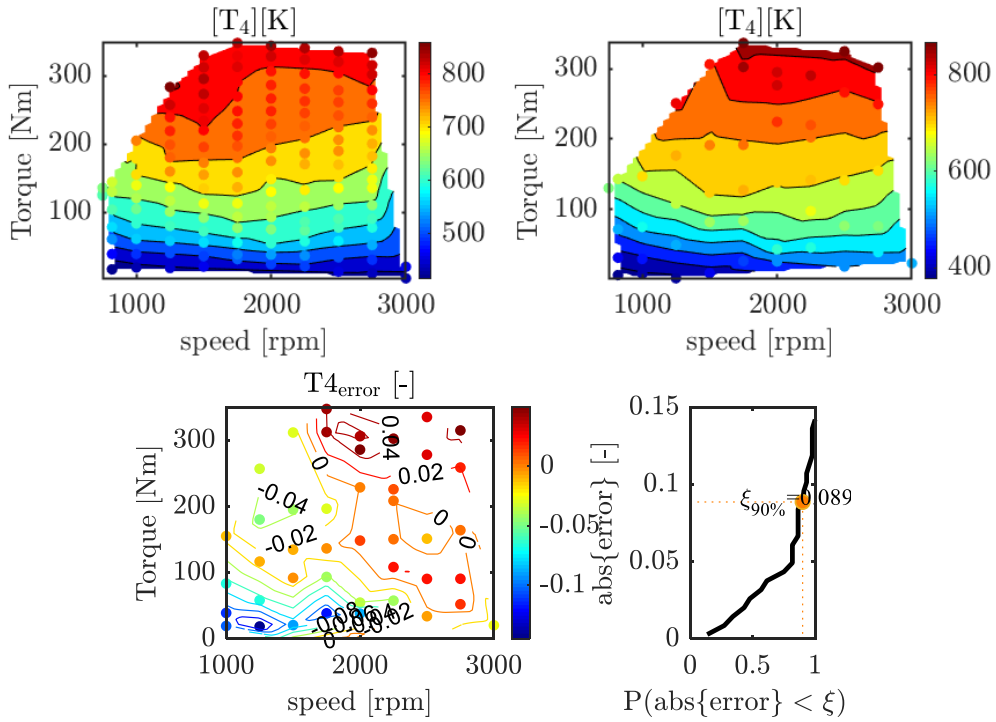

Figure 3.10: Measured turbine outlet temperature, modelled turbine outlet temperature, error map and error distribution (same reading order).

The error in magnitude of both turbine inlet and outlet temperatures is in the order of 10%.

NO_x emissions predicted by the model are in the similar range than measurements and error is less than 9% as shown in figure 3.11Figure. It can be noticed that, even though the NO_x emissions are modelled as a function of temperature in the intake manifold and the MAF, the influence of MAF on NO_x emissions is dominant which is evident in the figures for error in NO_x (figure 3.11) and MAF (figure 3.3), where the distribution of error is similar for both.

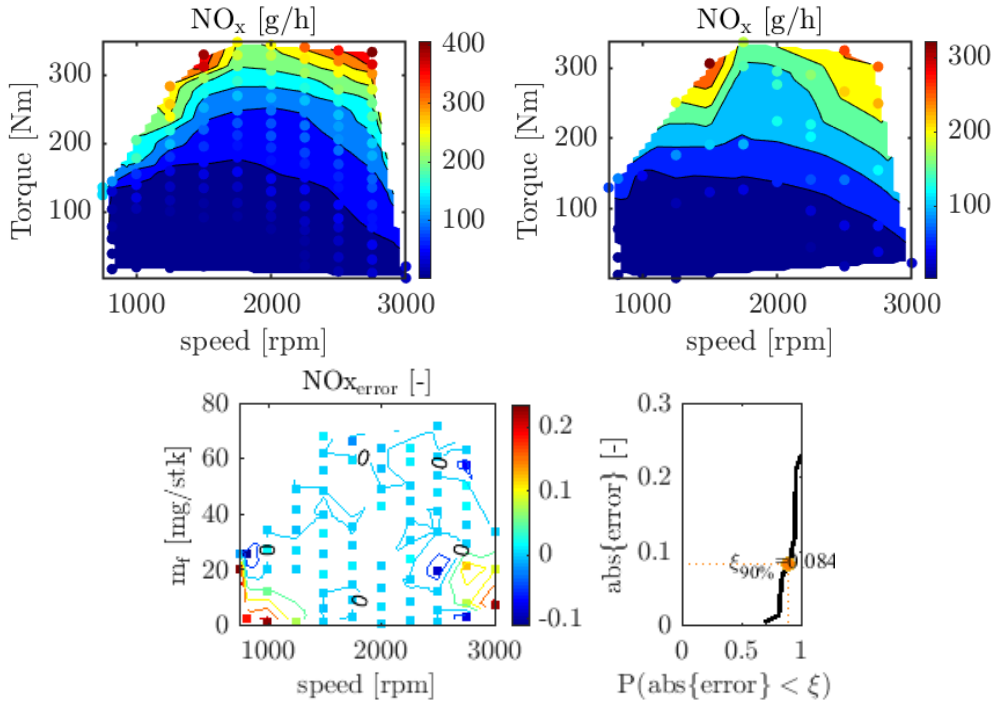

Figure 3.11: Measured NO_x emissions, modelled NO_x emissions, error map and error distribution (same reading order).

To conclude, the estimated EGR flow predicted from the model (figure 3.12) shows that, for the current engine, EGR is applied in the complete engine area, but mainly at high loads and low engine speeds, where small or even negligible EGR rates appear, maybe because limitations in the air loop. No available EGR rates or flows are available in files `"BLx.xls"`.

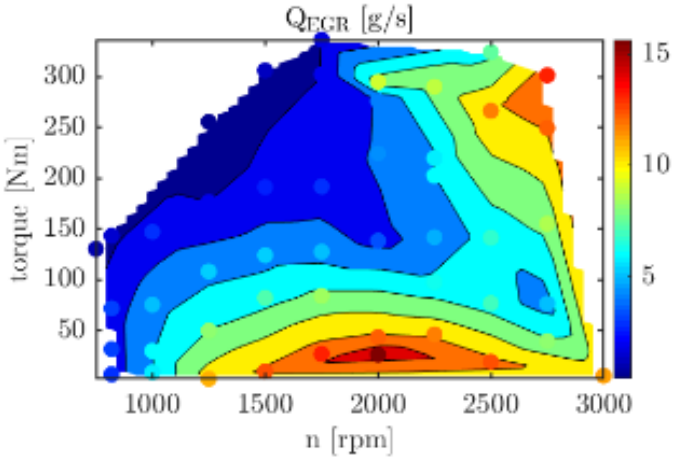

Figure 3.12: Modelled EGR flow with the baseline configuration (HPEGR).

Transient Model behavior (HPEGR)

The model has been used to run the transient simulation (WLTP cycle, Class 3). A couple of files where provided by *Groupe PSA*. One of them contains the engine speed and torque profiles, while the other has been used to extract the information about measured NO_x emissions, fueling rate, temperature after turbine (T4) and other cycle related information.

Figure 3.13 shows a comparison of measured and simulated results for the WLTP with the reference configuration, i.e. HPEGR. The first plot shows instantaneous measured vs the simulated MAF, where a satisfying correlation can be observed. Second plot shows instantaneous fueling rate and cumulative fuel consumption. In the same way, the third plot describes instantaneous and cumulative NO_x emissions, for measurements and simulation results. Finally, the fourth plot shows the error in cumulative NO_x emissions and fuel consumption for the cycle.

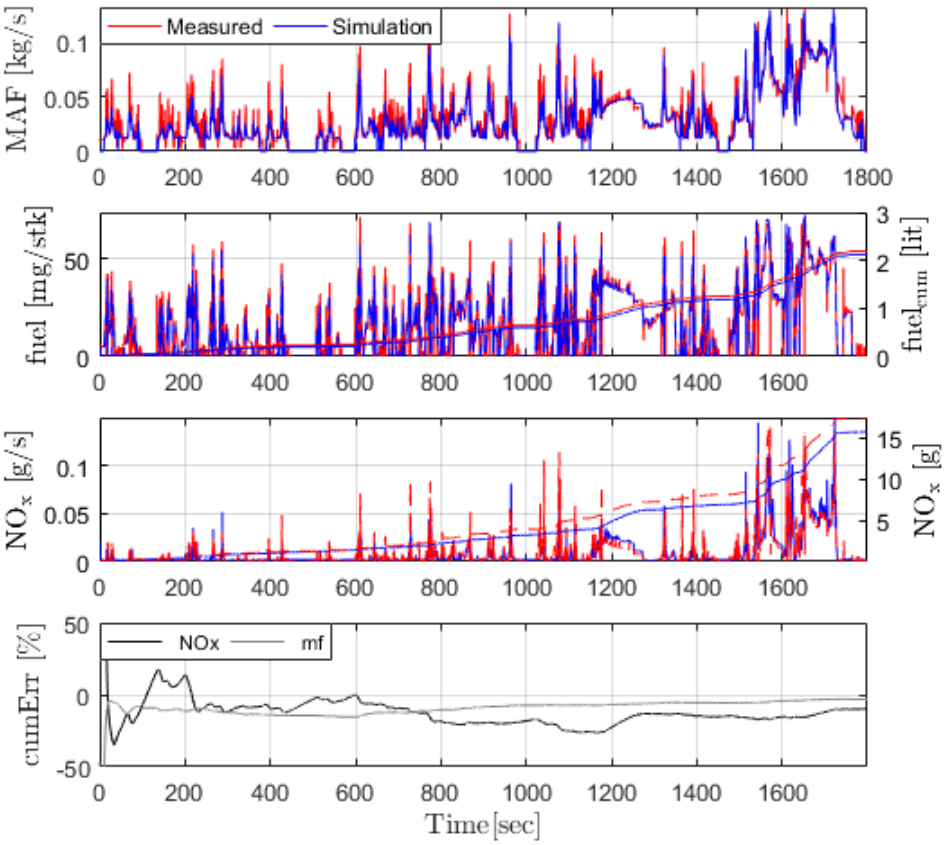

Figure 3.13: Comparison of the main model variables during the WLTP with the initial configuration (HPEGR).

The results are shown in figure 3.14, where the bar graphs represent the cumulative fuel consumption and NO_x emissions for the sake of readability.

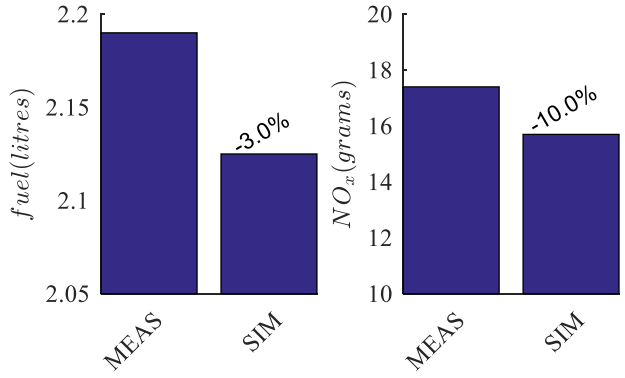

Figure 3.14: Comparison between obtained fuel consumption and NO_x emissions in the WLTP with the model and experiments for the HPEGR configuration.

At the end of the cycle, the differences between measured and modelled results are 3% and 10% in fuel consumption and NO_x emissions, respectively. It should be noted that errors in steady state points were bounded to 1% for torque and 8% for NO_x, so the accuracy levels obtained in the WLTP are in the order of magnitude of what can be considered certain with such a simple model.

Even though the model is simple and data based, it is able to capture to some extent the most important engine charaterstics for the study, i.e. engine fuel consumption and NO_x emissions.

Exploration of Low-Pressure Model (only LP-EGR circuit)

In the following subsections one on one comparison of important engine parameters (MAF, T2, T2', T2'', P2'', T3, T4, NOx and Qegr) for engine model with HPEGR and model with only LPEGR at 45 engine operating conditions is carried out. The followed structure is similar to that in previous section: the top plot to left presents the simulated results with HPEGR, right top plots are the results from simulations with LPEGR and the bottom plot shows the $y1_{error}$, which is the percentage variation between HP and LPEGR results defined as:

$$y1_{error} = \frac{y_{lpegr} - y_{hpegr}}{y_{hpegr}}$$

Steady State behavior (LPEGR)

Figure 3.15 shows the MAF obtained in simulations with HPEGR and LPEGR. The MAF increases to about 40% at low loads when using only LPEGR, compared to HPEGR. This is as expected because of the low EGR flow entering the compressor, consequence of the pressure ratio (PI in equation 19) being very close to one, due to low pressure in the exhaust line, and, as the compressor is receiving higher power from the turbine, more gas is to be supplied to the intake and only air is available for compression. At high loads, difference in MAF is zero, since the engine with the LPEGR circuit is able to reach the MAF demand, due to higher pressure-difference between intake and exhaust.

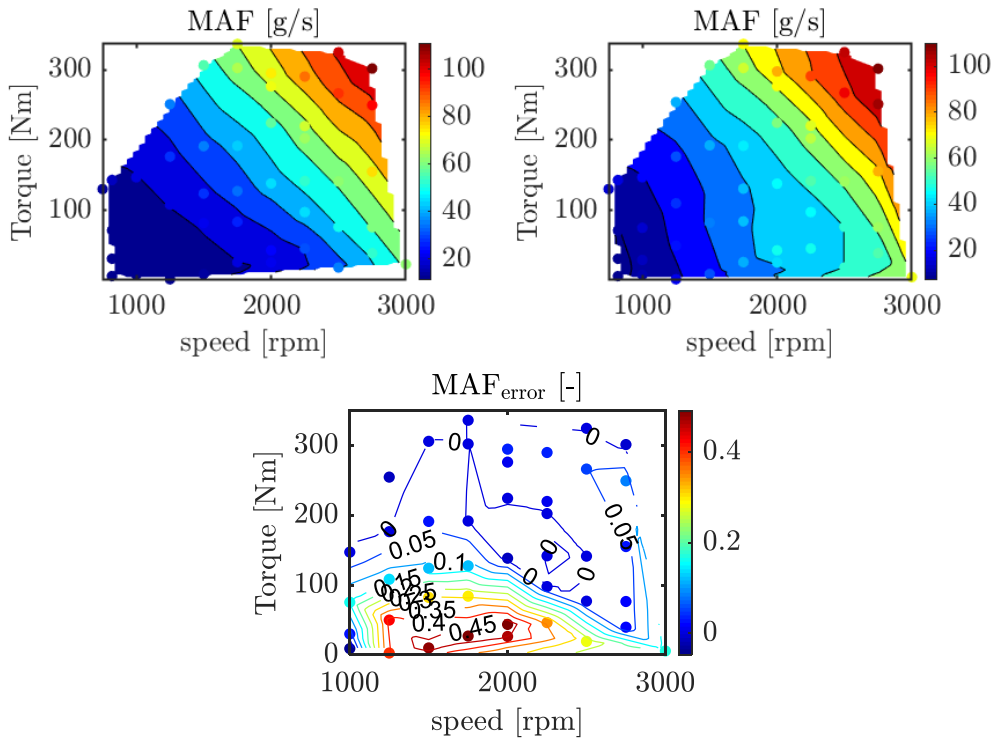

Figure 3.15: Comparison between air mass flow (MAF) obtained with the HPEGR system, LPEGR system and their difference (same reading order).

One of the main differences between HPEGR and LPEGR is the temperatures achieved in the compressor. Figure 3.16 shows this result. The temperatures after the compressor increases in case of LPEGR, which is as expected due to EGR introduction at the compressor inlet. Of course, this impact is especially evident at high loads, due to the amplification effect of the compression ratio. The maximum temperatures reach about 500K with the current calibration. These temperatures may pose a threat to the compressor reliability and hence a limit based on engine load may be applied in the LPEGR activation.

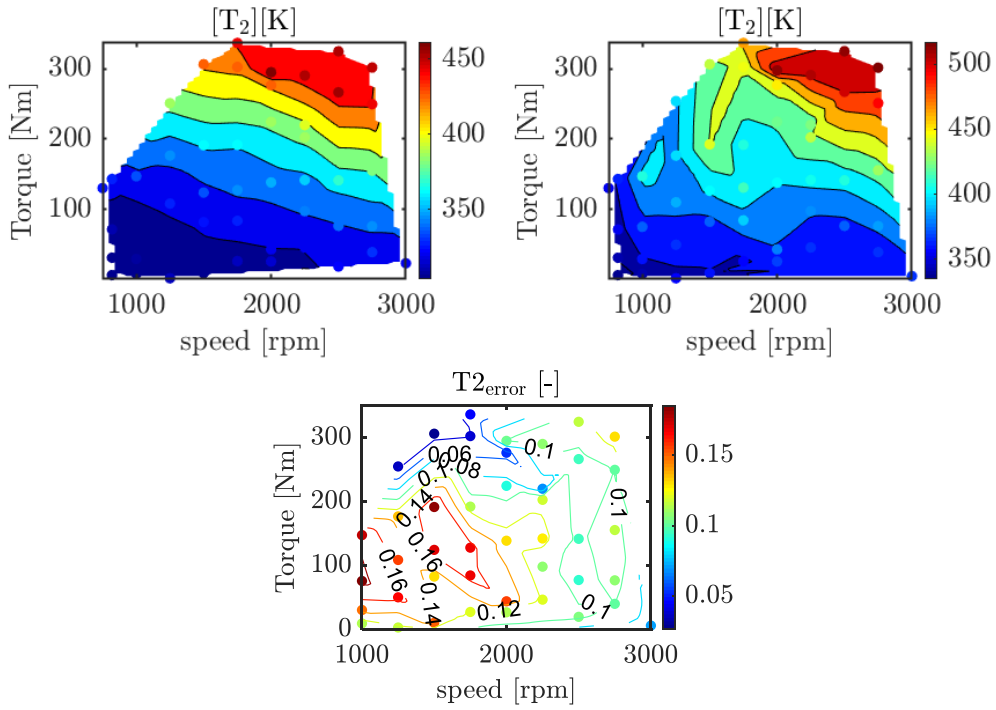

Figure 3.16: Comparison between compressor outlet temperature obtained with the HPEGR system, LPEGR system and their difference (same reading order).

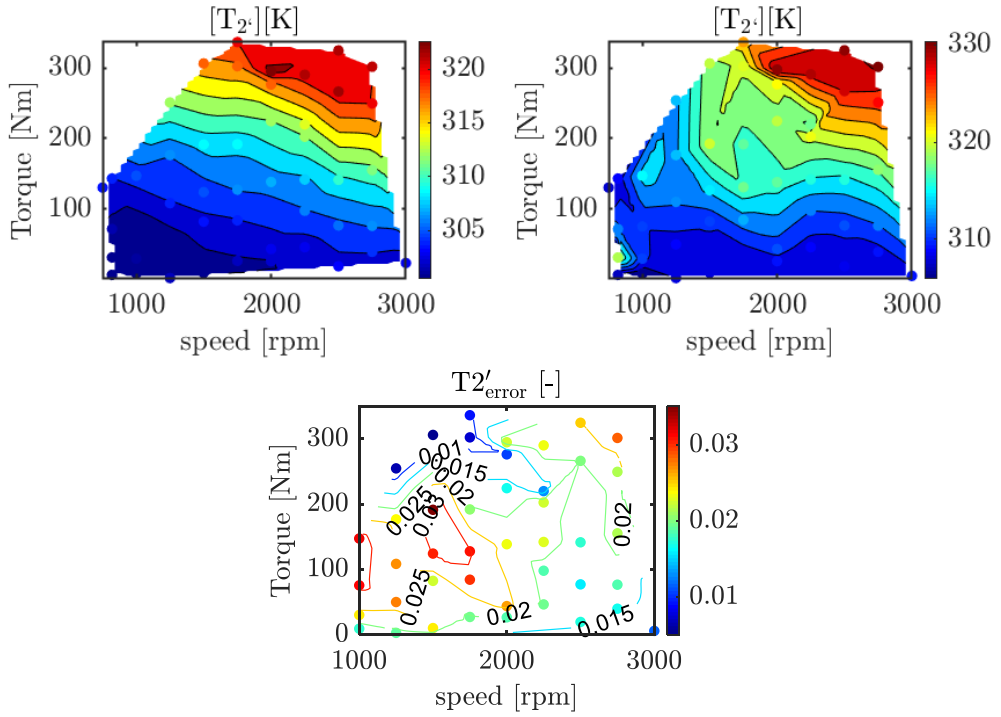

Figure 3.17: Comparison between WCAC outlet temperature obtained with the HPEGR system, LPEGR system and difference (same reading order).

Even though the temperatures in LPEGR shows very high values in T2, figure 3.17 shows how the reduction in the temperature due to WCAC subsystem reduces differences between HPEGR and LPEGR systems. In any case, the temperature is still 2-3 % higher than HPEGR model. At this point a limitation of the model becomes apparent since the efficiency of the WCAC has been assumed to be constant (0,85) but the impact of the exhaust gas going through the complete intake line (including WCAC) when LPEGR is used should have some negative impact on the efficiency due to progressive fouling.

As no further interactions exist in the intake line with LPEGR architecture, the intake manifold temperature is substantially lower than that achieved with HPEGR as observed in figure Figure3.18. Approximately 6% reduction can be expected in the entire engine map, but this difference can reach 10% at low loads, where maximum EGR rates appear. It should be noted that engine performance strongly depends on intake temperature, and particularly in the case of the considered model, the main impact of LPEGR on combustion is through this temperature.

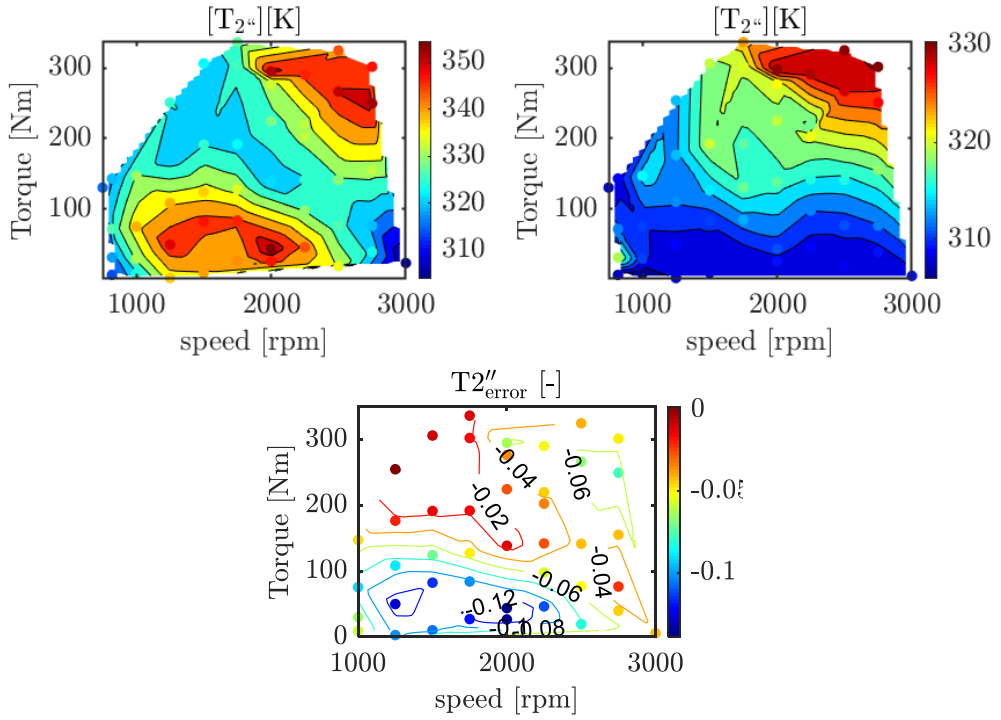

Figure 3.18: Comparison between intake temperature obtained with the HPEGR system, LPEGR system and difference (same reading order).

Another modification due to the LPEGR system is that all the gas (EGR and air) flows through the turbine and the compressor with this configuration. In this sense, there is more energy available to feed the turbine, but also higher power demands by the compressor. This balance is usually positive for the LPEGR, since increasing the flow moves the operating points of compressor and turbine towards higher efficiencies, as shown in figure 3.19 (see also Chapter 1). While the intake pressure set point is the same with both configurations, the higher energy availability in the turbine with the LPEGR system makes intake pressure be above the set point with completely open VGT. Those differences disappear at high loads and speeds, since the EGR rate is not that high and the operating points in the compressor map are more centered in the high efficiency area. This can be observed in the figure 3.19, where a single high-load operating point remains in the same position for both systems.

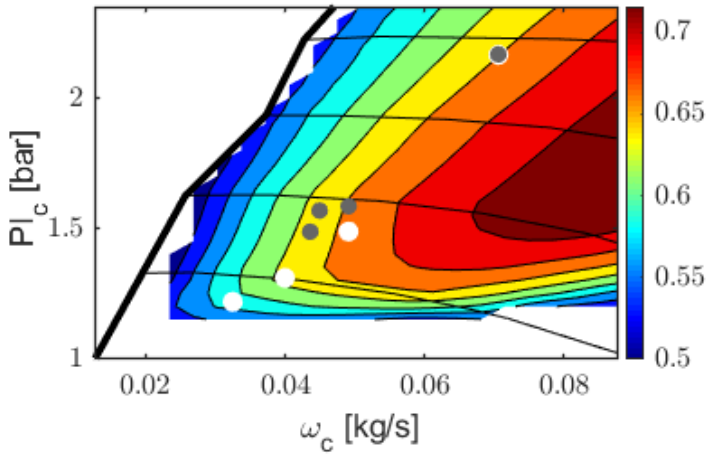

Figure 3.19: Compressor operating point displacement
over different compressor efficiencies (color scale),
by replacing HPEGR (white) for LPEGR (grey),
at the same four Steady State operative engine conditions

In this sense, figure 3.20 shows the differences obtained in intake pressure. It can be observed how, for low load and speed, higher intake pressures are obtained with the LPEGR system.

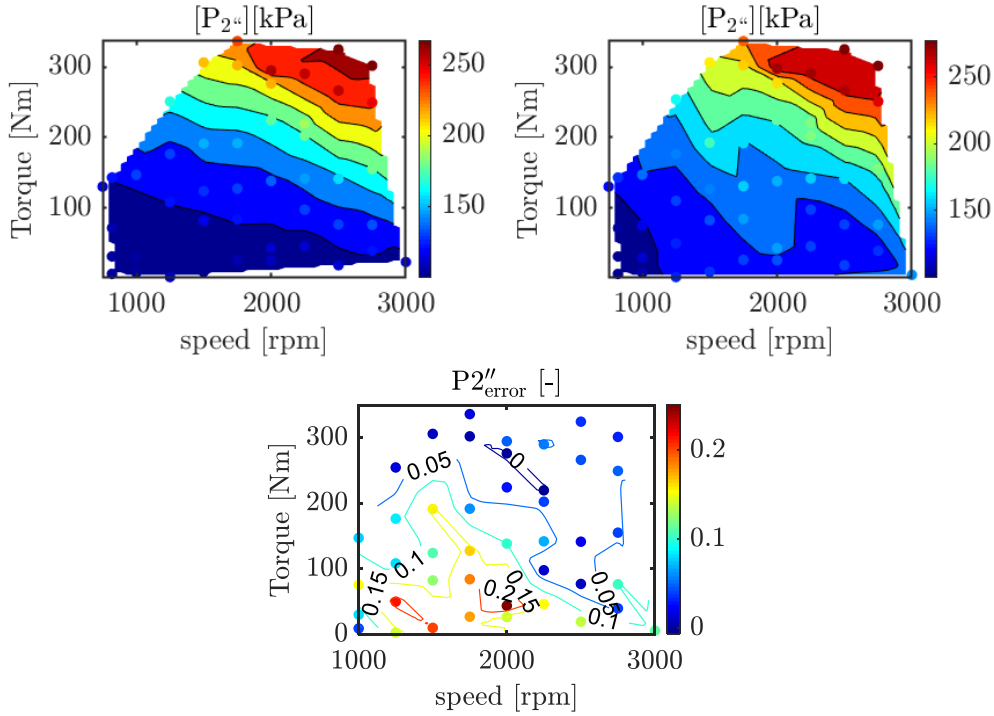

Figure 3.201: Comparison between intake pressure obtained with the HPEGR system, LPEGR system and difference (same reading order).

Similar results are obtained in terms of exhaust manifold pressure with small deviations at medium to high load, as showed in figure 3.21. However, important differences can be observed at low load conditions, where the predictive capabilities of the model are low due to its simplicity.

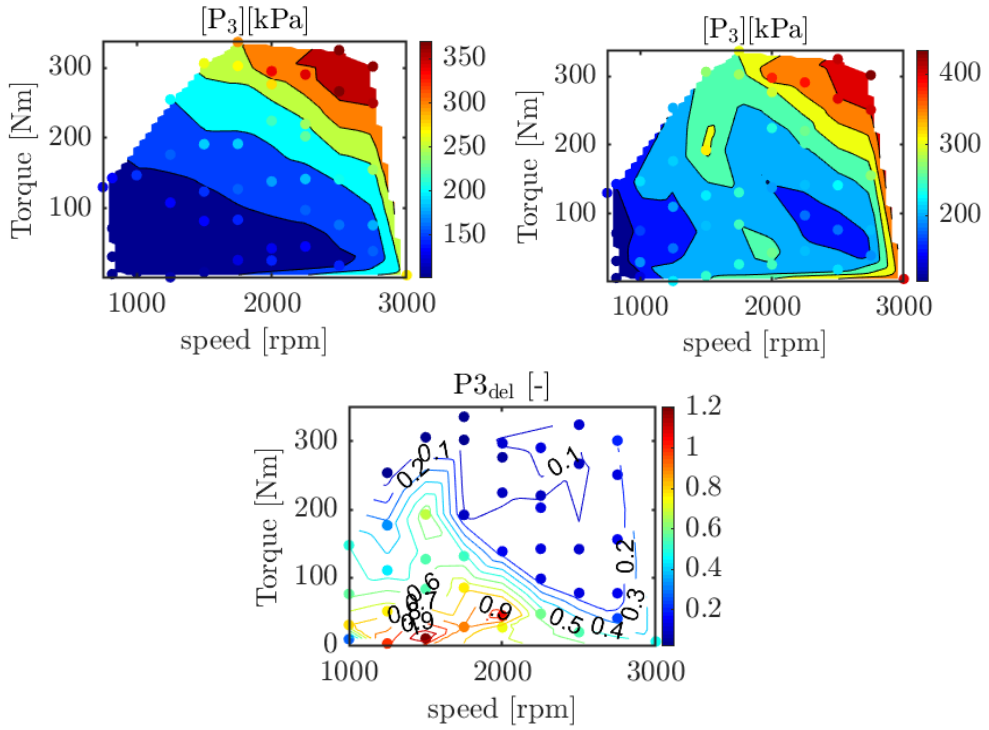

Figure 3.21: Comparison between exhaust pressure obtained with the HPEGR system, LPEGR system and difference (same reading order).

Regarding temperatures at the exhaust line, figures 3.22 and 3.23 show a reduction in both turbine inlet and outlet temperatures of around 1-5% with LPEGR.

Concerning NO_x emissions, it is observed in figure 3.24 how the flow with the LPEGR system is lower in the low speed-load region due to the lower pressure difference between the EGR duct inlet and outlet. This difference disapears at medium to high speed-load conditions where the flows are higher. According to this, NO_x emissions are expected to increase at low loads with only LPEGR, because high EGR rates would not be possible in these conditions, but at higher loads, it would be possible to maintain lower intake gas temperature while having higher EGR %.

Reduction of NO_x emissions at higher loads could be 20-40% as show by figure 3.25.

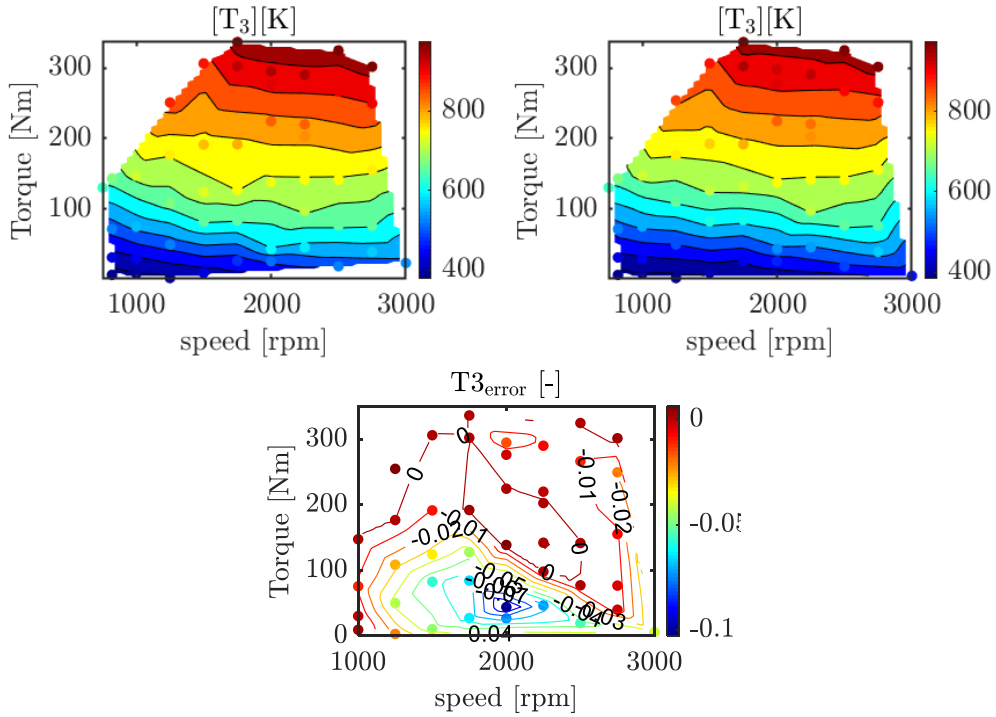

Figure 3.22: Comparison between turbine inlet temperature obtained with the HPEGR system, LPEGR system and difference (same reading order).

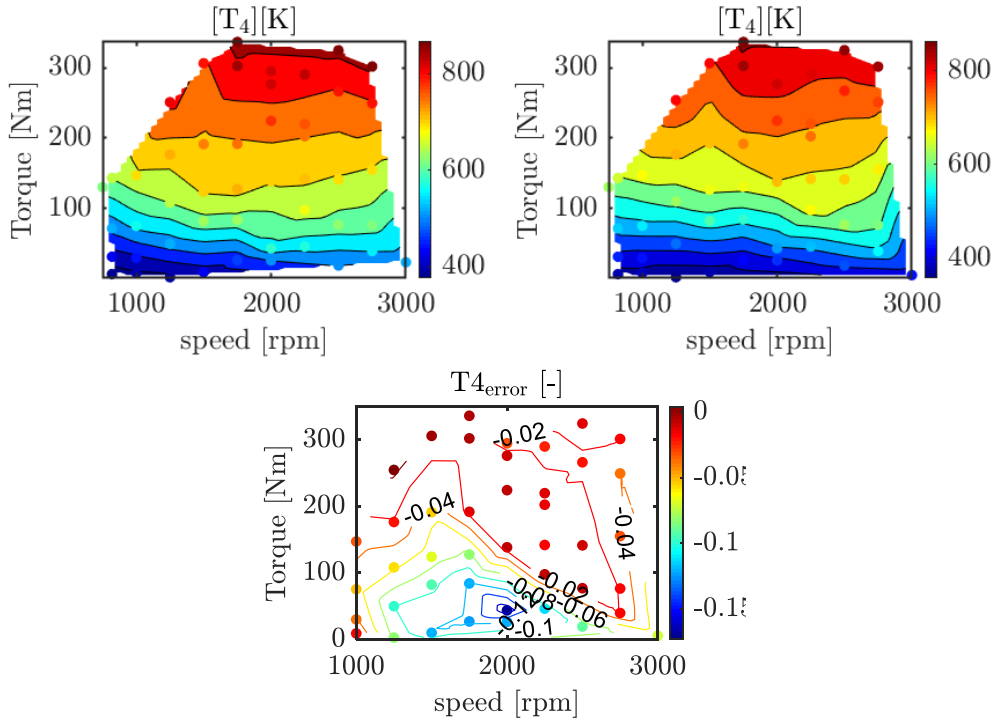

Figure 3.23: Comparison between turbine inlet temperature obtained with the HPEGR system, LPEGR system and difference (same reading order).

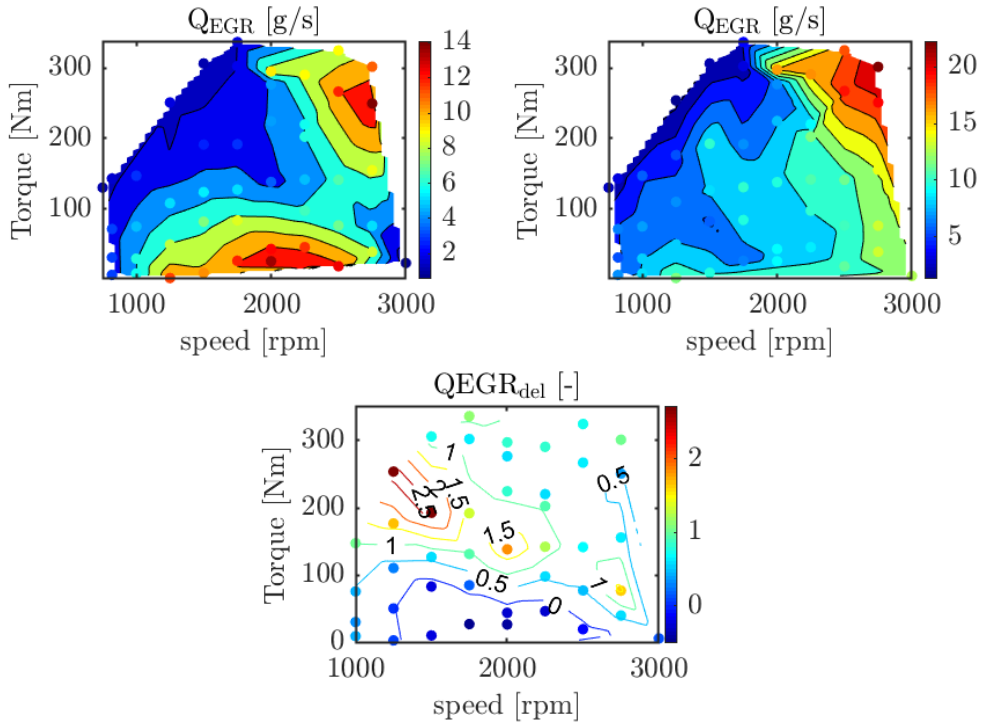

Figure 3.24: Comparison between the EGR flow obtained with the HPEGR system, LPEGR system and difference (same reading order).

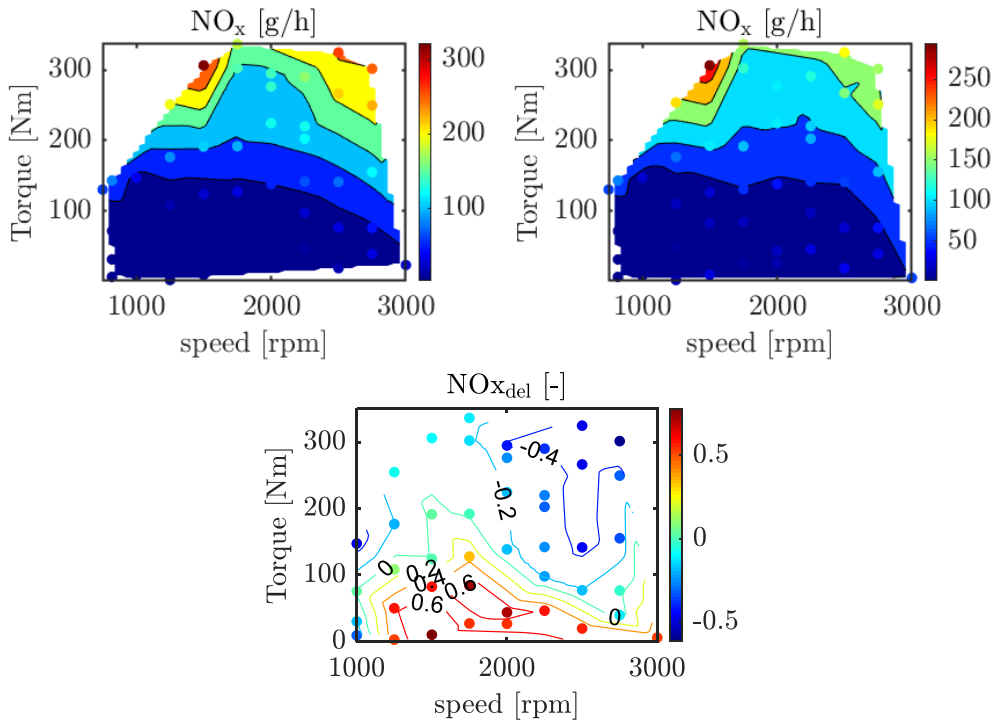

Figure 3.25: Comparison between NOx emissions obtained with the HPEGR system, LPEGR system and difference (same reading order).

Transient behavior (LPEGR)

In figure 3.26, a comparison of simulated results for engine with only HPEGR and only LPEGR are plotted for the WLTP cycle. The first plot shows instantaneous MAF for the two cases. Second plot shows instantaneous fueling rate and cumulative fuel consumption. The third plot for instantaneous and cumulative NO_x emissions. The fourth plot shows the percentual differences in terms of fuel consumption and NO_x emissions.

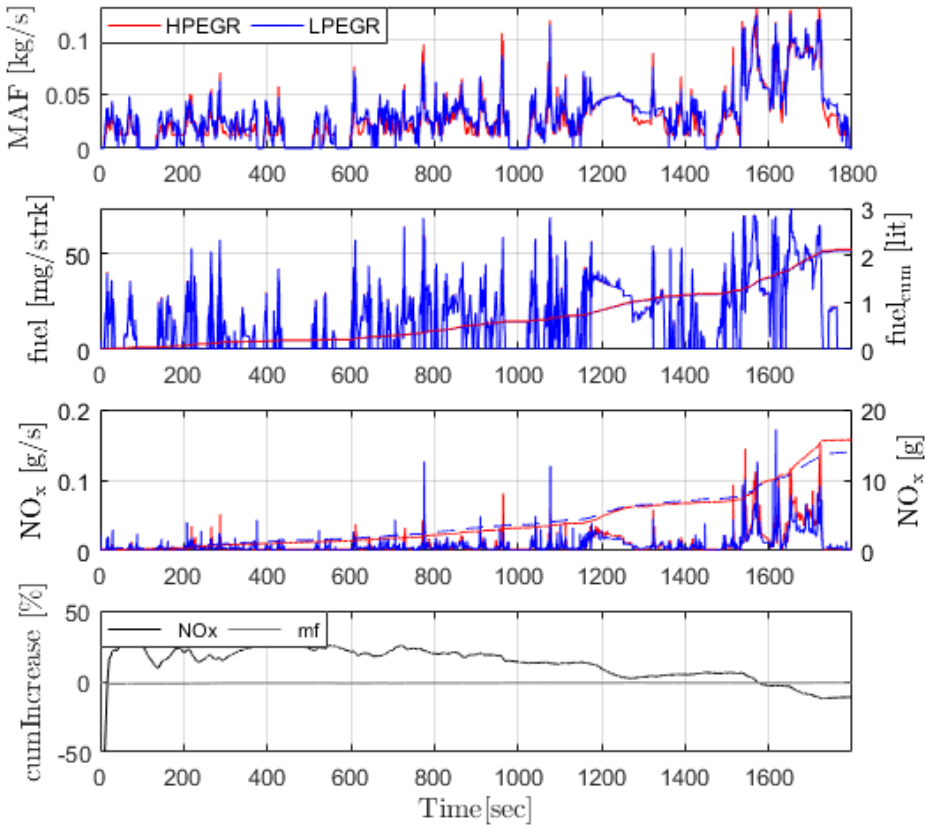

Figure 3.26: Comparison of the main model variables during the WLTP with HPEGR (red) and LPEGR (blue).

Despite the only difference between both simulations is the EGR system implemented, and the calibration has been kept constant, the upper plot in figure 3.26 points out differences in the air mass flow. During the first part of the cycle, the air mass flow with LPEGR is higher. The main reason for this is, as pointed out in the Steady State maps of previous subsection, that EGR flow is lower at the low speed and loads, typical of the beginning of the cycle the. In addition, the lower intake temperature achieved with the LPEGR system emphasizes this issue,

since this temperature implicates a higher mass of gases to be admitted by the cylinders and only air is available to flow through, given that the EGR flow cannot be increased due to the low pressure difference in the LPEGR duct. In the highway part of the cycle (from 1000s) the air mass flow is similar with both EGR systems since the pressure difference allows the LPEGR system to achieve the required EGR flows.

According to the model, negligible differences appear between HPEGR and LPEGR in terms of fuel consumption. Regarding NO_x, the emissions with LPEGR are higher during the first phase of the cycle due to the lower EGR rate, but this trend is quickly compensated at highway conditions where the LPEGR system can reach the air mass flow demand. Note that, since the intake temperature is lower with LPEGR, reaching the same air mass flow than HPEGR involves a higher EGR, so a positive impact on NO_x.

The accumulated fuel consumption and NO_x emissions at the end of the WLTP for both EGR architectures appears in figure 3.27. Results show that replacing HPEGR system with LPEGR may reduce NO_x emissions in the order of 10%, while keeping the same fuel consumption.

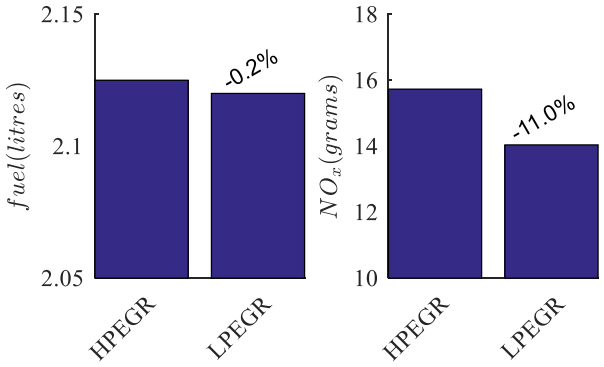

Figure 3.27: Accumulated fuel consumption (left) and NO_x emissions (right) in the WLTP with HPEGR and LPEGR.

Regarding intermediate variables of interest during the cycle, figures 3.28 & 3.29 show the evolution of engine speed and torque during the cycle, to verify that both configurations can follow the demanded torque profiles and results are fully comparable. In addition, the temperatures along the intake and exhaust lines show that temperatures at compressor inlet and outlet are substantially higher with LPEGR while intake temperatures are strongly reduced. Note that the temperature at the compressor outlet reaches >500K (>227ºC) which for sure will impact the compressor wheel durability. In this sense, the EGR rate should be limited at high loads (or other corrective measures are to be taken such as use hybrid EGR or reduce substantially the temperature of the LPEGR gas at the compressor inlet).

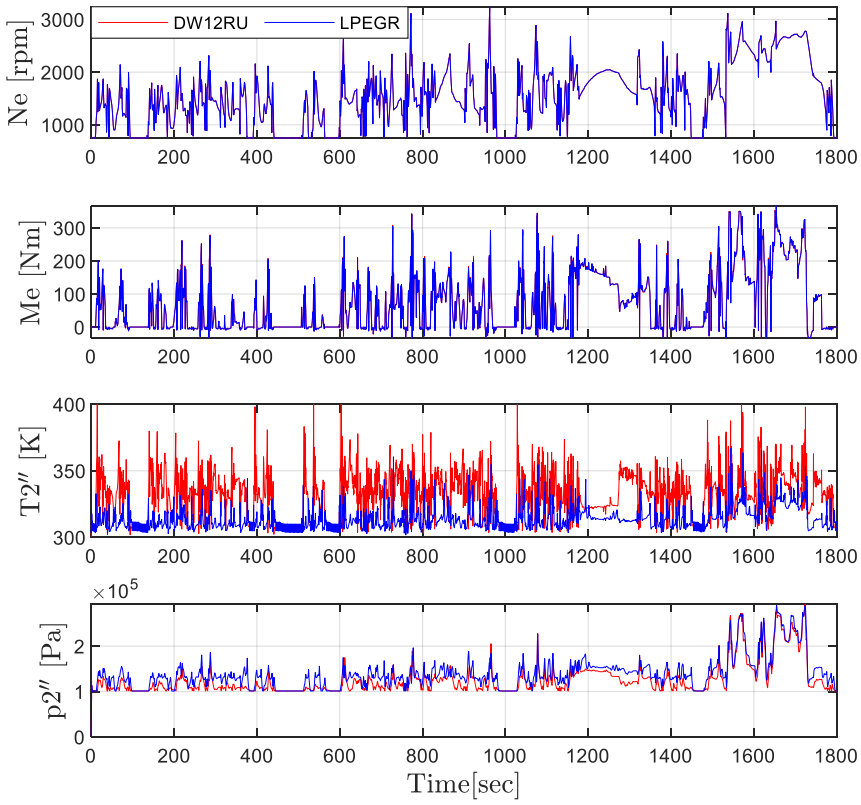

Figure 3.28: Evolution of engine variables during the WLTP with HPEGR (red) and LPEGR (blue). (Part 1)

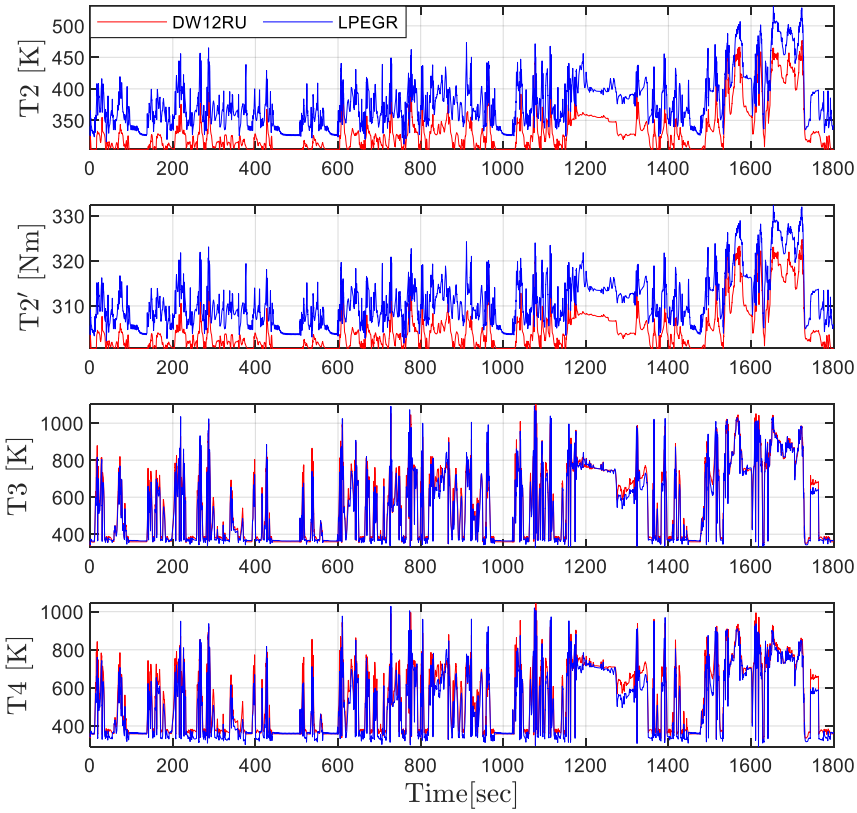

Figure 3.29: Evolution of engine variables during the WLTP with HPEGR (red) and LPEGR (blue). (Part 2)

Testing for Hybrid Model ($NO_{x_{Opt}}$, M_{opt})

In order to study the advantage of using both LP and HPEGR in a combination, forty-five engine-operating points covering the engine map have been selected to perform Steady State optimal calibrations for EGR related controls, by making a parametric swing on MAF and LP-HPEGR ratio defined as:

$$LPHP = \frac{m_{lpegr}}{m_{lpegr} + m_{hpegr}}$$

The results from swing were used to create the optimal calibration maps to choose the area (MAF, $LPHP$) where following conditions are satisfied:

- Torque, with the applied MAF setpoint and LP-HPEGR ratio, is greater than or equal to the torque obtained with only HPEGR.

- NO_x, with the new MAF setpoint and LP-HPEGR ratio is lower than or equal to that obtained with the HPEGR circuit:

$$Me(MAF, LPHP) \geq Me^{HP} \quad \& \quad NO_x(MAF, LPHP) \leq NO_x^{HP}$$

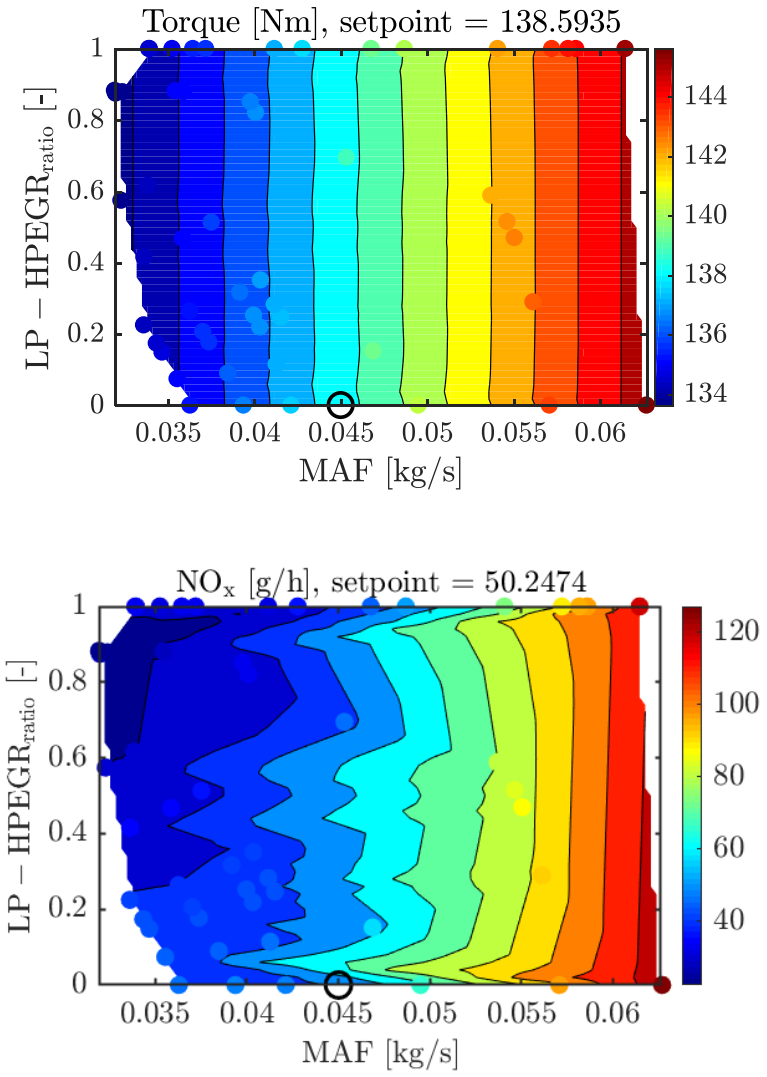

Figure 3.302: Swing on MAF and LP-HPEGR ratio and its impact on torque and NO_x emissions at a given engine operating point defined as 2250rpm - 30mg/strk.
The black circle represents the HPEGR reference operating conditions.

An example of the swing data is presented in figure 3.30 for one operating point of medium engine speed and load (2250rpm, 30mg/strk). Results show how, for a given LP-HPEGR ratio, reducing the air mass flow (then increasing the

EGR rate) lead to a reduction on NO_x emissions at the expense of a penalty on torque (and therefore efficiency). For a given air mass flow, increasing the LP-HPEGR ratio leads to a reduction in the NO_x emission, mainly due to two factors related with the lower intake temperature: on the one hand, reducing the intake temperature has a direct impact on NO_x reduction, since NO_x are temperature dependent. On the other hand, reducing the intake temperature at constant air mass flow involves an increase in the EGR rate, due to the higher mass to be admitted by the cylinders. Regarding the engine efficiency (torque in figure 3.30), the sensitivity to the LP-HPEGR ratio is low.

Maps like those presented in figure 3.30 have been obtained for the 45 operating conditions, spanning the complete engine map. Two different kinds of calibration have been obtained using the results from the swing simulations.

a. **Fuel (or torque) oriented calibration**: This calibration selects $LP-HPEGR_{ratio}$ and MAF_{sp}, where torque is maximum such that the NO_x emissions are lower or equal to the HPEGR case and temperature after the compressor is less than 450K.

$$\max_{MAF,\,LPHP}(M)$$

$$such\ that:$$

$$NO_x(MAF,\ LPHP) \leq NO_x^{HP}$$
$$T_{ac} \leq 450K$$

Calibration maps created using this process are called M_{opt}.

b. **NO_xOriented**: This calibration selects $LP-HPEGR_{ratio}$ and MAF_{sp} where NO_x is minimum such that the torque is higher or equal to the HPEGR case and temperature after the compressor is less than 450K.

$$\min_{MAF,\,LPHP}(NO_x)$$

$$such\ that:$$

$$M(MAF,\ LPHP) \geq M^{HP}$$
$$T_{ac} \leq 450K$$

Calibration maps created using this process are called $NO_{x_{Opt}}$.

Figure 3.31 shows an example of such process for three different operating conditions ranging from high load (top) to low load (bottom). After the MAF and LP-HPEGR ratio swing is done (see figure 3.30) all the combinations outside

previous conditions are removed. Then, from the subspace remaining, two points are selected as optimum calibration values, one for the M_{opt} calibration (that is the one with maximum torque), and other for $NO_{x_{Opt}}$ calibration (which is that with minimum NO_x). It can be noticed that, at some engine operating conditions, both calibrations share the same MAF and LP-HPEGR ratio, as pictured in the two medium-load points in figure 3.31. In general, the torque-oriented calibration leads to higher air mass flows due to the negative impact of EGR on torque.

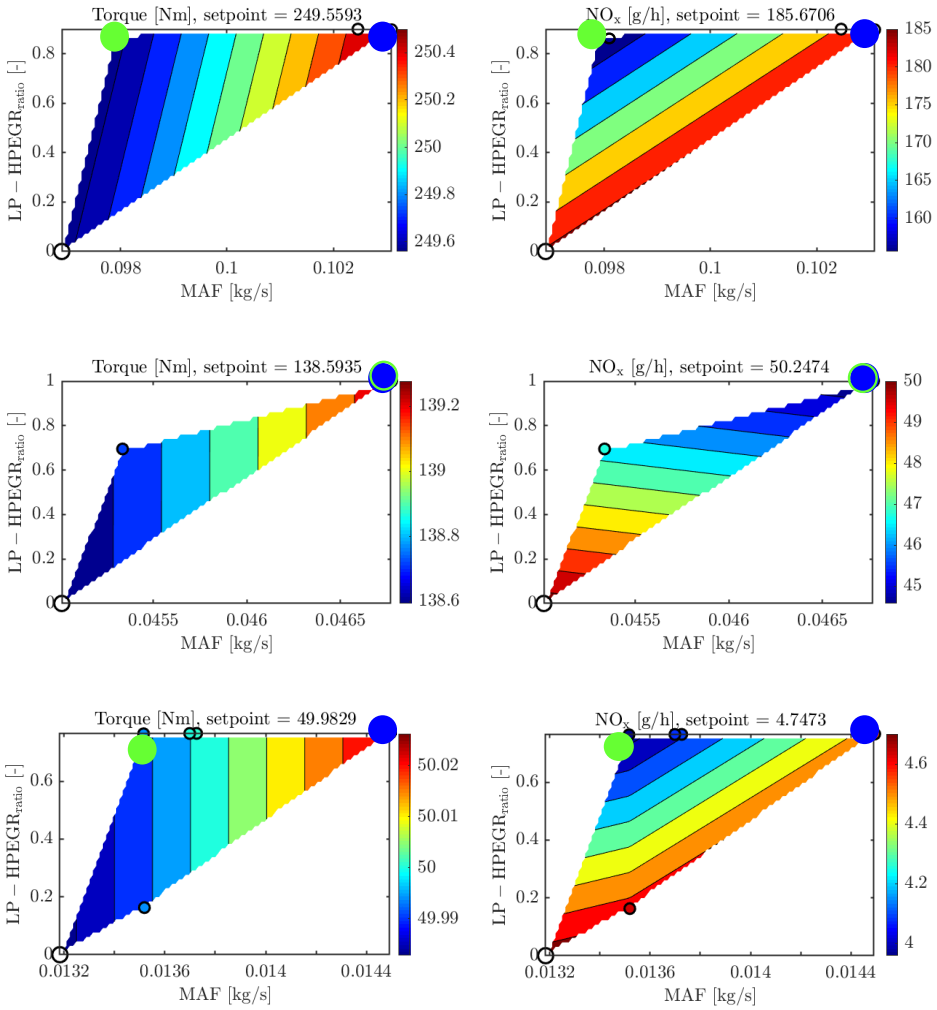

Figure 3.31: Swing on MAF and LP-HPEGR ratio, at three operating conditions, from low to high load, removing conditions where HPEGR torque is not reached or HPEGR NO_x emissions are exceeded. Black circle represents the reference HPEGR conditions, blue circle represents the Torque oriented calibration (M_{opt}) and the green circle represents the NO_x oriented calibration ($NO_{x_{Opt}}$).

According to this, figure 3.32 depicts the maps for the variable $LP - HPEGR_{ratio}$, for M_{opt} *and* $NO_{x_{Opt}}$ calibrations.

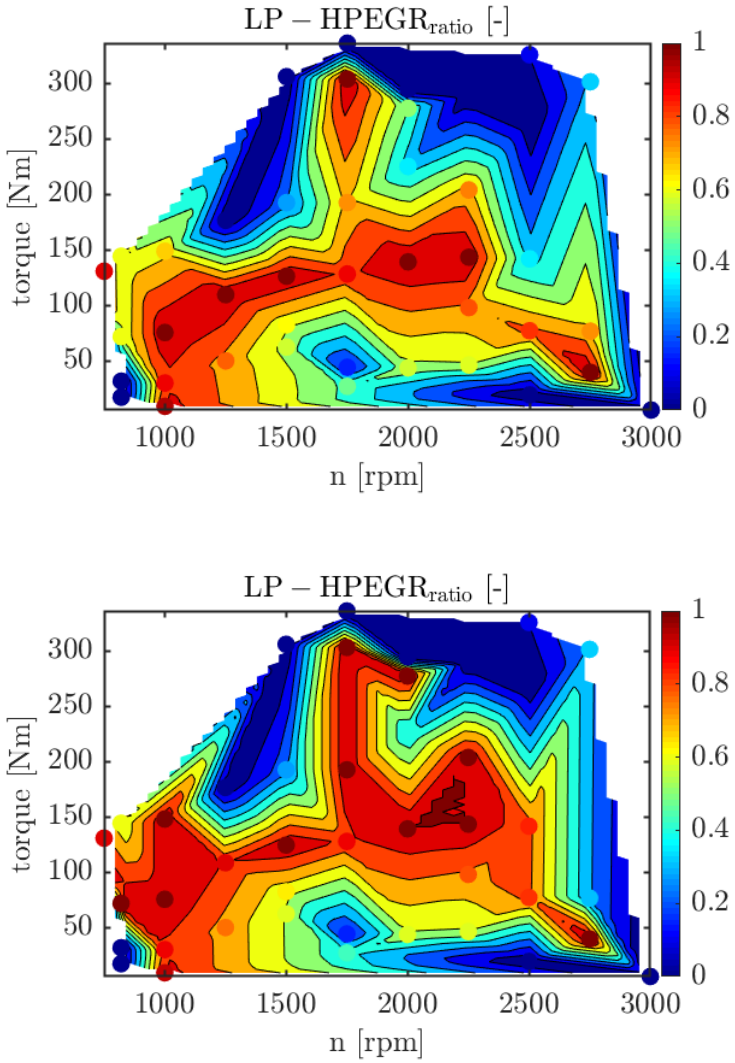

Figure 3.32: Calibration maps obtained for LPHP ratio as a function of engine speed and torque. M_{opt} calibration (top) and $NO_{x_{Opt}}$ calibration (bottom).

With the aim of pointing out the impact of the compressor temperature constraint, figure 3.33 shows the calibration maps obtained without considering the limit of 450K. It can be clearly observed how despite high LP-HPEGR ratios are interesting at high loads from torque and NO_x emissions point of view, the compressor limit regarding temperature forces the reduction of the LP-HPEGR ratio when the compression ratio is high and temperature at the compressor inlet are amplified.

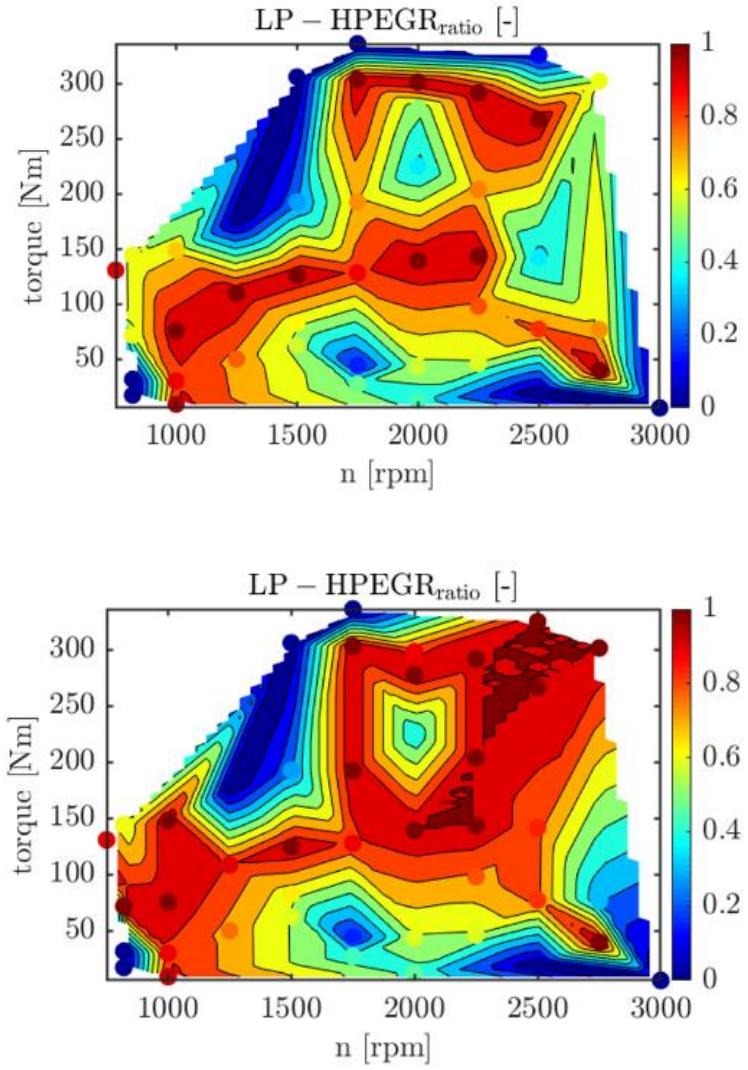

Figure 3.33: Calibration maps obtained for LPHP ratio as a function of engine speed and torque without considering the compressor temperature constraint at 450K. M_{opt} calibration (top) and NO_{xOpt} calibration (bottom).

Steady State engine behavior with optimal calibration maps

In the following subsection one on one comparison of important engine parameters (MAF, T2, T2', T2'', P2'', T3, T4, NOx and Qegr) for simulations with combined EGR with optimal calibrations $LP-HPEGR_{ratio}$ and $MAF_{sp}^{steadyOpt}$ at 45 engine operating conditions are presented.

For the sake of clarity, all the figures in this section share the same structure. The upper row shows the results with the M_{opt} calibration, while the lower row presents the results with the NO_{xOpt} calibration. In any row, the left plot shows the map on the considered variable while the right plot shows the relative differences with the HPEGR reference ($y2_{del}$) according to the following definition:

$$y2_{del} = \frac{y_{Mopt/NOxOpt} - y_{hpegr}}{y_{hpegr}}$$

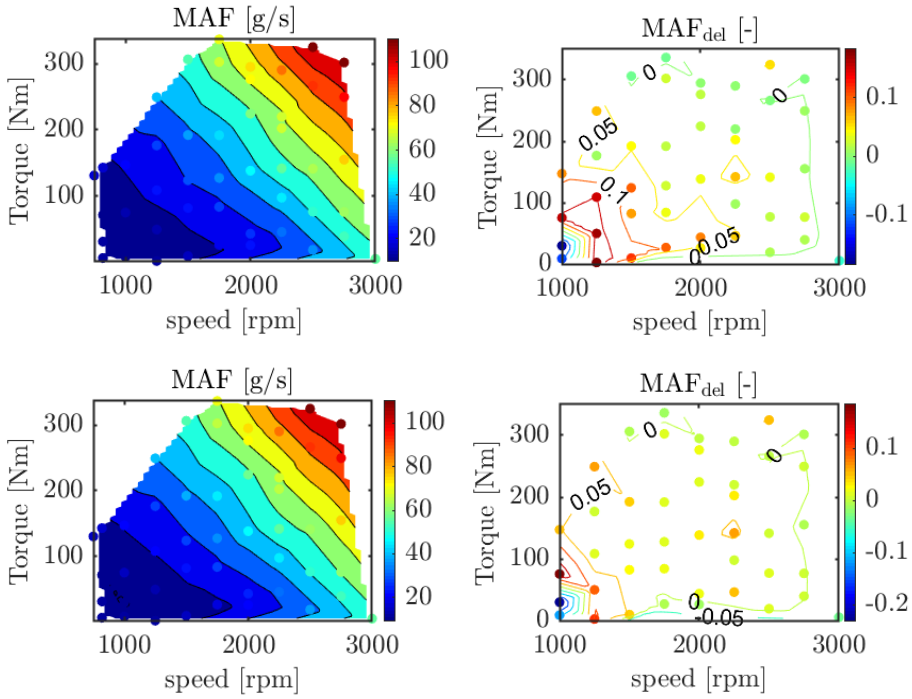

Figure 4.34: Air mass flow (left)
and difference with reference HPEGR configuration (right)
for the M_{opt} calibration (top row) and $NO_{x,opt}$ calibration (bottom row).

According to figure 3.34, the optimal MAF increases in comparison to HPEGR with both calibrations. This increase is more evident in the M_{opt} calibration (top plots) due to the negative impact of EGR on engine efficiency.

The restriction imposed in the compressor outlet temperature becomes apparent in figure 3.35, where maximum temperatures are limited to 450K at high loads and speed conditions. It can be checked that this restriction is achieved by reducing the LP-HPEGR ratio as shown in figure 3.32.

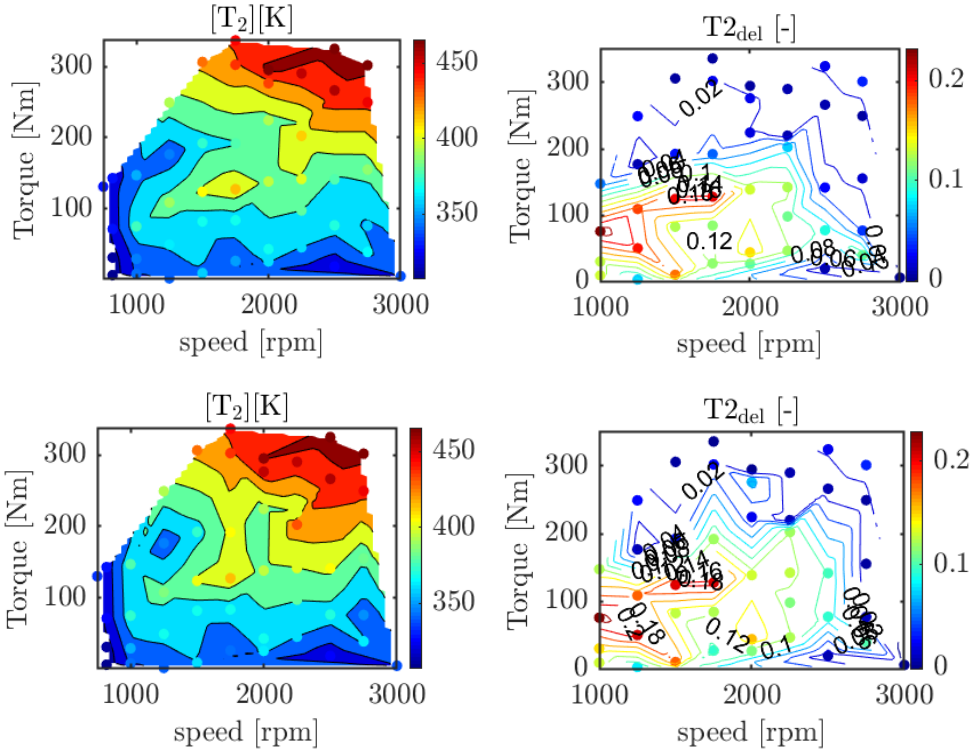

Figure 5.35: Compressor outlet temperature (left)
and difference with reference HPEGR configuration (right)
for the M_{opt} calibration (top row) and $NO_{x,opt}$ calibration (bottom row).

Temperature downstream WCAC (figure 3.36) are in the similar range of HPEGR engine, there seems to be increment in temperature of about 2% at low loads when high EGR rates are applied.

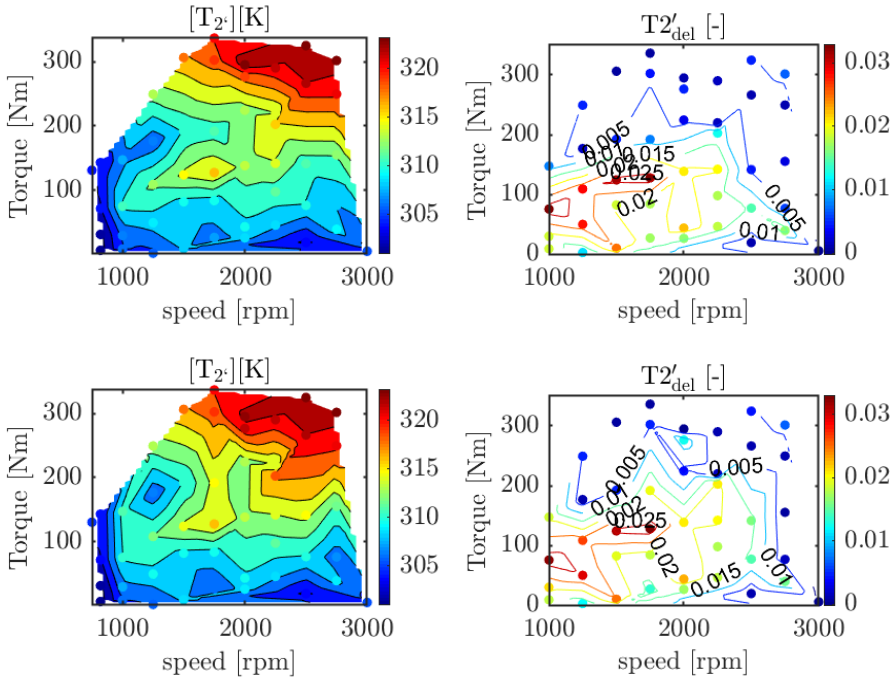

Figure 6.36: WCAC outlet temperature (left)
and difference with reference HPEGR configuration (right)
for the M_{opt} calibration (top row) and $NO_{x,opt}$calibration (bottom row).

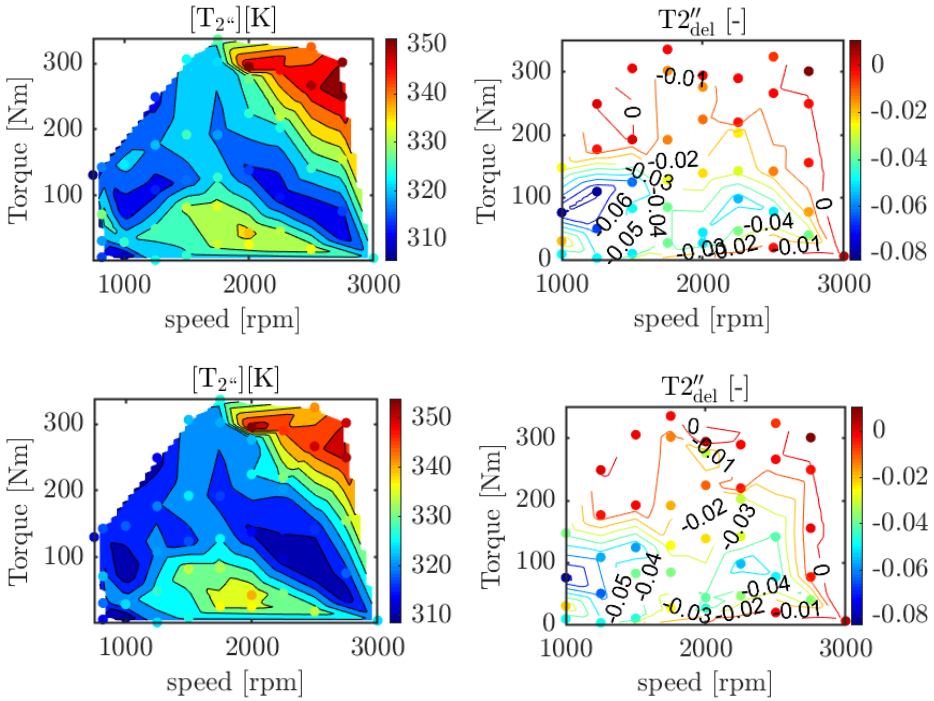

Figure 7.37: Intake temperature (left)
and difference with reference HPEGR configuration (right)

Temperatures in the intake manifold are reduced in the whole engine map, but specially at medium loads where reductions of about 5% are achieved due to the activation of LPEGR circuit (figure 3.37).

As happened with the LPEGR system (see figure 3.20) points at low loads show non-negligible differences with regards to the intake pressure of the HPEGR system (figure 3.38). The reason for that is that the mass flow through the turbine with the LPEGR system is higher, which also involves more energy available for the compressor and higher compression ratio.

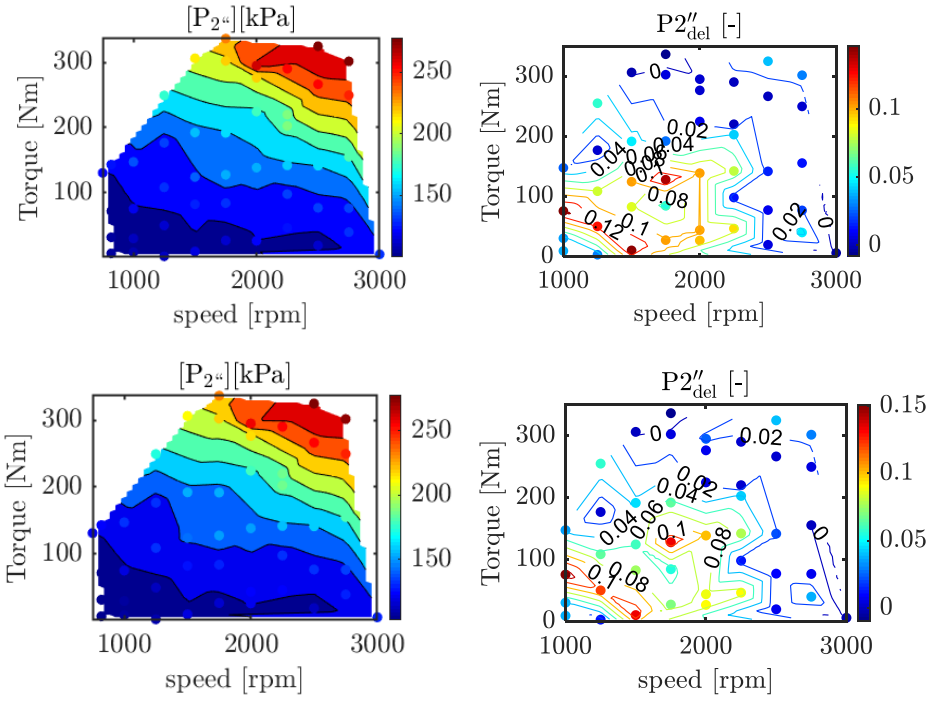

Figure 3.38: Intake pressure (left)
and difference with reference HPEGR configuration (right)
for the M_{opt} calibration (top row) and $NO_{x,opt}$calibration (bottom row).

Similarlly, the higher flow through the turbine and the exhaust line with LPEGR leads to higher pressure at the turbine inlet as can be observed in figure 3.39

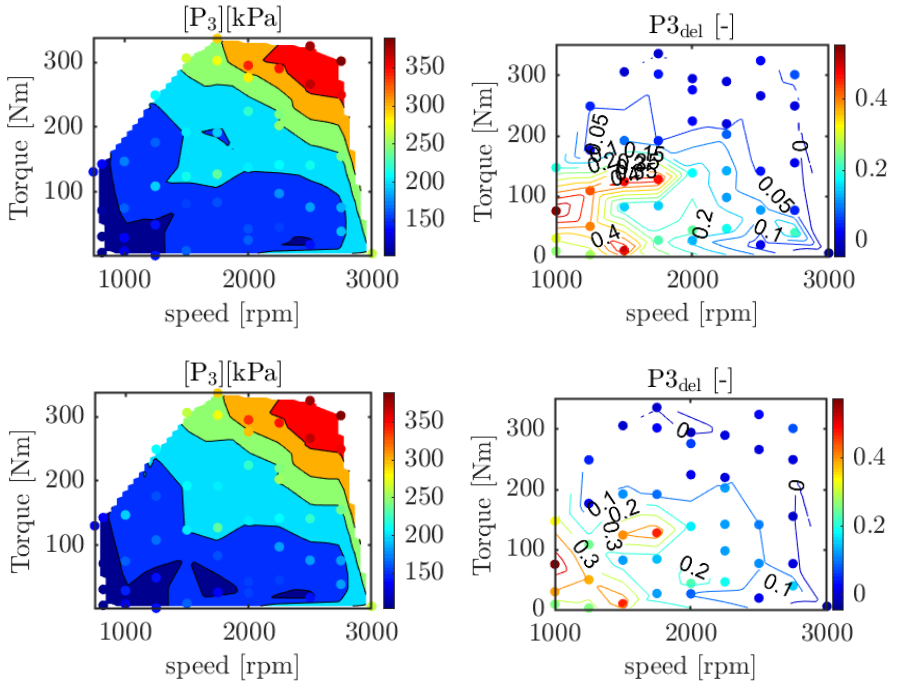

Figure 3.398: Exhaust pressure (left)
and difference with reference HPEGR configuration (right)
for the M_{opt} calibration (top row) and $NO_{x,opt}$calibration (bottom row).

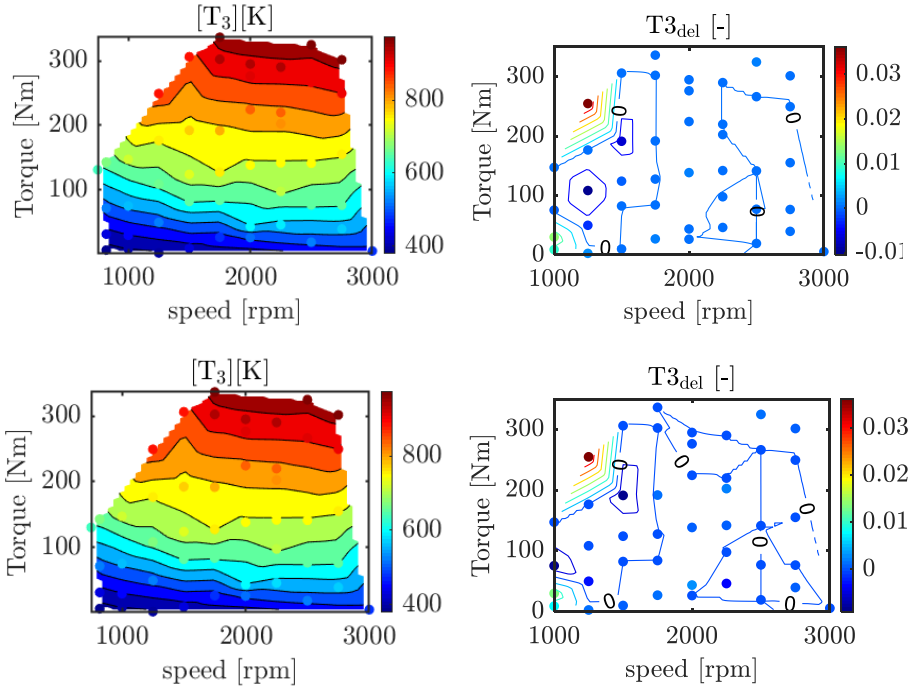

Figure 3.40: Exhaust temperature (left)
and difference with reference HPEGR configuration (right).

Regarding the temperatures in the exhaust line, the model does not show substantial variations with regards to the HPEGR reference configuration as can be checked in figure 3.40 and Figure 33.41.

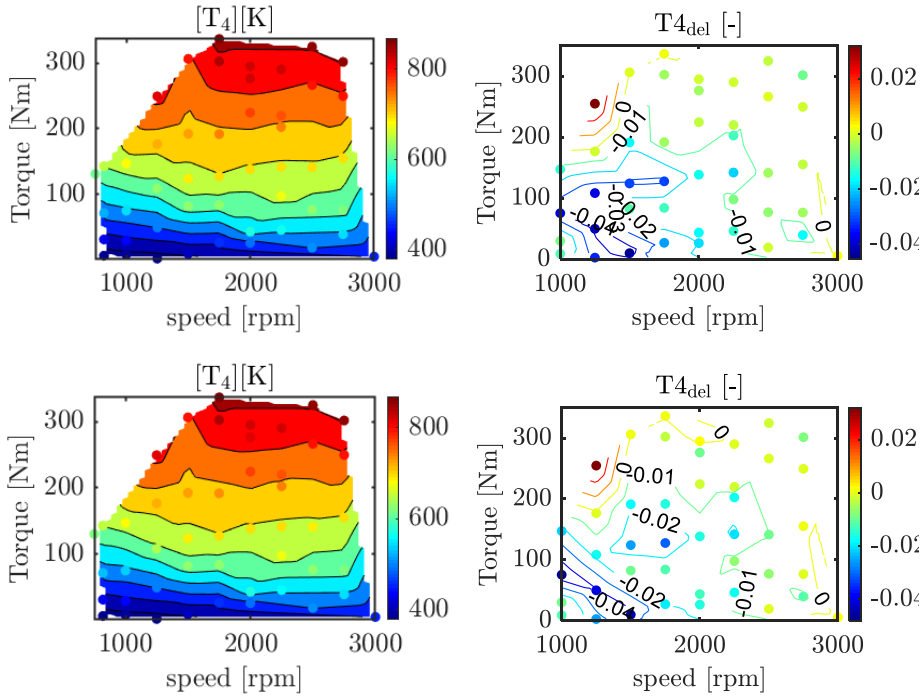

Figure 3.41: Turbine outlet temperature (left)
and difference with reference HPEGR configuration (right)
for the M_{opt} calibration (top row) and $NO_{x,opt}$calibration (bottom row).

The lower intake temperatures achieved with LPEGR lead to higher capacity to admit mass in the cylinders, that at the end, can revert in higher EGR flows as shown in Figure 3.429.42. Both calibrations show a general increase in the EGR flow respect to the HPEGR configuration, but this increase is more evident in the $NO_{x,opt}$ calibration (bottom plots) due to the positive impact of EGR on NO_x.

As a result of the lower intake temperatures, both calibrations and specially the $NO_{x,opt}$ show reductions in NO_x of 20-30%, mainly at medium and high loads, as showed in figure 3.43. This is possible due to lower intake manifold temperature with combined LP-HPEGR.

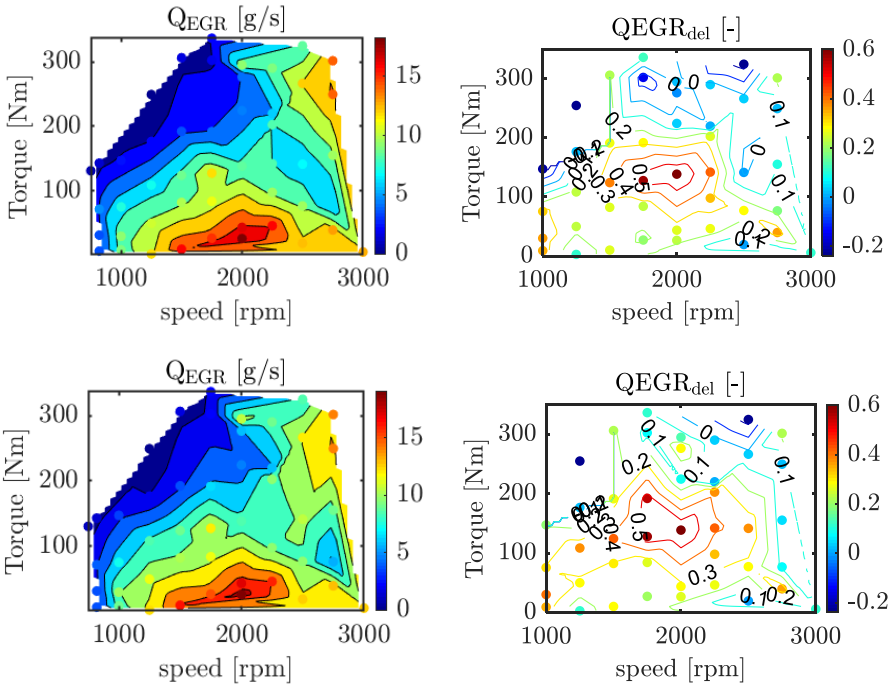

Figure 3.429: EGR flow (left)
and difference with reference HPEGR configuration (right)
for the M_{opt} calibration (top row) and $NO_{x,opt}$calibration (bottom row).

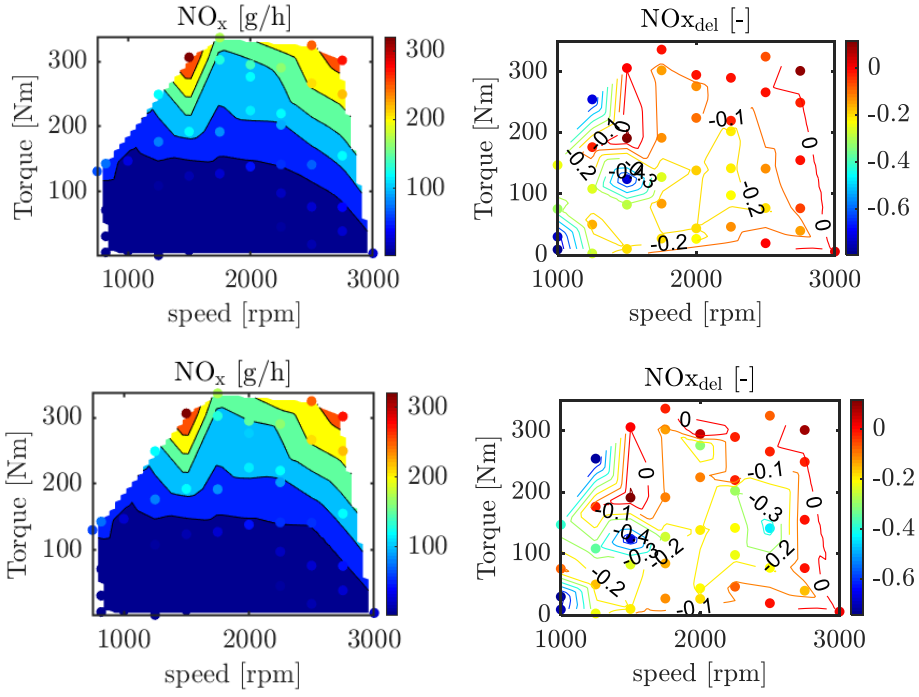

Figure 3.43: NOx emissions (left)
and difference with reference HPEGR configuration (right).

Transient engine behavior with optimal calibration maps

As explained in the introductory part of this chapter, the calibrations for minimum fuel consumption and minimum NO_x obtained from the Steady State simulations have been corrected with a linear transformation on the engine speed and fueling rate as:

$$MAF_{sp}^{Opt} = MAF_{sp}^{steadyOpt} \cdot \left(b_0 + b_1 \cdot n + b_2 \cdot m_f\right)$$

The parameters b_0, b_1 and b_2 for any of the two calibrations developed ($\mathbf{M_{opt}}$ and $NO_{x,opt}$) have been selected running a set of WLTPs with different combinations and solving the following optimization problems:

$$\min_{b_0, b_1, b_2} \int_{WLTC} \dot{m}_f dt$$

such that:

$$\int_{WLTC} \dot{m}_{NO_x} dt \leq NO_x^{HP,WLTC}$$

for the $\mathbf{M_{opt}}$ calibration, and

$$\min_{b_0, b_1, b_2} \int_{WLTC} \dot{m}_{NO_x} dt$$

such that:

$$\int_{WLTC} \dot{m}_f dt \leq Fuel^{HP,WLTC}$$

to obtain the $NO_{x,opt}$ calibration.

In the present subsection, the results obtained with both calibrations are compared with those obtained with HPEGR and LPEGR alone.

I. Results with calibration for minimum fuel consumption while keeping the same NO_x emissions ($\mathbf{M_{opt}}$)

As in previous sections, Figure 3.410 shows a comparison of simulated results for engine with only HPEGR and engine with LP-HPEGR, with the fuel oriented calibration $\mathbf{M_{opt}}$ in the WLTP cycle. The first plot shows instantaneous MAF for the two cases, and the LP-HPEGR ratio in grey. Second plot shows instantaneous fueling rate and cumulative fuel consumption. The third plot depicts instantaneous and cumulative NO_x emissions. The fourth plot is the percentual differences in terms of fuel consumption and NO_x emissions.

Despite differences in the air mass flow demands, as shown in Figure 434 between HPEGR and $\mathbf{M_{opt}}$ calibration, those differences where so low that are not appreciated in a dynamic cycle spanning the complete engine map, like the WLTP. However, the upper plot in Figure 44 points out how during the first phases of the cycle, with low engine speeds and loads, the LP-HPEGR ratio remains low, then giving rise to an often use of the HPEGR circuit. In the medium load and speed region, the LP-HPEGR ratio tends to 1, then using the LPEGR circuit because in this area shows its best potential (without exceeding the compressor temperature limit of 450K). Then, in the final part of the cycle, with high loads and speeds, despite the potential of LPEGR to reduce NO_x, the HP-LPEGR ratio remains low, for it is limited by the compressor temperature.

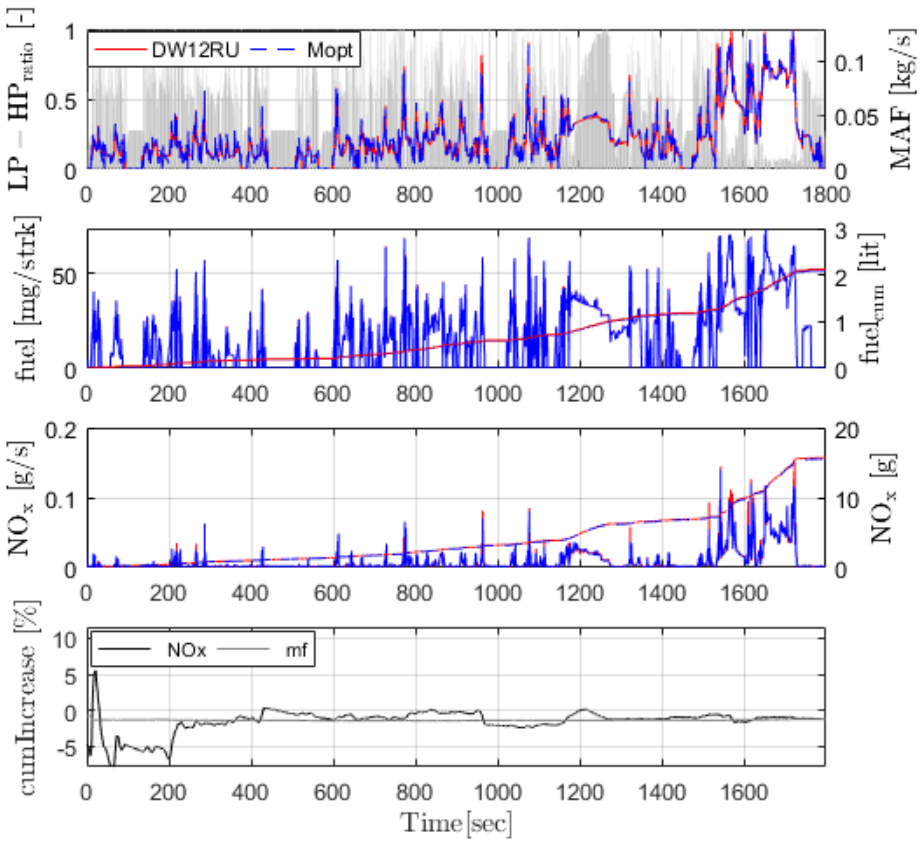

Figure 3.410: Comparison of the main model variables during the WLTP with HPEGR (red) and LP-HPEGR with M_{opt} calibration (blue).

Regarding fuel consumption and NO_x emissions is difficult to see the improvements, to this aim Figure 3.115 shows the accumulated results in the WLTC with the different configurations. The combination of HPEGR and

LPEGR with the $\mathbf{M_{opt}}$ calibration allows to reduce the fuel consumption by 1.2% while keeping the same NOx emissions than the HPEGR.

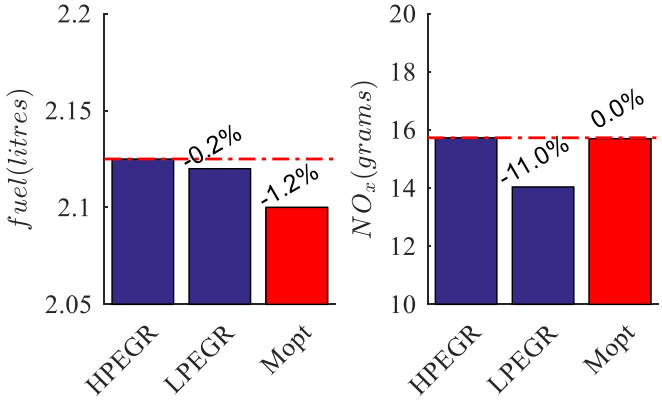

Figure 3.115: Comparison between fuel consumption (left)
and NOx emissions (right)
with HPEGR, LPEGR and LP-HPEGR with M_{opt} calibration in the WLTP.

The main concern regarding results in Figure 3.113.45 is related to the model simplicity and therefore limited accuracy that may make an improvement of 1.2% in the model to be completely negligible in the real engine.

For the sake of completeness, Figure 3.126 and 3.47 shows the evolution of some interesting variables, such as engine speed and torque that allow to check that both configurations follow the demanded torque profiles and results are fully comparable. Temperature evolutions allow to check the increased temperature at compressor and WCAC outlets when LPEGR is introduced and the reduction in intake temperature obtained with such system. Note that the temperature at the compressor outlet reaches the limit 450K (and occasionally exceeds it) with both HPEGR and LP-HPEGR configurations, but the LPEGR does not involve an increase in the maximum temperatures reached.

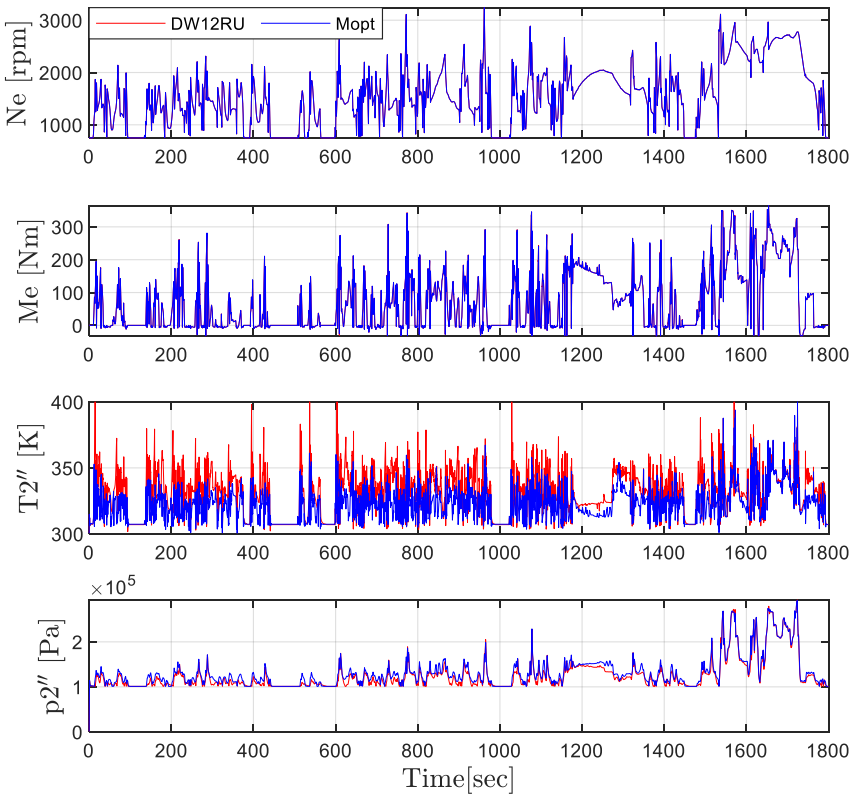

Figure 3.12: Comparison of simulation results with HPEGR model (red) and with combined LP-HPEGR model using M_{opt} calibration (blue) for WLTP cycle. (Part1)

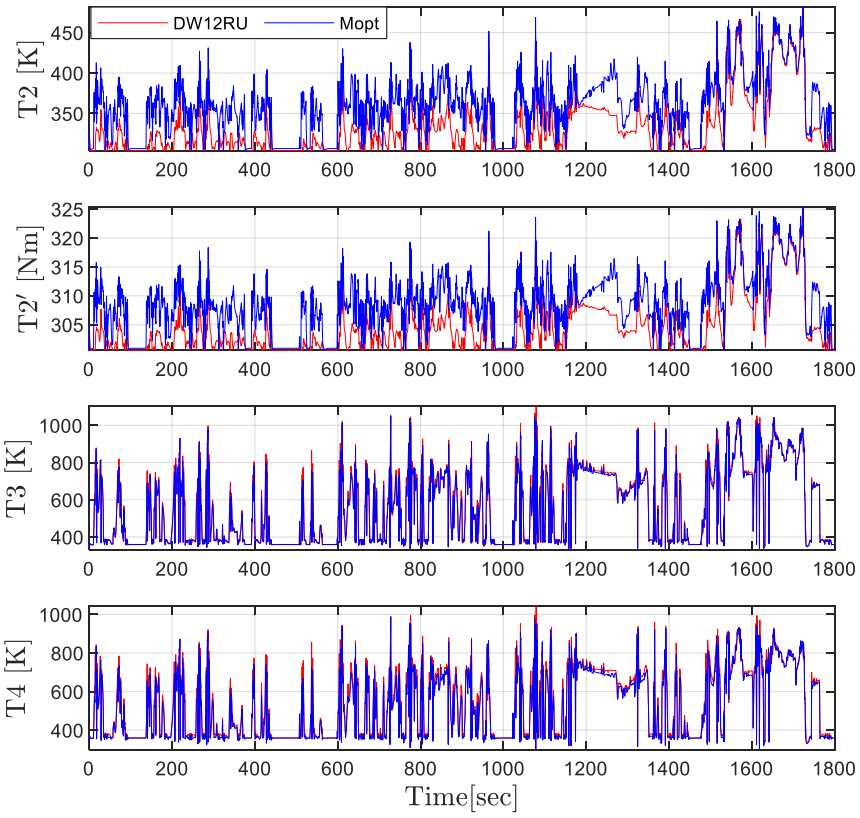

Figure 3.137: Comparison of simulation results with HPEGR model (red) and with combined LP-HPEGR model using M_{opt} calibration (blue) for WLTP cycle. (Part2)

II. Results with calibration for minimum fuel consumption while keeping the same NO_x emissions ($NO_{x,opt}$)

Figure 3.1448 shows how the LP-HPEGR ratio at medium loads reaches 1, to fully use LPEGR, whereas at low loads the LP-HPEGR ratio is reduced to increase the EGR rate, due to limitations in the pressure difference in the LPEGR line. At very high loads, the percentage of LPEGR is also reduced, in this case to keep the temperature after compressor below the 450K.

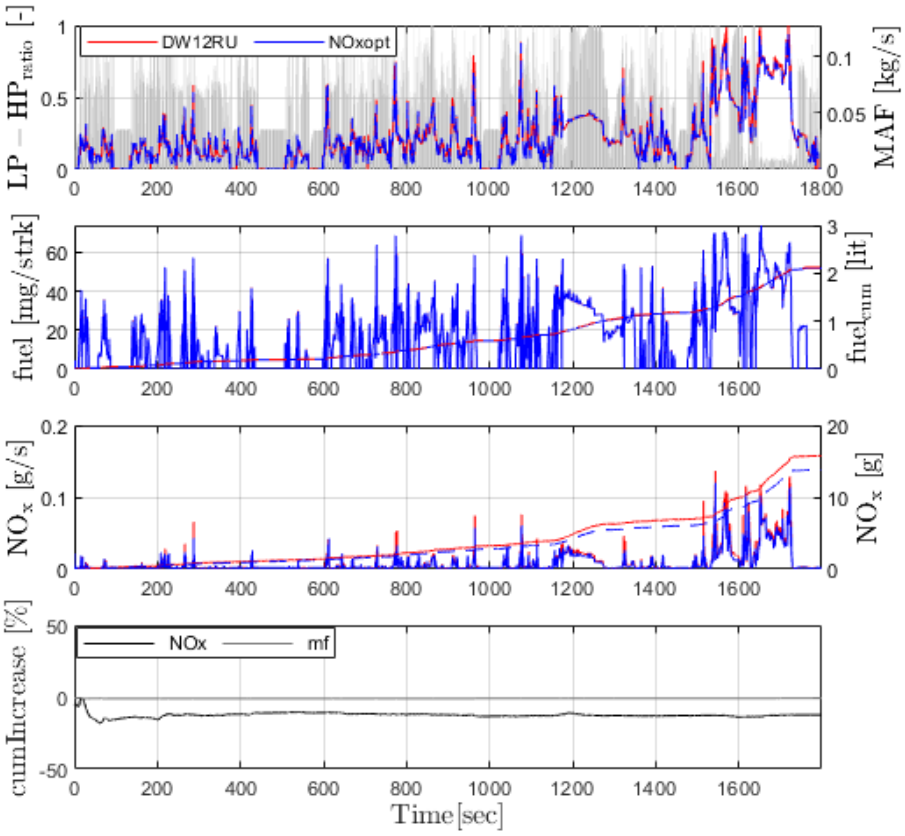

Figure 3.148: Comparison of the main model variables during the WLTP with HPEGR (red) and LP-HPEGR with $NO_{x,opt}$ calibration (blue).

As summary, Figure 15 shows that combining HP and LPEGR with the $NO_{x,opt}$ a reduction of 14% in NOx emissions can be obtained without penalty in fuel consumption.

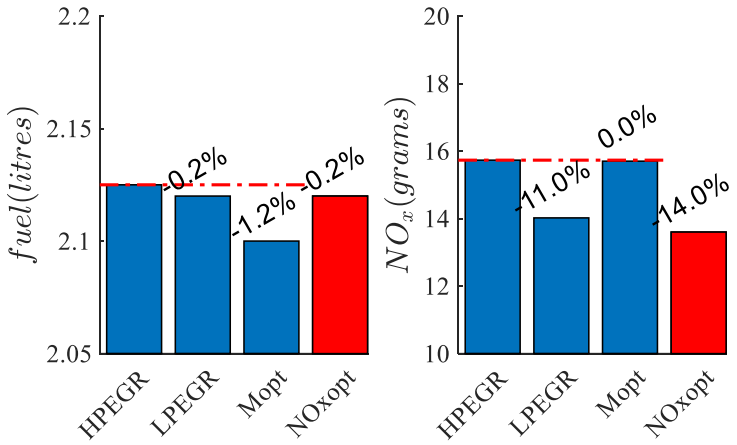

Figure 15: Comparison between fuel consumption (left)
and NOx emissions (right)
with HPEGR, LPEGR and LP-HPEGR
with M_{opt} and $NO_{x,opt}$ calibrations in the WLTP.

Despite the simplicity and limited accuracy of the model such an important difference in NOx should be observable in a real engine, moreover, those results are in line with experimental data in other engines (see Chapter 1).

Figure 160 and 3.51 may be used to verify that the $\mathtt{NO_{x,opt}}$ calibration also allows the engine to follow the torque demands in the WLTC and that maximum compressor outlet temperatures obtained with the HPEGR system are not exceeded.

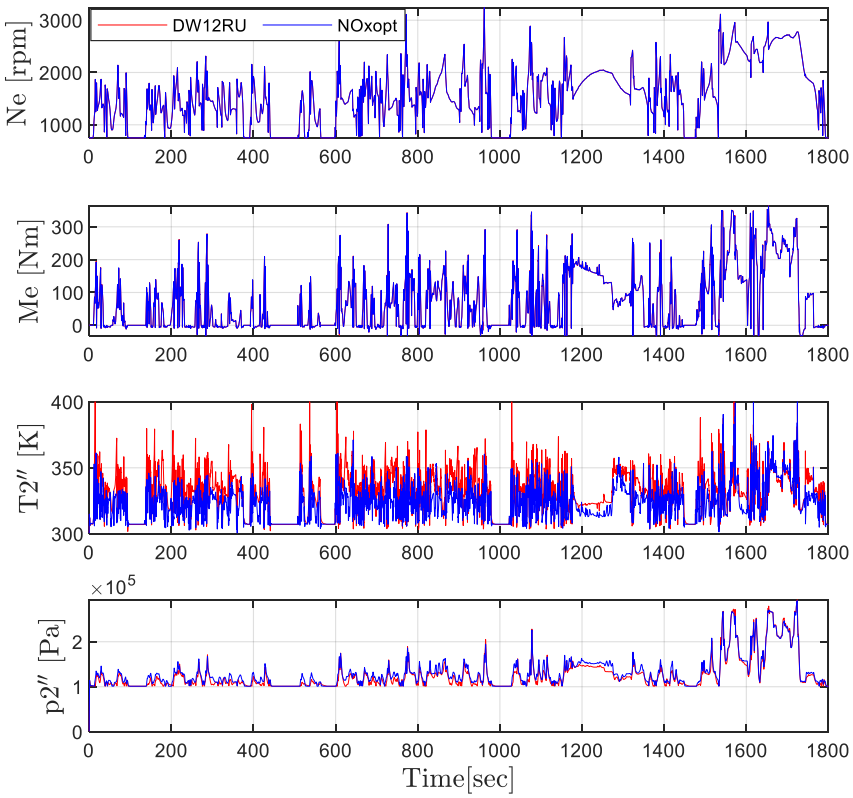

Figure 160: Comparison of simulation results with HPEGR model (red) and with combined LP-HPEGR model using $NO_{x,opt}$ calibration (blue) for WLTP cycle. (Part 1)

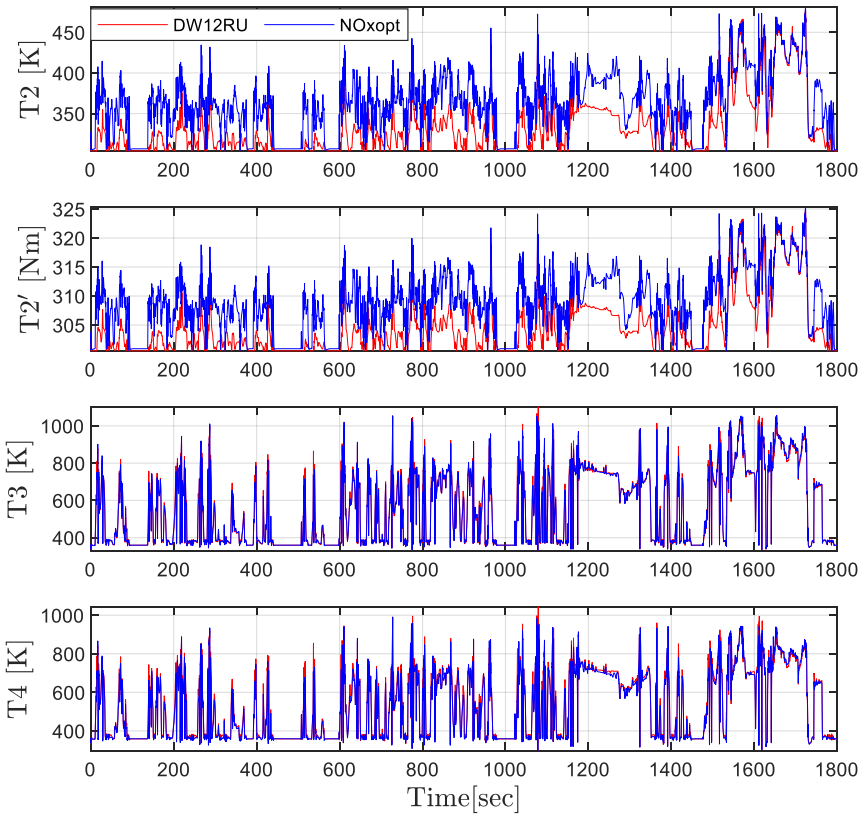

Figure 3.17: Comparison of simulation results with HPEGR model (red) and with combined LP-HPEGR model using $NO_{x,opt}$ calibration (blue) for WLTP cycle. (Part 1)

Chapter 4

Conclusion

An exhaustive review of state-of-the art knowledge, concerning LPEGR and Hybrid EGR systems, has been made in order to provide this project with a solid foundation that would lead to a high level of confidence towards its results, despite its entire computerized nature. In this sense, the amount of data provided from the manufacturer has been just enough to create a simplistic, yet quite precise computer model, which reflects the behavior of DW12RU engine close enough to identify its potential upgrade, when including the proposed air treatment techniques.

The results obtained convey that the calibration strategy implemented may be used to obtain an efficient, functional calibration for the control of new technologies introduced in the given engine, though real world parameters might include extra limitations (such as the one considered about compressor downstream temperature) in order to explore the real engine full potential.

Despite being a simple approach to explore the engine characterization, Steady State testing is not enough to fully reflect the entire engine behavior, so calibrations obtained from this path must be verify and modify via Transient tests, in order to fully understand and improve the dynamics inside the engine.

From the two calibrations generated in this project, improvements in fuel consumption and reduction of NO_x emissions are obtained in the DW12RU engine. Nevertheless, these results may be used not as exact values (like the ones shown in Chapter 3), but as a trend, given that more information would be needed to analyze this aspect. Real behavior of the engine would also take account of other

physical phenomena, so other parameters, such as friction losses and HC emissions, could be included in similar studies to, for example, make fuel consumption trends more sensible to intended changes.

With these previous statements, the objectives of this academic work are considered accomplished. Further experimental test of the given engine and others implemented in Light Duty Commercial Vehicles may make use of this information as reference and guideline for expected impact.

References and Bibliography

[1] Luján J, Pla B, Moroz S et al. Effect of low pressure egr on gas exchange processes and turbocharging of a hsdi engine. In THIESEL 2008 conference on thermo-and fluid dynamic processes in diesel engines. pp. 429–442.

[2] Luján JM, Galindo J, Serrano JR et al. A methodology to identify the intake charge cylinderto-cylinder distribution in turbocharged direct injection diesel engines. Measurement Science and Technology 2008; 19(6): 065401.

[3] Payri F, Luján J, Climent H et al. Effects of the intake charge distribution in hsdi engines. Technical report, SAE Technical Paper, 2010.

[4] Moroz S, Bourgoin G, Luján JM et al. Acidic condensation in low pressure egr systems using diesel and biodiesel fuels. SAE International Journal of Fuels and Lubricants 2010; 2(2): 305–312.

[5] Torregrosa AJ, Olmeda P, Martín J et al. Experiments on the influence of inlet charge and coolant temperature on performance and emissions of a DI diesel engine. Experimental Thermal and Fluid Science 2006; 30(7): 633–641.

[6] Broatch A, Luján JM, Serrano JR et al. A procedure to reduce pollutant gases from diesel combustion during European MVEG-A cycle by using electrical intake air-heaters. Fuel 2008; 87: 2760–2778.

[7] Luján JM, Pla B, Moroz S et al. Effect of low pressure egr on gas exchange processes and turbocharging of a HSDI engine. In THIESEL 2008 Conference on Thermo- and Fluid Dynamic Processes in Diesel Engines. Valencia, Spain.

[8] Ladommatos N, Abdelhalim SM and Zhao H. Effects of exhaust gas recirculation temperature on diesel engine combustion and emissions. Proceedings of the Institution of Mechanical Engineers, Part D: Journal of Automobile Engineering 1998; 212(6): 479–500.

[9] Hountalas DT, Mavropoulos GC and k B Binder. Effect of exhaust gas recirculation (EGR) temperature for various EGR rates on heavy duty DI diesel engine performance and emissions. Energy 2008; 33(2): 272–283.

[10] Maiboom A, Tauzia X and Hétet JF. Experimental study of various effects of exhaust gas recirculation (EGR) on combustion and emissions of an automotive direct injection diesel engine. Energy 2008; 33(1): 22–34.

[11] Desantes JM, Luján JM, Pla B et al. On the combination of high-pressure and low-pressure exhaust gas recirculation loops for improved fuel economy and reduced emissions in highspeed direct-injection engines. International Journal of Engine Research 2013; 14(1): 3–11.

[12] Bermúdez V, Luján JM, Pla B et al. Effects of low pressure exhaust gas recirculation on regulated and unregulated gaseous emissions during NEDC in a light-duty diesel engine. Energy 2011; 36(9): 5655–5665.

[13] Kolmanovsky I, Morall P, Van Nieuwstadt M et al. Issues in modelling and control of intake flow in variable geometry turbocharged engines. Chapman and Hall CRC research notes in mathematics 1999; : 436–445.

[14] Wahlström J. Control of EGR and VGT for emission control and pumping work minimization in diesel engines. PhD Thesis, Institutionen för systemteknik, 2006.

[15] Luján JM, Guardiola C, Pla B et al. Considerations on the low-pressure exhaust gas recirculation system control in turbocharged diesel engines. International Journal of Engine Research 2014; 15(2): 250–260.

[16] Lapuerta M, Ramos A, Fernandez-Rodriguez D et al. High-pressure versus low-pressure egr in a euro 6 diesel engine with lnt. effectiveness to reduce nox emissions. In THIESEL 2018 conference on thermo-and fluid dynamic processes in direct injection engines.

[17] Yan F and Wang J. Control of diesel engine dual-loop EGR air-path systems by a singular perturbation method. Control Engineering Practice 2013; 21: 981–988.

[18] Castillo F, Witrant E, Talon V et al. Simultaneous air fraction and low-pressure EGR mass flow rate estimation for diesel engines. In 5th Symposium on System Structure and Control. Grenoble, France.

[19] Grondin O, Moulin P and Chauvin J. Control of a turbocharged diesel engine fitted with high pressure and low pressure exhaust gas recirculation systems. In 48th IEEE Conference on Decision and Control. Shanghai, P.R. China.

[20] Luján JM, Guardiola C, Pla B et al. Switching strategy between hp (high pressure)-and lpegr (low pressure exhaust gas recirculation) systems for reduced fuel consumption and emissions. Energy 2015; 90: 1790–1798.

[21] Mao B, Yao M, Zheng Z et al. Effects of dual loop egr on performance and emissions of a diesel engine. Technical report, SAE Technical Paper, 2015.

[22] Mao B, Yao M, Zheng Z et al. Effects of dual loop egr and variable geometry turbocharger on performance and emissions of a diesel engine. Technical report, SAE Technical Paper, 2016.

[23] Zamboni G, Moggia S and Capobianco M. Hybrid egr and turbocharging systems control for low nox and fuel consumption in an automotive diesel engine. Applied Energy 2016; 165: 839–848.

[24] Svensson E, Yin L, Tunestal P et al. Combined low and high pressure egr for higher brake efficiency with partially premixed combustion. Technical report, SAE Technical Paper, 2017.

[25] Koli R, Arunachalam H, Zhu Q et al. Nonlinear model predictive control of dual loopexhaust gas recirculation in a turbocharged spark ignited engine. In 2018 Annual American Control Conference (ACC). IEEE, pp. 2437–2442.

[26] Yan F and Wang J. Control of diesel engine dual-loop egr air-path systems by a singular perturbation method. Control Engineering Practice 2013; 21(7): 981–988.

[27] Park J and Choi J. Optimization of dual-loop exhaust gas recirculation splitting for a light-duty diesel engine with model-based control. Applied Energy 2016; 181: 268–277.

II Document

Project Budget

Introduction

The objective of this document is the quantification of the expenses derived from this academic work. Given that the nature of the project is entirely computer-oriented and a relatively small amount of resources were utilized, the budget doesn't fit the typical formal structure of those focused in manufacture, traditionally applied to projects at this level. Even so, a relatively similar statement is provided, intending to be a much more pragmatic approach to the situation at hand. In following sections, the project is separated in its stages of development and a detailed explanation of the expenses made for each section is listed.

I. Prices Breakdown Appendix

1. 0-D Engine Modeling and Calibration

1.1 Creative Planning

Ref	un	Description
MCL	u	Review of the information given by the contracting party and analysis of the method to be implemented on the given engine. Comparative studies are carried out in this phase, identifying relations between similar engines which already make use of the suggested technology to be installed

Ref	un	Description	Qtty.	Price	Value
MEg	h	Mechanical Engineer	80,00	50,00	4000,00
PHME	h	Senior Mechanical Engineer	30,00	75,00	2250,00
Direct expenses	%	Complementary Direct Expenses	0,02	6250,00	125,00
				Sub-total:	6375,00

1.2 Model Development and Calibration

Ref	un	Description
MDC	u	Implementation of a data-based model for DW12RU engine in MathWorks Simulink. The model combines physical and empirical models for the different subsystems and control volumes. Model corresponds to a Euro 6 Diesel turbocharged internal combustion engine (ICE) with VGT and High-Pressure Exhaust Gas Recirculation systems (HPEGR). Model parameters are fitted to a set of experimental data set of steady state experiments (“BL7.xls”), that explore different combinations of operating conditions and controls.

Ref	un	Description	Qtty.	Price	Value
MEg	h	Mechanical Engineer	120,00	50,00	6000,00
MEds	h	Simulation and Analysis Engineer	120,00	60,00	7200,00
Direct expenses	%	Complementary Direct Expenses	0,02	13200,00	264,00
				Sub-total:	13464,00

1.3 Office Tools Amortization

Acquisition Cost		Description	(years) Amt. P	T.B.Amt.	Value
980,00	€	Laptop Asus GL552V	4	0,125	30,63
1200,00	€	Intel® Core™ i7-8550U CPU @1.80GHz	4	0,125	37,50
15000,00	€	MATLAB-Simulink Software	5	0,125	375,00
				Sub-total:	443,13

2. Model Exploration and Optimization Activities

2.1 Model Upgrade for LP-EGR Architecture

Ref	un	Descriptions
VUL	u	Creation of the LPEGR subsystem inside the Simulink Model. It follows the same calibration and control points considered for HPEGR calibration. An additional control (LP-HP_ratio) has been implemented to switch between systems. This switch could be set to one in order to activate LPEGR and zero to activate HPEGR; and any rational values between zero and one could be set to achieve a desired combination of LP and HP EGR.

Ref	un	Description	Qtty.	Price	Value
MEds	h	Simulation and Analysis Engineer	40,00	60,00	2400,00
PHME	h	Senior Mechanical Engineer	5,00	75,00	375,00
MEg	h	Mechanical Engineer	40,00	50,00	2000,00
Direct expenses	%	Complementary Direct Expenses	0,02	4775,00	95,50
				Sub-total:	4870,50

2.2 Obtaining of Optimal Maps and Steady State Analysis

Ref	un	Description
VOOPM	u	Creation of two Calibration Maps for the engine. The maps stablish a value for LP-HP_ratio, depending on operative conditions. The process consists in a parametric study to explore a wide range of LP-HP_ratios in several simulations, for later organizing the data to obtain the one combination with minimum value of NOx emissions while maintaining fuel consumption, for 45 engine operating points

Ref	un	Description	Qtty.	Price	Value
MEds	h	Simulation and Analysis Engineer	30,00	60,00	1800,00
MEg	h	Mechanical Engineer	60,00	50,00	3000,00
Direct expenses	%	Complementary Direct Expenses	0,02	4800,00	96,00
				Sub-total:	4896,00

2.3 WLTP Validation of Optimal Maps

Ref	un	Description
VWOPM	u	WLTP Cycle simulations are run, applying the optimal calibration, and values of NOx emissions are verified. Then, another set of simulation take place, for each calibration, with the objective of including cycle dynamics. A linear correction is made by applying optimizers on parametric coefficients that explore the proximities of steady state calibration and find improvements on fuel consumption and NOx emissions

Ref	un	Description	Qtty.	Price	Value
MEds	h	Simulation and Analysis Engineer	30,00	60,00	1800,00
MEg	h	Mechanical Engineer	60,00	50,00	3000,00
Direct expenses	%	Complementary Direct Expenses	0,02	4800,00	96,00
				Sub-total:	4896,00

2.4 Office Tools Amortization

Acquisition Cost		Description	Amt. P (years)	T.B.Amt.	Value
980,00	€	Laptop Asus GL552V	4	0,208	50,96
1200,00	€	Intel® Core™ i7-8550U CPU @1.80GHz	4	0,208	62,40
15000,00	€	MATLAB-Simulink Software	5	0,208	624,00
				Sub-total:	737,36

3. Development of Data-Management and Analysis Programs

3.1 Coding and Writing

Ref	un	Description
DCR	u	MATLAB codes for data extraction and management are created in order to portray findings in a clear way. The programs allow visual analysis and other informative resources for communication with the contracting party. Reports and instructive documents are also developed for this purpose.

Ref	un	Description	Qtty.	Price	Value
MEds	h	Simulation and Analysis Engineer	50,00	60,00	3000,00
MEg	h	Mechanical Engineer	60,00	50,00	3000,00
Direct expenses	%	Complementary Direct Expenses	0,02	6000,00	120,00
				Sub-total:	6120,00

3.2 Office Tools Amortization

Acquisition Cost		Description	Amt. P (years)	T.B.Amt.	Value
980,00	€	Laptop Asus GL552V	4	0,083	20,34
1200,00	€	Intel® Core™ i7-8550U CPU @1.80GHz	4	0,042	12,60
15000,00	€	MATLAB-Simulink Software	5	0,083	249,00
				Sub-total:	281,94

II. Measurements & Partial Budget

1. 0-D Engine Modeling and Calibration

Concept	Ref	Value	
Creative Planning	MCL	6375,00	€
Model Development and Calibration	MDC	13464,00	€
Office Tools Amortization		443,13	€
	Total:	20282,13	€

2. Model Exploration and Optimization Activities

Concept	Ref	Value	
Model Upgrade for LP-EGR Architecture	VUL	4870,50	€
Obtaining of Optimal Maps and Steady State Analysis	VOOPM	4896,00	€
WLTP Validation of Optimal Maps	VWOPM	4896,00	€
Office Tools Amortization		737,36	€
	Total:	15399.86	€

3. Development of Data-Management and Analysis Programs

Concept	Ref	Value	
Coding and Writing	DCR	6120,00	€
Office Tools Amortization		281,94	€
	Total:	6401,94	€

III. Budget Summary

Phase		**Value**	
I	0-D ENGINE MODELING AND CALIBRATION	20282,13	€
II	MODEL EXPLORATION AND OPTIMIZATION ACTIVITIES	15399,86	€
III	DEVELOPMENT OF DATA-MANAGEMENT AND ANALYSIS PROGRAMS	6401,94	€
Execution preliminary budget		42083,93	€
3% general expenses		1262,52	€
5% industrial benefit		2104,20	€
Sum		45450,65	€
21% IVA		9544,64	€
Execution final budget		**54995,29**	**€**

The overall cost regarding the development of this project rises to FIFTY-FOUR THOUSAND, NINE-HUNDRED AND NINETY-FIVE EUROS WITH TWENTY-NINE CENTS.